UNIVERSITY OF CALIFORNIA
Los Angeles

# Spectroscopy of Polarons, Bipolarons, and Excitons in Semiconducting Polymers

A dissertation submitted in partial satisfaction
of the requirements for the degree
Doctor of Philosophy in Chemistry

by

Matthew Gregory Voss

2020

ABSTRACT OF THE DISSERTATION

Spectroscopy of Polarons, Bipolarons, and Excitons in Semiconducting Polymers

by

Matthew Gregory Voss
Doctor of Philosophy in Chemistry
University of California, Los Angeles, 2020
Professor Benjamin Joel Schwartz, Chair

Organic electronics are an exciting alternative to traditional inorganic electronics. Compared to inorganic materials, organic electronics are lightweight, flexible, solution-processable, and inexpensive, and are made with non-toxic earth-abundant elements. Semiconducting polymers, discovered in the 1970s, are promising materials for use in organic electronics; the materials are easily tunable through organic synthesis, and their promise allowed researchers to earn the Nobel Prize for their discovery in 2000. Semiconducting polymers have potential applications in LEDs, solar cells, electrochromics, and thermoelectrics. Like the case with inorganic semiconductors, doping of organic semiconductors produces a charge (usually a positive charge) on the polymer. If the charge is mobile, the material's electrical conductivity is enhanced. The belief in the literature is that initially, at low dopant concentrations, trapped polarons (singly-charged cation radicals) form, which can be Coulombically-bound to the dopant counterion. As the concentration increases, the Coulomb wells of the dopants overlap and create mobile free polarons. As the dopant concentration increases further, polarons become too crowded on the polymer chains and can pair up to form doubly-charged bipolarons instead. My thesis work investigates polarons and bipolarons in conjugated polymers to better understand the nature and formation of these charge carriers.

The work presented in this thesis is the first use of ultrafast spectroscopy to understand and identify the electronic structure of the doped species on conjugated polymers. The first chapter in my thesis introduces semiconducting polymers and their applications, as well as the techniques I used to study them. The second chapter in my thesis demonstrates that ultrafast transient absorption

spectroscopy can be used to distinguish the roles of free carriers and carriers that are Coulomb-bound to the dopant counterions. The work presented in Chapter 2 also refutes one model of polaron energy levels, the band-bending model, based upon the transitions observed in the ultrafast transient absorption experiments. The final chapter of my thesis applies the ultrafast spectroscopy techniques developed in Chapter 2 to rule out the formation of polarons in a novel doped polymer system and to show that in this novel polymer, doping produces solely bipolarons instead of single polarons. We argue based on quantum chemistry calculations that it is the particular chemical structure of the polymer that produces this unusual behavior. Overall, my thesis work has made great strides in identifying and understanding the charge carrier(s) present in doped polymer systems.

The dissertation of Matthew Gregory Voss is approved.

Stuart Brown

Yves F. Rubin

Benjamin Joel Schwartz, Committee Chair

University of California, Los Angeles

2020

*To my friends and family, without whom none of this would have been possible.*

# TABLE OF CONTENTS

# LIST OF FIGURES

# LIST OF TABLES

# ACKNOWLEDGMENTS

I would like to start off by first and foremost thanking my family whose loving support and dedication allowed me to focus on my work. They were a constant source of inspiration and chaos in my life that helped me grow. They were always understanding of the sacrifices I was making.

I would like to thank my advisor Big Ben. I appreciate all of the guidance and support you showed me over the years in your office, from teaching me how to become a better scientist and salesman, helping me express clearly what I have discovered.

I want to thank the former grad students who were so instrumental in my success. Jordan and Steve who first showed me how to make polymer films. I want to thank Erik and Reddy and Eric who taught me about the lasers. I want to thank Taylor, Tyler, KJ, Omar and Dane for bouncing ideas off of and making all the samples I studied. I cannot forget to mention how my lab mates, particularly Jordan, Erik, Taylor and Chen-Chen improved my quality of life in grad school, keeping me sane during the years.

Finally I wish to thank those with whom I collaborated so often, many of which contributed much towards my graduate career success. Tyler and Reddy who were heavily involved in all of my projects. Xiaolin, Xiao, Sanghyun, and Peiqi, who made sure I kept up with all the theoretical calculations they did. I appreciate all the work Patrick and KJ did with GIWAXS, and particularly KJ for all the fluorescence and absorption measurements we did together. I thank Selvam and Sam for synthesizing a very unique polymer. I would like to thank Yves, Sarah, and Justin and their groups for all the enlightening discussions that have helped me understand so much more about polymers.

**Chapter 2** is a version reproduced from Voss, M. G.; Scholes, D. T., Challa, J. R., Schwartz, B. J. Ultrafast Transient Absorption Spectroscopy of Doped P3HT Films: Distinguishing Free and Trapped Polarons. *Faraday Discussions* **2018** with permission from the Royal Society of Chemistry. This work was supported by the National Science Foundation under grant numbers CBET-1510353 and CHE-1608957. This material is based upon work supported by the National Science Foundation Graduate Research Fellowship under Grant No. DGE-1650604. Any opinion, findings, and conclusions or recommendations expressed in this material are those of the authors and

do not necessarily reflect the views of the National Science Foundation. I performed the majority of measurements and writing the manuscript as well as developing its conclusions. Tyler made the samples and performed the steady state spectroscopy, and Reddy helped with the ultrafast spectroscopy. The PI was Benjamin J. Schwartz.

**Chapter 3** and Appendix A were supported in the National Science Foundation under grant numbers CBET-1510353 and CHE-1608957. This material is based upon work supported by the National Science Foundation Graduate Research Fellowship under Grant No. DGE-1650604. Any opinion, findings, and conclusions or recommendations expressed in this material are those of the authors and do not necessarily reflect the views of the National Science Foundation. X.L.W. was supported by the China Scholarship Council under grant number 201806035001. MGV, JRC, DTS, and BJS designed the experiments. MGV and JRC performed the transient absorption spectroscopy. MGV also analyzed the data. DTS made the films, took the steady state spectroscopy measurements, and performed the conductivity measurements. SS and SAJ synthesized the polymer. PYY and SHT took and analyzed the GIWAXS measurements. XLW and MDC ran the computational predictions of PBTDTP and XL and SJP ran the computational predictions of P3HT. OLR performed the measurements on PTB7. MGV and BJS wrote the paper with contributions from all authors. The PIs involved were Samson A. Jenekhe, Xiaolin Wang, Sarah H. Tolbert, and Benjamin J. Schwartz.

# VITA

| | |
|---|---|
| 2014–2015 | MS Chemistry, University of California Los Angeles (UCLA), Los Angeles |
| 2010–2014 | BS Chemistry, BS Engineering and Applied Science: Material Science, California Institute of Technology (Caltech), Pasadena |
| 2015 | National Science Foundation Graduate Research Fellowship |

## PUBLICATIONS AND PRESENTATIONS

**Voss, M. G.;** Scholes, D. T., Challa, J. R., Schwartz, B. J. Ultrafast Transient Absorption Spectroscopy of Doped P3HT Films: Distinguishing Free and Trapped Polarons. *Faraday Discussions* **2018**.

**Litman, Y.;** Voss, M. G., Rodríguez, H. B., San Román, E. Effect of Concentration on the Formation of Rose Bengal Triplet State on Microcrystalline Cellulose: A Combined Laser-Induced Optoacoustic Spectroscopy, Diffuse Reflectance Flash Photolysis, and Luminescence Study. *The Journal of Physical Chemistry A* **2014**, 118 *45*, 10531–10537.

**Voss, M. G.*;** Scholes, D. T.; Challa, J. R; Tolbert, S. H.; Schwartz, B. J.; Ultrafast Photophysics of Polarons and Bipolarons in Doped Semiconducting Polymers. *257th ACS National Meeting*, Poster, 2019

**Winchell, K. J.;** Voss, M. G.*; Schwartz, B. J.; Tolbert, S. H.; Polarized Optical Spectroscopy of Semiconducting Polymers in an Aligned Mesoporous Silica System for the Study of Polaron

Dynamics. *253rd ACS National Meeting*, Poster, 2017

**Voss, M. G.*;** Scholes, D. T.; Challa, J. R; Lindemuth, J. R.; Schwartz, B. J.; Photophysics of Polarons and Bipolarons in F4TCNQ-doped Semiconducting Polymers. *253rd ACS National Meeting*, Poster, 2017

# CHAPTER 1

# Introduction

Using light-active polymers to create organic electronics allows for lightweight, flexible, easily-processable, and cost-effective materials relative to silicon or other inorganic materials. Altering a polymer's π-conjugated backbone and side chains tunes its behavior. Being able to tune a polymer's behavior enables a degree of control over the characteristics of polymer-based electronics that is absent in inorganic systems. Polymer electronics are made using solution processing techniques that enable easy scalability and thus are a promising direction of research.

My current research explores *p*-doping of semiconducting polymers, that is, the removal of an electron from the π-conjugated backbone to create a conductive hole. Doped polymers are useful as charge transport and charge injection layers, which could provide a nice alternative to metal electrodes. They would be particularly useful to pair with other organic electronics as organic-organic interfaces form better junctions than metal-organic interfaces.[1]

Another promising application of doped semiconducting polymers is in thermoelectric devices.[2–4] A thermoelectric device can convert a heat gradient into a current due to thermally-driven diffusion of electrons (or conversely, it can use an applied voltage to generate a temperature gradient). The best thermoelectric materials have high electrical conductivity and low thermal conductivity in order to have the largest temperature gradient and best movement of charge over the smallest distance. Semiconducting polymers have low thermal conductivity relative to alternative materials but suffer from low electrical conductivity unless the electrical conductivity is improved by doping.[2–4]

In order to design higher conducting polymer films, the nature of the charge carriers responsible for conductivity must be understood. The carriers formed in a conjugated polymer upon *p*-doping can take several forms. During the *p*-doping of a polymer, a small molecule dopant oxidizes

the polymer backbone, removing a single electron. The removal of an electron leaves behind an unpaired electron and a hole, making a cation radical. The cation radical behaves as a single quasiparticle, a single delocalized species. The cation and radical move together to conduct a current, and this cation and radical quasiparticle is called a polaron. The structure of a polymer with a polaron is shown in Figure 1.1.

A polaron can be delocalized along the polymer backbone, or it can delocalize onto neighboring polymer chains as well. Polarons can be free to conduct along the polymer backbone, or the dopant counterion's negative charge can hold on to the polaron's positive charge, trapping the polaron Coulombically. If two polarons pair up, they can become a dication, which is also called a bipolaron, and is shown in the lower part of Figure 1.1.

These different polaronic species have distinct optical signatures.[5] Briefly, undoped conjugated polymers have a single absorption in the visible region, the bandgap transition, as shown in Figure 2.2a. When a polymer is doped to form a polaron, an electron is removed from the valence band in the polymer. Polarons have a low energy transition, called P1, absorbing in the near infrared region, and an absorption on the edge between visible and near infrared, called P2.[5] When a polaron delocalizes onto neighboring polymer chains, additional peaks may appear, as shown in Figure 2.2b,d.[6] When a polaron becomes trapped, the P1 peak shifts to higher energy. Alternatively, as seen in Figure 2.2c a bipolaron has a single absorption, called BP1 that absorbs at an energy between the P1 and P2 absorption peaks of polarons.[5] In steady-state spectroscopy, all of these peaks look similar to each other and can overlap if multiple species are present simultaneously; thus assigning which species is present is difficult.

These overlapping peaks can be resolved using time-resolved spectroscopy methods; however, to perform time-resolved spectroscopy, one needs high quality films. Recent advances from our group in how doped polymers are fabricated[7, 8] have improved doped polymer film quality significantly, enabling new optical measurements on doped polymer films to understand the nature of the charge carriers present. My thesis work takes these high-quality films and investigates them using ultrafast transient absorption spectroscopy, a femtosecond resolution technique described in the following section. My thesis demonstrates that transient absorption spectroscopy is a powerful technique that is well-suited towards understanding which carriers are present in a given doped polymer film.

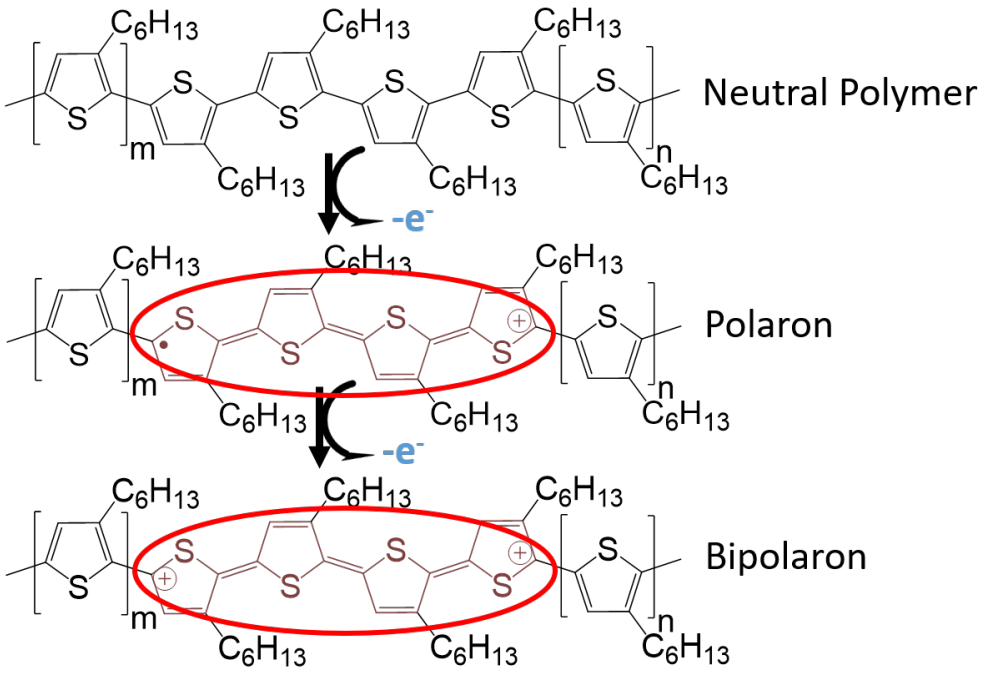


**Figure 1.1: A representation of an example polymer (P3HT, poly-3-hexylthiophene) shows how its chemical structure changes upon doping. Top: the structure and arrangement of bonds of neutral P3HT, middle: the structure of P3HT once one electron has been removed and a polaron forms, bottom: the structure of P3HT when a second electron is removed and a bipolaron forms.**

## 1.1 Transient Absorption Spectroscopy

In transient absorption spectroscopy, a femtosecond duration excitation pulse promotes a fraction of the sample to an electronically excited state. A weak probe pulse is then sent through the sample following a controlled time delay relative to the excitation pulse. This weak probe pulse is often a white light continuum pulse, short in time but broad in wavelength. A difference absorption spectrum (the baseline ground-state absorption spectrum subtracted from the excited absorption spectrum) is then measured. By seeing how the difference absorption spectrum changes with respect to the time delay between the pump and probe pulses, the kinetics of the relaxation of the excited states can be determined.

As mentioned above, previous work using ultrafast transient absorption spectroscopy to investigate the carriers had been stymied by the lack of optical quality chemically-doped polymer films. Instead, most transient absorption measurements have come from studying photoinduced carriers.[9–11] Photoinduced carriers are produced after exciting a polymer's bandgap transition to

make excitons in the presence of an acceptor molecule that has been mixed into the polymer film to split the exciton into polarons. The problem with studying photoinduced polarons is that there are also many other absorbing species present, including excitons, excimers, and polaron pairs, which can overlap the transient signals of any potential polarons and bipolarons. Additionally, the signal-to-noise in photoinduced carrier experiments is marginal, as the signal is a change in the change in the transient absorption. The difficulty of proper assignment of the spectra in photoinduced polaron experiments has been summarized by the Rumbles group.[9]

In my work, I avoid the these difficulties by studying charge carriers that are already formed in chemically-doped polymer films. The films were excited in the near infrared to avoid spectrally congested regions where multiple transitions might overlap. Specifically, we excite the near infrared P1 and BP1 peaks of polarons and bipolarons, cleanly targeting the species of interest and avoiding the complications of also exciting the bandgap transition, the dopant absorption, and other species that absorb in the visible region. As described in Chapters 2 and 3, applying transient absorption spectroscopy to chemically-doped polymer films allows clean assignment of the charge carriers present, distinguishing free and trapped polarons and bipolarons from each other. This is a significant advancement over previous works, enabling a clear picture of the electronic species present in a polymer film.

## 1.2 Overview of Thesis

This thesis contains two additional chapters focused on insights from using spectroscopic methods to understand the nature of carriers in semiconducting polymer systems. The following is a brief summary of each of these chapters as well as a description highlighting how this original work contributed to the field.

### 1.2.1 Chapter 2: Ultrafast Transient Absorption Spectroscopy of Doped P3HT Films: Distinguishing Free and Trapped Polarons

In this chapter, we demonstrate that ultrafast transient absorption spectroscopy can disentangle the presence and roles of free and trapped polarons in doped polymer films. It is generally presumed that the vast majority of carriers created by chemical doping of semiconducting polymer films are Coulombically trapped by the counteranion, with only a small fraction that are free and responsible for the increased conductivity essential for organic electronic applications. At higher doping levels, it is also possible for bipolarons to form, which are expected to be less conductive than single polarons. Unfortunately, there is no simple way to distinguish free polarons, trapped polarons and bipolarons from steady-state spectroscopy. Thus, in this work, we use ultrafast transient absorption spectroscopy to study the dynamics of polarons in 2,3,5,6-tetrafluoro-7,7,8,8-tetracyanoquinodimethane ($F_4$TCNQ)-doped films of poly(3-hexylthiophene-2,5-diyl) (P3HT) as a function of dopant concentration and excitation wavelength. When exciting on the red side of the polaron P1 transition, our transient absorption spectra and kinetics match well with what is expected for free 2-D-delocalized polarons; the measurements are not consistent with a recent theory of doped conjugated polymer electronic structure that suggests that the half-filled state lies deeper in the conduction band rather than in the bandgap. As we tune the excitation wavelength to the blue, our measurements reveal an increasing amount of slower transient kinetics that are consistent with the presence of Coulombically-trapped polarons rather than bipolarons. Taking advantage of their distinct ultrafast relaxation kinetics as a type of action spectroscopy, we are able to extract the steady-state absorption spectra of free and trapped polarons as a function of dopant concentration. By comparing the results to theoretical models, we determine that in $F_4$TCNQ-doped P3HT films, trapped polarons sit $\sim$0.4 nm away from the anion while free polarons reside between 0.7 and 0.9 nm from the counteranion. Perhaps counterintuitively, the ratio of trapped to free polarons increases at higher doping levels, an observation that is consistent with a plateau in the concentration-dependent conductivity of $F_4$TCNQ-doped P3HT films.

### 1.2.2 Chapter 3: The Effects of Crystallinity on Charge Transport and the Structure of Sequentially-Processed $F_4$TCNQ-doped Conjugated Polymer Films

In this chapter, we explore the driving force behind bipolaron formation in chemically-doped semiconducting polymers. Molecular dopants are often added to semiconducting polymers to improve electrical conductivity. However, the use of such dopants does not always produce mobile charge carriers. We use ultrafast spectroscopy to explore the nature of the carriers created following doping of a conjugated push-pull polymer with both $F_4$TCNQ (2,3,5,6-tetrafluoro-7,7,8,8-tetracyanoquinodimethane) and $FeCl_3$. We show that the low conductivity results from the fact that the charge carriers created by doping are entirely bipolarons and not single polarons, and that transient absorption spectroscopy can readily distinguish the two types of charge carriers. Based on density functional theory calculations, we argue that for push-pull conjugated polymers, the size of the donor push unit determines the relative stabilities of polarons and bipolarons, with larger donor units stabilizing the bipolarons by providing more area for two charges to co-reside.

## References


(1) Deschler, F.; Riedel, D.; Deák, A.; Ecker, B.; Hauff, E. V.; Da, E. Imaging of morphological changes and phase segregation in doped polymeric semiconductors.*Synthetic Metals* **2015**, *199*, 381–387.

(2) Hynynen, J.; Kiefer, D. Influence of crystallinity on the thermoelectric power factor of P3HT vapour-doped with F4TCNQ.*RSC Adv.* **2018**, 1593–1599.

(3) Liang, Z.; Zhang, Y.; Souri, M.; Luo, X.; Boehm, A. M.; Li, R.; Zhang, Y.; Wang, T.; Kim, D.-Y.; Mei, J.; Marder, S. R.; Graham, K. R. Influence of dopant size and electron affinity on the electrical conductivity and thermoelectric properties of a series of conjugated polymers.*Journal of Materials Chemistry A* **2018**, *6*, 16495–16505.

(4) Lim, E.; Peterson, K. A.; Su, G. M.; Chabinyc, M. L. Thermoelectric Properties of Poly(3-hexylthiophene) (P3HT) Doped with 2,3,5,6-Tetrafluoro-7,7,8,8-tetracyanoquinodimethane (F 4 TCNQ) by Vapor-Phase Infiltration.*Chemistry of Materials* **2018**, *30*, 998–1010.

(5) Bredas, J. L.; Street, G. B. Polarons, bipolarons, and solitons in conducting polymers.*Accounts of Chemical Research* **1985**, *18*, 309–315.

(6) Cornil, J.; Brédas, J.-L. Nature of the optical transitions in charged oligothiophenes.*Advanced Materials* **1995**, *7*, 295–297.

(7) Scholes, D. T.; Hawks, S. A.; Yee, P. Y.; Wu, H.; Lindemuth, J. R.; Tolbert, S. H.; Schwartz, B. J. Overcoming Film Quality Issues for Conjugated Polymers Doped with F 4 TCNQ by Solution Sequential Processing: Hall Effect, Structural, and Optical Measurements.*The Journal of Physical Chemistry Letters* **2015**, *6*, 4786–4793.

(8) Scholes, D. T.; Yee, P. Y.; Lindemuth, J. R.; Kang, H.; Onorato, J.; Ghosh, R.; Luscombe, C. K.; Spano, F. C.; Tolbert, S. H.; Schwartz, B. J. The Effects of Crystallinity on Charge Transport and the Structure of Sequentially Processed F 4 TCNQ-Doped Conjugated Polymer Films.*Advanced Functional Materials* **2017**, *27*, 1702654.

(9) Reid, O. G.; Pensack, R. D.; Song, Y.; Scholes, G. D.; Rumbles, G. Charge Photogeneration in Neat Conjugated Polymers.*Chemistry of Materials* **2014**, *26*, 561–575.

(10) Das, S.; Khlyabich, P. P.; Burkhart, B.; Roberts, S. T.; Couderc, E.; Thompson, B. C.; Bradforth, S. E. Quantifying Charge Recombination in Solar Cells Based on Donor–Acceptor P3HT Analogues.*The Journal of Physical Chemistry C* **2014**, *118*, 6650–6660.

(11) Ohkita, H.; Cook, S.; Astuti, Y.; Duffy, W.; Tierney, S.; Zhang, W.; Heeney, M.; McCulloch, I.; Nelson, J.; Bradley, D. D. C.; Durrant, J. R. Charge Carrier Formation in Polythiophene/Fullerene Blend Films Studied by Transient Absorption Spectroscopy.*Journal of the American Chemical Society* **2008**, *130*, 3030–3042.

# CHAPTER 2

# Ultrafast Transient Absorption Spectroscopy of Doped P3HT Films: Distinguishing Free and Trapped Polarons

## 2.1 Introduction

Like all organic semiconductors, conjugated polymers have several disadvantages relative to their inorganic counterparts when it comes to serving as functional electronic materials. The conductivity of conjugated polymers is generally poor, the result of intrinsically low charge mobilities and meager equilibrium carrier densities. As with inorganic materials, the carrier density and mobility can be improved by doping, which places additional charge carriers in the valence or conduction band. For inorganic semiconductors, atomic replacement of just a few parts per billion dopes these materials enough to become effective conductors. In contrast, the density of charge carriers needed to increase the conductivity of conjugated polymers by several orders of magnitude is quite high, and can be on the order of parts per thousand or even parts per hundred.[1–3]

Doping of plastic semiconductors is achieved by either oxidizing (for *p*-type doping) or reducing (for *n*-type doping) the conjugated polymer. The oxidation/reduction of conjugated polymers can be accomplished through a variety of means, including electrochemical doping,[4–6] which uses an applied bias and counterions from an electrolyte, or direct electrical methods, such as gate-doping in a field-effect transistor.[5, 7] To permanently dope polymers, the best approach is chemical doping by adding a molecule to a conjugated polymer that is either a strong electron donor or acceptor, so that ground-state charge transfer reactions occur to produce equilibrium charge carriers.

Of course, conjugated polymers are full of defects (chain ends, oxidized or chemically altered monomers, kink sites, catalyst left over from the synthesis, etc.), that can trap or localize a charge

carrier. Moreover, the low dielectric constant of organic semiconductors allows the carriers created by doping to have strong Coulomb interactions with the dopant counterions, interactions that are largely screened in doped inorganic materials. This means that at low doping concentrations in conjugated polymers, the carriers (also referred to as polarons) created are largely trapped. At higher concentrations, molecular doping is expected to create free carriers that contribute to improved charge transport and thus can be used as charge injection layers for organic-organic interfaces with good connections to organic active layers.[1] Applications of highly-doped semiconducting polymers include spintronics, thermoelectrics, biological sensors as well as OLEDs and polymer-based solar cells. [8–12]

Much of the work studying conjugated polymer doping has focused on the prototypical semiconducting polymer, poly(3-hexylthiophene-2,5-diyl) (P3HT), whose chemical structure is pictured at the top left in Figure 2.1.[1] One of the more common molecular dopants is 2,3,5,6-tetrafluoro-7,7,8,8-tetracyanoquinodimethane (F4TCNQ), whose chemical structure is shown in the upper right of Fig. 2.1. F4TCNQ has its LUMO level at 5.24 eV relative to vacuum, in a position relative to the HOMO/valence band of P3HT at 5.2 eV[13] to allow electrons to be transferred from P3HT to F4TCNQ, creating holes on P3HT.[2] F4TCNQ doping of P3HT dramatically increases the polymer's electrical conductivity by multiple orders of magnitude, although at the highest doping levels explored, the conductivity is observed to plateau with increased dopant loading.[3]

There are two main questions concerning the doping of polymers like P3HT with dopants like F4TCNQ that we will explore in this paper. First is the issue of free versus trapped carriers in molecularly-doped conjugated polymer films. Previous work has estimated that $\sim$95% of the polarons created by F4TCNQ-doping of P3HT at low concentrations remain trapped due to Coulomb binding with the F4TCNQ anion.[2] It is not clear, however, how this number changes with doping concentration or how Coulomb binding changes the spectroscopic and electrical properties of the polarons created by doping. Structural studies suggest that F4TCNQ resides in the lamellar region of P3HT crystallites, causing a reorganization of the P3HT crystal structure; F4TCNQ is also thought to increase order in the amorphous region of P3HT films.[14, 15] Thus, the first main question we address in this paper is: can we use spectroscopic methods to separate the contributions of free and trapped carriers, and in doing so determine where the counterion resides relative to the polarons?

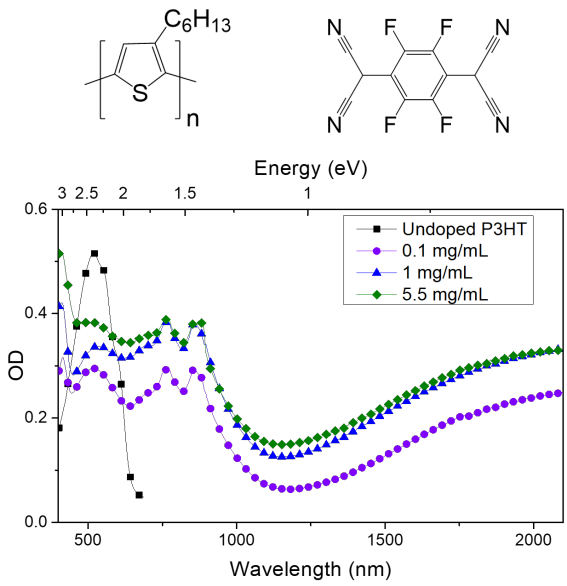


**Figure 2.1: Top Right: Chemical structure of the dopant F4TCNQ (2,3,5,6-tetrafluoro-7,7,8,8-tetracyanoquinodimethane. Top Left: Chemical structure of P3HT (poly(3-hexylthiophene-2,5-diyl). Lower Panel: Steady-state UV-Vis-NIR absorption spectra of: an undoped P3HT film (black squares); an identical P3HT film after sequential doping using a 5.5-mg/mL solution of F4TCNQ in 70:30 THF:DCM (green diamonds); an identical P3HT film sequentially doped with a 1 mg/mL solution of F4TCNQ in DCM (blue triangles); and an identical P3HT film sequentially doped using a solution that was 0.1 mg/mL F4TCNQ in DCM (purple circles).**

The second main issue we address in this work is the electronic nature of the charged carriers created by doping. The standard picture of doping for inorganic semiconductors, which has been extended to doped conjugated polymers, is shown in Figs. 2.2a and b.[16, 17] The electronic structure associated with the polarons, however, can change if the holes pair at high concentrations to form bipolarons (Fig. 2.2c) or if the holes can delocalize to a neighboring P3HT chain as well as along the chain backbone (Fig. 2.2d).[18] Moreover, there are even competing theories as to the intrinsic electronic structure of a polaron, with a recent alternative model that we refer to as the 'band-bending' model, which puts the polaronic states in the valence band rather than the bandgap, shown in Fig. 2.2e.[19–22] All of these different pictures predict different allowed transitions between the different polaronic electronic states. Thus, the second question we will address in this paper is: by studying the ultrafast relaxation dynamics of photoexcited polarons, can we distinguish between the various theoretical scenarios of polaron electronic structure outlined in Fig. 2.2?

To address both of these questions, we performed a series of ultrafast spectroscopy experiments

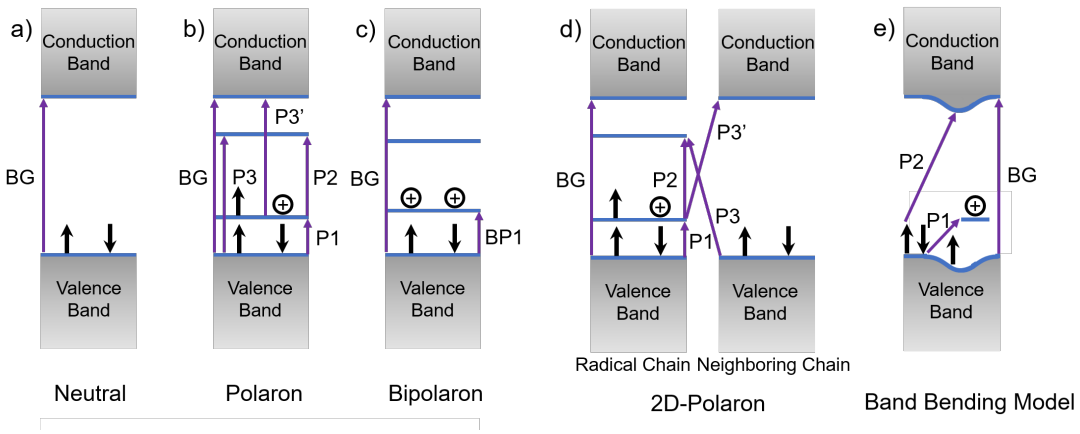


**Figure 2.2: a) The band diagram for neutral semiconducting polymers, which shows only a single optical transition (labeled BG); b) the traditional, longstanding electronic structure model for polarons in semiconducting polymers and their corresponding optical transitions. The P3 and P3′ transitions are usually believed to be optically forbidden; c) the traditional model for bipolarons and their allowed BP1 optical transition; d) the model for 2-D-delocalized polarons, where optical transitions can occur both on the chain containing the majority of the radical cation character as well as diagonally between that chain and a neighboring, predominantly neutral chain. This makes the P3 and P3′ transitions become optically allowed and breaks their degeneracy; e) a new band-bending model for the electronic structure of polarons on conjugated polymers that does not predict that a positively-charged polymer chain is easier to ionize than a neutral polymer chain.[19] There are no bipolarons or P3 or P3′ transitions in this model.**

examining the behavior of photoexcited polarons in F4TCNQ-doped P3HT films. We find clear evidence for two distinct polaron populations with different relaxation dynamics, which we assign to free and Coulombically-trapped polarons. By monitoring how the amplitudes of the two species change as the excitation wavelength is tuned, we are able to disentangle the spectra of the free and trapped polarons in our samples. We find that, perhaps counterintuitively, the number of trapped polarons increases with increasing doping levels, with the trapped polaron spectrum blue-shifting at higher doping concentrations. We also find that based on the features of the transient spectroscopy, there is little evidence for bipolaron formation at high doping levels. Instead, the transient spectroscopy appears to be consistent with that expected for 2-D-delocalized polarons, and not with band-bending models in which the electronic states of hole polarons lie in the valence band rather than the bandgap. Taken together, our results help to build a better understanding of how polarons in doped conjugated polymers contribute to electrical conductivity.

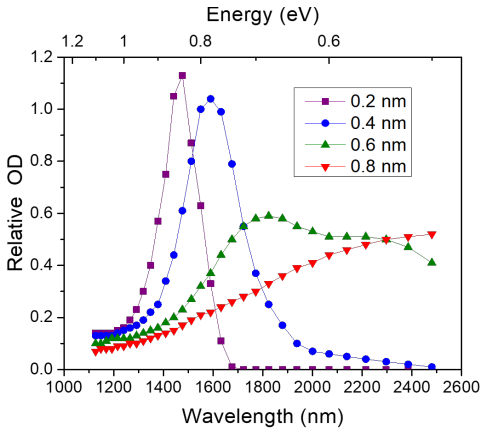


**Figure 2.3: A reproduction of theoretical calculations of the P3HT P1 polaron absorption band as a function of an anion distance from the P3HT chain, taken from Ref. [23]; as the anion distance decreases from 0.8 nm to 0.2 nm, the P1 peak shifts towards smaller wavelengths and narrows significantly.[23] The calculations used a 10-mer of P3HT with a point-charge counteranion situated at the given distance away from the center of the polymer chain, along with a dielectric constant and a Huang-Rhys parameter of 1.0.[23] The vibrational frequency was chosen to be 0.17 eV, the intrachain coupling as $-0.4$ eV, the Gaussian disorder width as 0.3 eV, and the homogeneous linewidth to be 0.03 eV.[23] See Ref. [23] for details.**

## 2.2 Methods

### 2.2.1 Sample Preparation

All of the F4TCNQ-doped P3HT films in this work were prepared via solution sequential processing[3] to ensure high optical quality and control over the doping levels. Briefly, 120-nm thick films of undoped P3HT (purchased commercially from Rieke Metals) were fabricated by spin-coating a 20 mg/mL solution of P3HT in *o*-dichlorobenzene at 1000 rpm for 60 s onto glass substrates. The films were then doped following the solution sequential processing procedure outlined by Scholes *et al.*[3] by spinning solutions of F4TCNQ on top of the pristine P3HT films at 4000 rpm for 10 s. For lower doping levels ($\leq$ 1 mg/mL), the F4TCNQ solutions were prepared in dicholormethane, which is known to swell but not dissolve P3HT, allowing for infiltration of the dopant into the P3HT underlayer. For higher doping levels of 5.5 mg/mL, the F4TCNQ dopant was dissolved in a 70:30 v:v tetrahydrofuran:dichloromethane mixture, with the THF fraction needed to solubilize the higher concentration of dopant. All samples were stored under an inert argon atmosphere at 1 atm and all measurements were taken with the samples in an inert atmosphere within 72 hours of fabrication

to limit any effects from F4TCNQ subliming or other de-doping mechanisms that could affect the sample over time.

### 2.2.2 Transient Absorption Spectroscopy

All of the ultrafast transient absorption experiments were performed using a commercial Ti:sapphire regenerative amplifier (Coherent, Inc.) and a Helios transient absorption spectrometer that together provide ∼75-fs time resolution. The amplified laser system produced pulses of light at 800 nm with ∼3 mJ of energy at a 1 kHz repetition rate. Part of the amplified 800-nm beam was used to pump an optical parametric amplifier, which was used to create ∼10-$\mu$J pulses at 1200, 1500, 1700, or 2000 nm to serve as the pump beam. The other part of the 800-nm pulse was focused into a sapphire plate to generate white light continuum in either the NIR (850 to 1300 nm) or visible regions (450 to 725 nm) to serve as the probe beam. We note that for both the NIR- and visible-probe experiments, scatter from the laser fundamental prevented transient absorption data from being collected in the region near 800 nm. The timing between the pump pulse and the probe pulse was modulated using a double-pass delay stage. Scans were averaged over at least 5 seconds per time point and at least three independent scans were taken.

### 2.2.3 Deconvoluting the Transient Absorption Spectroscopy via Differential Kinetics

To determine the nature of the underlying and overlapping species in the ultrafast transient absorption measurements, we used the matrix decomposition technique Singular Value Decomposition. Singular Value Decomposition, which we applied according to methods elaborated by Doan *et al.*, factorizes a set of data into its significant components.[24] In our application, we took the data to be a function of wavelength on one dimension, and represented time steps, excitation wavelength and dopant concentration on the other dimension. Data was used from delays of 0.3 ps to 20 ps and for probe wavelengths from 500 to 720 nm and 900 to 1120 nm, including excitation of both 1 mg/mL and 5.5 mg/mL samples at 1200 nm, 1500 nm, 1700 nm and 2000 nm.

In our application of SVD, $D$ holds the spectral components of our system, which is calculated from $U$, $S$, and $V$, which come from the Singular Value Decomposition of the data set in wavelength,

excitation wavelength and concentration and time, along with $F$, which is a fitted model of how the measured absorption spectra change in time, excitation wavelength, and concentration:

$$\text{Data} = USV^T = DF^T \tag{2.1}$$

$$D = US(V^T F^{T+}) \tag{2.2}$$

We constructed the model $F$ as a two-column matrix that described independent exponential decays for the two components. One row of $F$ represents the fast component and the other the slow component. $F$ is thus a function of the decay constants $\tau_1$ and $\tau_2$, which correspond to the fast and slow decay components, respectively, as well as the initial relative amplitudes of each component at each excitation wavelength and doping concentration. The columns of $F$ run over time, describing the exponential decay of each component as a function of the initial amplitude of the spectral component and the time constant of its exponential decay.

We started by modeling the transient absorption data following 1200-nm excitation of the 1 mg/mL F4TCNQ-doped P3HT sample. After modeling this transient absorption decay, the matrix $F$ would then be used to map out the decay following 1500-nm excitation, then that at 1700-nm excitation and so forth. This procedure was then repeated for the transient absorption data for different excitation wavelengths on the 5.5 mg/mL F4TCNQ-doped P3HT films. The two spectral components were constrained to have the same shape, regardless of excitation wavelength and doping concentration.

The difference between the transient absorption data and $DF^T$ was minimized using a least squares technique to solve for the ratio of amplitudes, the spectral shape of the components, and the time constants of each component's exponential decay. Our attempts to include a third spectral component did not change the overall fit, as the first two components remained essentially unchanged and the third component had nearly zero amplitude.

Based upon initial fitting, the spectral shape and decay rate of each component were assumed to be constant for each excitation wavelength and the initial amplitude of each component was varied based upon the dopant concentration and excitation wavelength. We also explored several

other models, such as one component decaying into the other or an inverse time dependence for the decay of one component, but none of the alternative models fit the data better, and most of the other models had more fitting parameters than the simple model of two independently-decaying transient species.

Error bars were generated by fixing the ratio of the slow and fast components' starting amplitudes for the corresponding excitation wavelength, and calculating the root-mean-square error of the fit for a particular fitting parameter. The ratio of the root-mean-square error of the constrained fit to the unconstrained fit compared well to an estimate of the general variance of the data constructed by fitting four time-dependent single-probe-wavelength traces for each excitation wavelength and concentration to the simple model and averaging their root-mean-square errors.

## 2.3 Results and Discussion

### 2.3.1 The Electronic Structure of Polarons and Bipolarons in Conjugated Polymer Films

One of the key motivators for the experiments we present here is that the nature of the electronic quasiparticle species present in doped semiconducting polymers has been the subject of debate in the literature.[2, 16, 19, 20, 22, 25] The basic band structure of a neutral conjugated polymer is shown in Fig. 2.2a. When the neutral polymer becomes positively doped, the polymer relaxes from a benzoid to a quinoid structure to stabilize the charge, creating a polaron.[16] In the standard picture, this rearrangement shifts the occupied half-filled state from the valence band into the bandgap and lowers an equivalent state from the bottom of the conduction band, leading to the situation in Fig. 2.2b.[16] Within this picture, doping should lead to three new optical transitions in addition to the original bandgap transition: the P1 transition, which consists of exciting an electron from the valence band to the half-filled state, the P2 transition, which involves exciting the electron in the half-filled state to the other state inside the bandgap, and a degenerate pair of transitions known as P3 and P3$'$, which involve excitation of an electron between the valence band and the empty state or between the half-filled state and the conduction band, respectively.[16]

For an ideal, doped single conjugated polymer chain, the P3 and P3$'$ transitions are optically

forbidden, but in a disordered system or a material in which there is partial delocalization of the polarons between neighboring polymer chains (so-called 2-D delocalization), one or both of these transitions may be observable.[18, 25] In this 2-D delocalization picture, shown in Fig. 2.2d, one polymer chain carries most of the radical cation character, but there can be optical transitions involving electrons to or from neighboring chains.[18] When this happens, the P3 and P3′ transitions become symmetry-allowed and the P2 transition is expected to become more optically forbidden.[18] In addition, with 2-D-delocalization the P3 and P3′ transitions are no longer required to be degenerate in energy.

At high doping levels, it is possible that polarons on conjugated polymers can pair, forming bipolarons. This is because it can be energetically less costly to put two like charges near each other than to distort the backbone of the conjugated polymer in two separate locations.[16] Bipolaron formation is particularly likely when the concentration of dopants is so high that the delocalization of polarons becomes limited by the total concentration of carriers.[16] Figure 2.2c shows the standard electronic structure picture for bipolaron formation, in which there are two empty states within the bandgap, with the only optically-allowed transition going from the valence band to the lower-energy empty intragap state, termed the BP1 transition.[16, 26, 27]

Recently, however, several groups have proposed a new electronic structure scheme to explain polaron formation in doped conjugated polymers.[19, 20] The new scheme, which is summarized in Fig. 2.2e, was motivated by the physical idea that it should be harder to ionize a positively-doped conjugated polymer chain than a neutral chain; the standard picture predicts that the half-filled polaronic state is closer to the vacuum level than the valence band.[19] In this new 'band-bending' model, which is based on density functional theory calculations, when a polaron forms, the state from which the electron was removed splits in half. After the state splits, a half-occupancy state containing the remaining electron bends below the bandgap into the valence band and the half-filled state containing the hole rises into the gap. The conduction band then bends down locally with the hole, forming another state that projects into the gap. The P1 transition would then result from promotion of an electron from the valence band to the intergap state and the P2 transition would arise when as valence band electron is promoted to the lowered part of the bent conduction band. Rather than being optically forbidden, there are no P3 or P3′ transitions in the band-bending model.[19,

20] The band-bending model also provides no obvious mechanism for bipolaron formation.[19]

When a polaron is in close spatial proximity to its counteranion, the polaron can localize and become trapped in the Coulomb well of the counteranion.[2, 28] Both experimental and theoretical work indicates that trapped polarons have a blue-shifted P1 peak due to their decreased delocalization and the presence of the Coulomb well.[23, 29–31] Spano and his co-workers have pioneered calculations of polaron localization and trapping as a function of the distance of a counteranion from the doped polymer chain. These calculations show a clear shift to smaller wavelengths as well as a change in shape of the absorption band as the counteranion moves closer to the polaron, as shown in Figure 2.3.[23] Of course, there may be an inhomogeneous distribution of free and weakly or more deeply trapped polarons in any given conjugated polymer film, but it is clear that polarons can absorb in different spectral regions depending on their degree of delocalization, which is directly related to their proximity to a dopant counterion.

Overall, there is still a great deal of complexity and controversy when it comes to describing polaronic states in conjugated polymers. There are multiple different pictures of the electronic structure of polarons, including the possibilities of traditional polarons, 2-D delocalized polarons and the new band-bending picture of polaron electronic structure. When this is combined with the fact that most polarons in chemically-doped conjugated polymer films are thought to be Coulombically trapped rather than freely mobile, it is simply not at all clear how to best interpret the spectroscopy of doped conjugated polymer films. Our goal in this paper is to elucidate the spectroscopy of doped conjugated polymers by performing the ultrafast transient absorption experiments: as we will see below, the shape of the excited-state absorption spectrum will tell us about polaron electronic structure, and the dynamics will tell us about the degree of Coulombic polaron trapping.

### 2.3.2 The Steady-State Spectroscopy of F4TCNQ-Doped P3HT Films

We begin our study of the electronic structure of doped conjugated polymers in Fig. 2.1, which shows the steady-state optical absorption spectra of a neutral P3HT film (black squares) and P3HT films doped via sequential processing[3, 32] with increasing concentrations of F4TCNQ (purple circles, blue triangles and green diamonds). The figure shows clearly that as neutral P3HT becomes

doped, the absorption associated with the bandgap transition at 525 nm decreases in intensity, while new absorbing features grow in at 400, 700, 780, 880 and 2400 nm. All of these features have been observed in previous work and their assignments are well understood.[33–36] The peak near 2400 nm is assigned to the low-energy P1 transition of polarons on the doped P3HT. The new peaks that appear at 700, 780, and 880 nm are vibronic structure associated with the F4TCNQ anion, and the new peak at 400 nm is associated with neutral F4TCNQ.[33] We also expect that much of the absorption in the 650–900 nm region is the result of a P2 transition (and possibly P3 and/or P3′ transitions) that lie underneath the F4TCNQ anion absorption in this region.

Figure 2.1 also shows that as the dopant concentration increases from 0.1 mg/mL to 1.0 mg/mL, the intensity of the doped P3HT P1 and P2/F4TCNQ anion absorption peaks increases. As the dopant concentration is further increased to 5.5 mg/mL, however, there is no further increase in the absorption intensity of these peaks; instead, a shoulder appears on the high-energy side of the broad P1 band in the region between 1200 and 1500 nm. This new absorption feature could be consistent with that expected for the BP1 transition of bipolarons that form at high dopant concentrations,[16] but it also is potentially consistent with the P1 transition of single polarons that are Coulombically localized by their counterions.[14]

### 2.3.3 Connection Between the Electronic Structure and Expected Ultrafast Dynamics of Doped Conjugated Polymer Films

To better understand the spectral changes that take place upon doping P3HT with different concentrations of F4TCNQ, we performed a series of pump/probe transient absorption experiments. Most groups have used three-pulse pump-probe experiments to study polarons, in which a first laser pulse is used to create a polaron, a second, time-delayed pulse excites the polaronic species, and then a third pulse probes the resulting spectral dynamics.[37–41] These experiments suffer from being unable to cleanly excite polarons with the second laser pulse because of spectral congestion from other excited-state species (excitons, triplets, etc.).[37, 42–44] Here, we excite already-formed polarons in our F4TCNQ-doped P3HT films, avoiding spectral congestion. Our idea was to perform one set of experiments exciting the low-energy P1 peak near 2400 nm (0.5 eV), and a second set

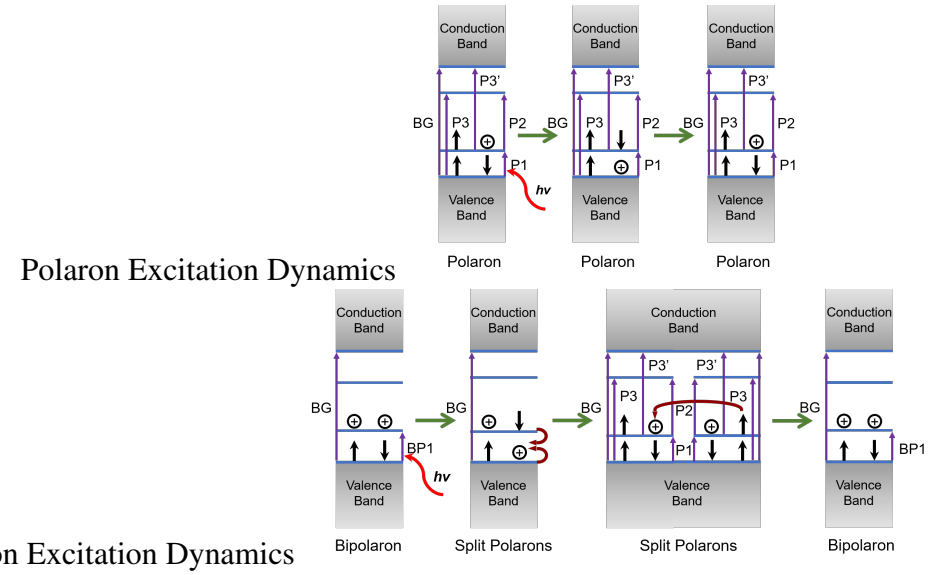


**Figure 2.4: Band diagrams explaining the dynamics expected following photoexcitation of polarons (top) and bipolarons (bottom) in the traditional conjugated polymer electronic structure picture; time flows from left to right. Following excitation of the low-energy polaron P1 transition, an electron is removed from the valence band and used to fill the pre-existing hole, creating a half-filled lower state and a filled P1 state. After rapid relaxation around the new hole, the system returns to the original ground-state polaron configuration. In contrast, when the BP1 transition of bipolarons is excited, an electron is taken from the valence band and used to fill one of the two holes, creating two single polarons in half-filled orbitals in different locations in the film. After any fast relaxation processes are complete, the two separated polarons must diffuse back together to reform the equilibrium bipolaron state, a process that is expected to occur on longer timescales.**

of experiments exciting at wavelengths further to the blue to learn more about the nature of the absorbing species that gives rise to the blue shoulder at higher doping concentrations.

Figure 2.4 shows roughly what can be expected in our pump/probe experiments based on the traditional model for the electronic structure of polarons and bipolarons in conjugated polymers,[16] with time flowing from left to right. For the case of polarons, shown in the upper part of the figure, exciting the low-energy P1 transition should bleach both the P1 peak and the neutral bandgap absorption since an electron is removed from the valence band. The addition of a second electron in the intra-gap state should also lead to an increase in absorption of the P2 peak. In this picture, one can think of exciting the P1 band as taking an electron from the valence band and using to fill the pre-existing polaronic hole, leaving a new hole somewhere else in the material; in other words, the P1 transition is essentially a charge-transfer band for moving the hole polaron from one place in the polymer to another. Once the polymer backbone relaxes around the new hole, which should

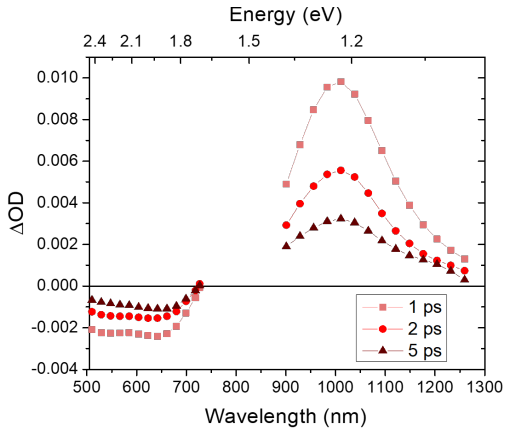


**Figure 2.5: Ultrafast transient absorption spectra of P3HT films sequentially doped with a 1 mg/mL F4TCNQ solution in DCM following excitation at 2000 nm; spectra are shown at delays of 1, 2, and 5 ps between excitation and collection. The data show two bleaches in the visible region, at 520 nm and 650 nm, and one broad transient absorption in the visible region near 1000 nm, which we assign to the bleach of neutral P3HT, the bleach of the P3 transition, and an increase of the P2 transition in the 2-D-delocalized polaron picture, respectively (*cf.* Fig. 2d).**

take place relatively quickly, the electronic states will rearrange to recover the initial electronic configuration and thus the equilibrium absorption spectrum.

If we extend these ideas to the case of 2-D-delocalized polarons, in addition to all of the aforementioned changes in absorption, we would expect that exciting the P1 band of the polaron would also bleach the now-allowed P3 transition and cause a corresponding increase in absorption intensity for the P3′ transition. If the P3 and P3′ transitions are degenerate, then there would be no net change in absorbance at the P3 transition energy, but if the degeneracy is broken, this could produce an additional transient absorption signature.

This picture could change even further in the case of trapped polarons, where the P1 transition will occur at higher energy, and the positions of the P2, P3, and P3′ peaks all will shift depending on how Coulomb trapping affects the corresponding energy levels. In the band-bending model of polaron electronic structure, the picture would be modified yet again, as exciting the P1 polaron band should temporarily bleach the P1, P2 and neutral bandgap transitions and there are no P3 or P3′ transitions to potentially bleach or increase in absorption intensity.

Finally, the lower part of Figure 2.4 shows our expectations following excitation of the BP1 band of bipolarons. Here, one can think of the BP1 band as a charge-transfer transition that takes

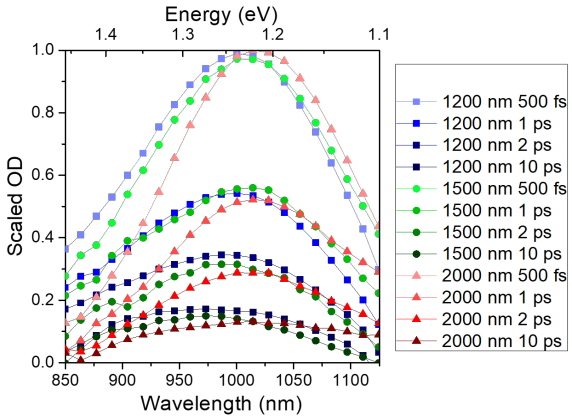


**Figure 2.6: Ultrafast transient absorption spectra of a P3HT film sequentially doped with a 1 mg/mL F4TCNQ solution in DCM following excitation at either 1200 nm (blue squares), 1500 nm (green circles) or 2000 nm (red triangles). Data are shown at 0.5, 1, 2, and 10 ps delays between excitation and collection, with darker colors used for later delay times. The observed transient absorption feature shifts to the blue, with the blue feature decaying more slowly, as the excitation wavelength is tuned to the blue.**

an electron from the valence band and moves it to fill one of the two original paired holes. This effectively dissociates the bipolaron into two single polarons, one of which remains in the original bipolaron location and the other of which appears somewhere else. Following excitation of the BP1 band, we expect both the BP1 and neutral bandgap transitions to be bleached by removal of the electron from the valence band. The two polaron-like states created will have new P1- and P2-like absorptions, and depending on the degree of delocalization between neighboring chains, there also could be new P3 and P3′ absorption transitions. As time progresses, the split single polarons will diffuse until they ultimately recombine back into an equilibrium bipolaron. Currently, there are no predictions regarding how bipolaron states might be affected upon excitation for the band-bending model.[19, 20]

### 2.3.4 Pump-Probe Transient Absorption Spectroscopy of F4TCNQ-Doped P3HT

To understand the nature of the steady-state optical absorption spectrum of F4TCNQ-doped P3HT shown in Fig. 2.1, we started by performing pump/probe experiments exciting near the peak of the P1 transition. Figure 2.5 shows that when exciting the 1 mg/mL F4TCNQ-doped P3HT film at 2000 nm, there is a bleach of the P3HT neutral bandgap transition at 525 nm (2.4 eV), a second bleach

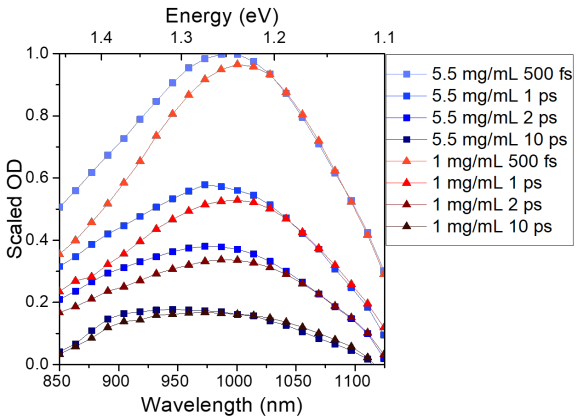


**Figure 2.7: Ultrafast transient absorption spectra of P3HT films that have been sequentially doped either with a 1 mg/mL solution of F4TCNQ in DCM (red triangles) or a 5.5 mg/mL solution of F4TCNQ in a 70:30 v:v mixture of THF:DCM (blue squares) following excitation at 1200 nm. Data are shown for 0.5, 1, 2, and 10 ps delays between excitation and collection, with darker colors corresponding to later delay times. The more highly-doped samples have the transient absorption shifted to the blue and the blue feature decaying more slowly than the lower-doped sample.**

that appears near 650 nm (1.9 eV), and a new, broad transient absorption that appears near 1000 nm (1.24 eV). The transient bleaches and absorption all decay at similar rates, suggesting that they all arise from the same electronic species.

These transient spectral signatures are not consistent with what is expected from the traditional polaron model outlined at the top of Fig. 2.4. In this picture, we would expect bleaching of the bandgap transition at 525 nm and an increase in absorption of the P2 transition near 1000 nm, but there is no way to explain the bleach that appears near 650 nm, below the bandgap of neutral P3HT. Instead, the data in Fig. 2.5 are consistent with the photoexcitation of 2-D delocalized polarons, with the 1000-nm transient absorption corresponding to the expected increase in the P2 transition and the 650-nm bleach corresponding to removal of the partially-allowed P3 transition. We might also expect 2-D delocalized polarons to show an increase in absorption due to the P3$'$ transition, but this is likely obscured by scatter from the laser fundamental at 800 nm (or possibly has significant overlap with the P3 and/or P2 bands). It is also worth noting that the bleach of the P3 transition at 650 nm is not consistent either with the photoexcitation of bipolarons, which would show increased absorption at this wavelength, or with the band-bending model, which does not predict any P3 or P3$'$ transitions.[19, 20]

With the basic features of the ultrafast transient spectroscopy of polarons on P3HT established, we turn next to identifying the nature of the species that contributes to blue shoulder of the P1 band seen for P3HT at higher doping concentrations in Fig. 2.1. To this end, we repeated the experiment using a series of different excitation wavelengths spanning the range from 1200 to 2000 nm; the results for three such wavelengths are shown in Fig. 2.6. As we tune the excitation wavelength to the blue, we see clear shifts in the P2 transient absorption of P3HT that peaks near 1000 nm. In particular, the higher the energy of the excitation wavelength, the more blue-shifted the peak of the resulting P2 transient absorption. Moreover, higher-energy excitation also leads to a broadening on the blue side of the P2 transient absorption signature. But most importantly, the data in Fig. 2.6 show that transient absorption no longer decays uniformly with time: the blue side of the transient absorption that is enhanced when exciting further to the blue decays more slowly than the peak of the transient absorption band. All of these observations indicate that bluer excitation wavelengths are indeed accessing a new electronic species that was not significantly excited at 2000 nm.

To better understand the origin of the new electronic species, we also repeated our ultrafast transient absorption experiments on P3HT films as a function of dopant concentration. Figure 2.7 shows the results when the bluest wavelength, 1200 nm, is used to excite P3HT films sequentially doped with F4TCNQ at concentrations of 1 mg/mL (red-colored curves) and 5.5 mg/mL (blue-colored curves). The data show that as the doping concentration is increased, the transient absorption spectrum shifts to the blue and shows a broadening on the blue side, similar to what is seen when using higher-energy excitation. Moreover, also like what we saw above, the blue portion of the transient absorption spectrum decays more slowly than the peak. Thus, whatever the new electronic species is, its presence is manifest both when exciting at higher energies and when the doping concentration is increased.

### 2.3.5 Analysis of the Ultrafast Transient Absorption Spectra of F4TCNQ-Doped P3HT Films

To elucidate the nature of the second electronic species that is excited more at 1200 nm than 2000 nm and is more prevalent in P3HT films doped with F4TCNQ at 5.5 mg/mL than at 1 mg/mL

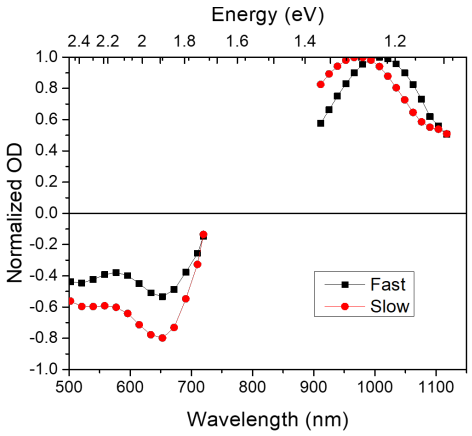


**Figure 2.8: The two spectral components extracted using SVD from our global fits to the transient absorption spectra of P3HT films sequentially doped with several different concentration solutions of F4TCNQ and excited at multiple wavelengths. The more slowly-decaying component (red circles) has a ∼15 ps lifetime while the faster decaying component (black squares) has a 0.37 ps lifetime. Both components have two clear negative peaks in the visible region, at 530 nm and 650 nm, corresponding to bleaches of the BG and P3′ transitions. The slow component, which we assign to trapped polarons, shows a blue-shifted P2 peak in the NIR and more intense bleaching in the visible region relative to that of the fast component, which we assign to free polarons.**

doping level, we globally analyzed our transient absorption data across excitation wavelength and doping concentration. For our global analysis, we assumed a model in which there are precisely two species excited in the doped films. Each species in the model has a different absorbance at each excitation wavelength, is present in different amounts at different doping concentrations, and each has its own transient absorption spectrum and decay rate. We then used SVD, as described above, to extract the transient absorption spectra and decay times of each of the two species.

With the SVD procedure applied globally to all of our transient absorption data for the 1 and 5.5 mg/mL-doped samples (not just the subset of data shown in Figs. 2.5-2.7), we found that indeed SVD yielded a quickly-decaying (lifetime of ∼0.37 ps), red-shifted transient absorption component with a larger initial amplitude and a more slowly-decaying (lifetime of ∼15 ps), blue-shifted transient absorption component with a lower initial amplitude. The spectra of the two components are shown in Fig. 2.8. Based on their shapes, it makes sense to assign both of the spectral components as arising from what would be expected following photoexcitation of a 2-D-delocalized polaron, with a bleach of the bandgap and P3 transitions and the transient appearance of P2 and P3′ peaks. Our hypothesis is thus that the two species can be assigned to free and Coulombically-trapped 2-D-delocalized

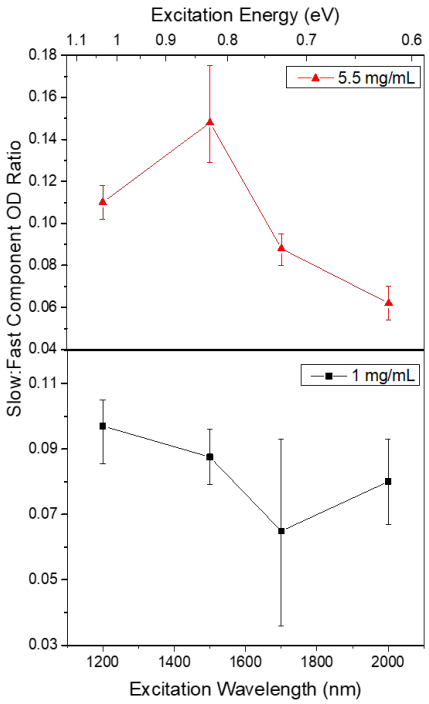


**Figure 2.9: The ratio of the initial optical densities of the extracted slow to fast components from the global fit of the transient absorption measurements as a function of excitation wavelength for: a) a P3HT film sequentially doped with a 5.5 mg/mL F4TCNQ solution, and b) a P3HT film sequentially doped with a 1 mg/mL F4TCNQ solution. It is clear that there is more of the slow component produced using 1200 and 1500 nm excitation wavelengths, particularly for the more highly-doped sample.**

polarons: the species with the redder transient absorption spectrum and faster decay corresponds to that from free polarons, while the species with the blue-shifted transient absorption spectrum and slower recovery corresponds to trapped polarons.

To better characterize the SVD components, we fit each of the two SVD components that describe the transient spectroscopy to a sum of four Gaussian peaks, with the idea that each Gaussian peak reflects one of the expected transient 2-D-delocalized polaron transitions. Both the slow- and the fast-decaying spectral components, which we assign to trapped and free polarons, have two negative Gaussian peaks in the visible region, corresponding to the bleaches of bandgap and P3 transitions. Both transient spectra also have two positive Gaussian peaks, corresponding to newly-created P3′ and P2 absorptions. The Gaussian fitting parameters for both transient species are summarized in Table 2.1.

The Gaussian fits to the two SVD spectral components summarized in Table 2.1 make sense

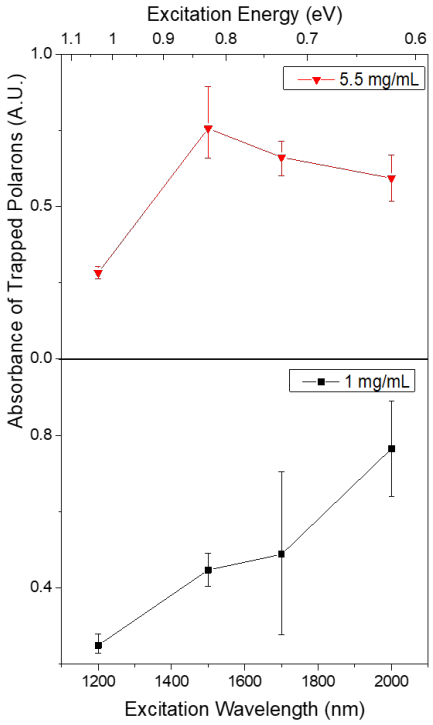


**Figure 2.10: The calculated action spectrum of trapped polarons for: a) a P3HT film sequentially doped with a 5.5 mg/mL F4TCNQ solution, and b) a P3HT film sequentially doped with a 1 mg/mL F4TCNQ solution. This spectrum was calculated by scaling the measured ratios of the slow to fast components in Fig. 2.9 by the absorption of a P3HT films sequentially doped with a 0.1 mg/mL F4TCNQ solution, which we expect has few trapped polarons. The data make clear that the more highly-doped sample has trapped polarons with a more blue-shifted absorption spectrum, indicating that these polarons are more highly trapped than those in the lower-doped sample.**

in terms our assignment of these as transitions arising from excited 2-D-delocalized polarons. As seen in Fig. 2.2d, the energy of the P2 transition plus twice the energy of the P1 transition should equal the optical bandgap energy, as should the sum of P3 and P3′ transition energies minus the P2 transition energy. In both cases, the energies of the fitted Gaussian peaks sum to within ∼0.1 eV of the known ∼2.2-eV bandgap of P3HT.[45]

With this assignment of the two transient species as arising from free and trapped polarons, the ∼0.37 and ∼15 ps time constants we observe imply that photoexcited free polarons in P3HT recover roughly forty times faster than the trapped polarons. This makes sense given what we expect from the standard 2-D-delocalized polaron picture. For free polarons, photoexcitation relocalizes the polaron and the system recovers to equilibrium as soon as the polymer backbone can relax to accommodate the hole in its new location, a process that can easily happen on sub-ps time scales.

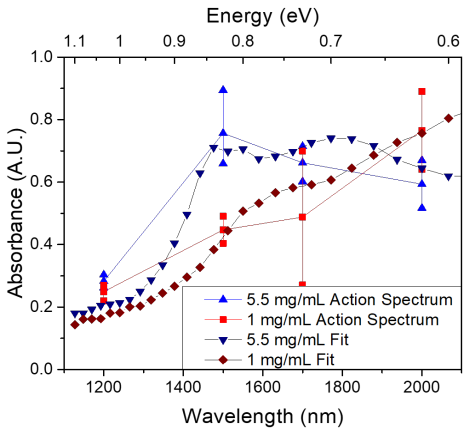


**Figure 2.11: The action spectra of trapped polarons from Fig. 2.10 fit to linear combinations of the anion-distance-dependent P1 spectra calculated by Spano and co-workers shown in Fig. 2.3.[23] The 5.5 mg/mL F4TCNQ-doped P3HT film (blue triangles) fits best to a sum of the theoretical spectra with anion distances calculated for 0.2, 0.4, and 0.6 nm spacing between the anion and the polymer chain with 20, 7, and 73% relative weightings, respectively. The 1 mg/mL F4TCNQ-doped P3HT film (red squares) fits best to a sum of the spectra for anion distances calculated for 0.4, 0.6, and 0.8 nm spacing between the anion and the polymer chain with 6, 4 and 90% relative weightings, respectively.**

For Coulombically-trapped polarons, it is reasonable to expect that the excited-state absorption is slightly blue-shifted from that of free polarons, much like the ground-state absorption spectra of free and trapped polarons shown above in Fig. 2.3. Moreover, we expect that photoexcitation of Coulombically-bound polarons likely moves the hole away from the trap site, to where it must diffuse back to recover to equilibrium. Since diffusion is a much slower process (and since we expect polarons near traps to have lower mobilities than their free counterparts), it is not surprising that the excited-state recovery of trapped polarons is more than an order of magnitude slower than that of free polarons.

We turn next turned to exploring the relative amplitudes of the free and trapped polaron transient absorptions at each excitation wavelength and both doping levels. Figure 2.9 shows the ratio of the slow (trapped) to fast (free) polaron components as a function of excitation wavelength for the 5.5-mg/mL-doped sample (upper panel) and the 1-mg/mL-doped sample (lower panel). The figure makes clear that more of the slow transient absorption component is excited near 1400 nm than at other wavelengths, particularly in the 5.5-mg/mL-doped sample. This fits perfectly with our expectation that trapped polarons absorb to the blue of free polarons, and that the blue shoulder observed on the P1 band of the 5.5-mg/mL-doped sample (Fig. 2.1) is indeed due to the presence of

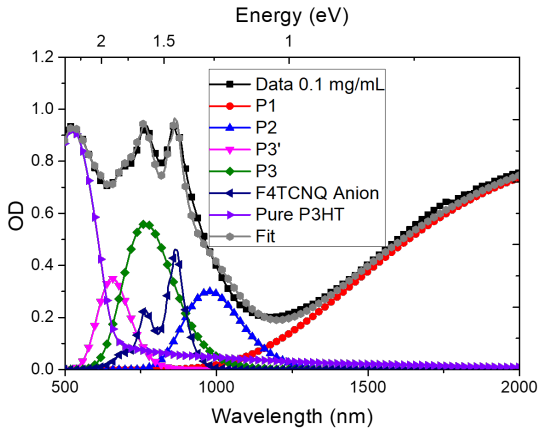


**Figure 2.12: Reconstruction of the absorption spectrum of a P3HT film sequentially doped with a 0.1 mg/mL solution of F4TCNQ in DCM using a linear combination of the known F4TCNQ anion spectra (taken from Wang *et al.*),[33] the known spectrum of neutral P3HT (Fig. 2.1), and the Gaussian fits of the peak positions of the fast component (which we assign to free polarons) extracted from the global model of our transient absorption measurements (Table 2.1); see text for details. The excellent agreement between the measured spectrum and the reconstructed fit shows that our transient absorption measurements, global fit, and steady-state absorption measurements are all internally consistent.**

an increased number of trapped polarons. The fact that many of the polarons added at high doping concentrations are trapped fits well with the observation that doping at this level does not improve the overall film conductivity.[3, 14]

Given our assignment of the two transient absorption species to free and trapped 2-D-delocalized polarons, one important question that needs to be addressed is why does the number of trapped polarons appear to increase at higher doping concentrations? Previous work has shown that when P3HT is doped by F4TCNQ at low concentrations, the dopant intercalates into the lamellar regions of the P3HT crystallites, leading to a reorientation of the P3HT crystalline unit cell.[14, 46–48] Because the F4TCNQ anion sits in the lamellar region, it lies relatively far from the P3HT backbone where the polaron resides, thus minimizing the Coulomb interaction between them. Once the crystalline reorganization is complete, there is no room for additional dopant in the P3HT crystallites, so at high doping concentrations F4TCNQ is forced to reside in the amorphous regions of the P3HT films. We speculate that when the anion is in the amorphous regions of the film, it can sit closer to the polymer backbone, thus increasing the Coulomb attraction and the degree of polaron trapping.

We also can analyze the relative amplitudes of free and trapped polarons in Fig. 2.9 in another

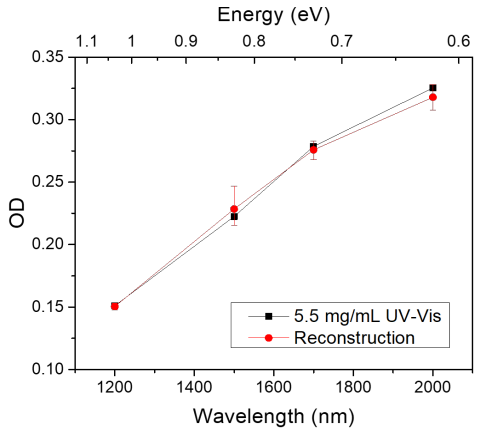


**Figure 2.13: Reconstruction of the absorption spectrum of a highly-doped P3HT film (created using a 5.5 mg/mL solution of F4TCNQ). The reconstructed spectrum uses the spectrum of a low-doped P3HT film (created using an 0.1 mg/mL F4TCNQ solution) and the action spectrum of trapped polarons that we extracted from the ultrafast transient absorption data in Fig. 2.10; see text for details. The excellent agreement provides confirmation that the action spectrum taken from our ultrafast measurements can be used to account for the spectral shape changes observed between the high- and low-doped P3HT films seen in Fig. 2.1.**

way. If we follow the logic in the preceding paragraph, we can assume that the 0.1-mg/mL-doped P3HT sample has a negligible amount of trapped polarons. This means that the P1 band of this film is largely that of free polarons. If we then scale our measured ratio of trapped-to-free polarons by the 0.1-mg/mL-doped film absorption spectrum, we can obtain the absorption spectrum of the trapped polarons in the higher-doped P3HT films. These spectra, which are one of the principal results of this work, are shown in Fig. 2.10. Essentially, these are reconstructed action spectra of the slow transient absorption component that we assign to the presence of trapped polarons.

The data in Fig. 2.10 make clear that the spectrum of trapped polarons is different at different doping concentrations. If we compare our extracted trapped polaron action spectra to what is expected from theory (Fig. 2.3, above),[14, 23, 29] we can estimate the average distance the polaron lies from its counterion at each doping concentration. We accomplished this by using a least squares regression to fit our measured action spectra of the trapped polaron in P3HT films doped with different F4TCNQ concentrations to a weighted sum of the simulated polaron spectra for varying anion distances,[23] as shown in Fig. 2.11. We conclude that the 'free' polarons in 0.1-mg/mL-F4TCNQ-doped P3HT films are still somewhat Coulombically bound by their counterions, with an average polaron-to-anion distance of 0.7 to 0.9 nm, consistent with the idea that the dopant

**Table 2.1: Fitted Gaussian peak locations for the free and trapped polaron spectral components**

| Assignment | Wavelength nm | Energy eV | Amplitude | Width eV |
|---|---|---|---|---|
| **Free Polarons** | | | | |
| Neutral | 517 | 2.40 | -0.45 | 0.22 |
| P3′ | 658 | 1.89 | -0.52 | 0.16 |
| P3 | 765 | 1.62 | 0.12 | 0.17 |
| P2 | 1000 | 1.24 | 1 | 0.11 |
| P1 | 2400 | 0.52 | N/A | N/A |
| **Trapped Polarons** | | | | |
| Neutral | 519 | 2.39 | -0.60 | 0.22 |
| P3′ | 670 | 1.85 | -0.86 | 0.19 |
| P3 | 742 | 1.67 | 0.48 | 0.12 |
| P2 | 969 | 1.28 | 1 | 0.11 |
| P1 | 1500 | 0.83 | N/A | N/A |

counterions sit in the lamellar regions of the P3HT crystallites. We also see that the distance between the trapped polarons in the 5.5-mg/mL-doped P3HT films and their F4TCNQ counteranions is 0.2 nm to 0.6 nm, and the corresponding distance in the 1-mg/mL-doped films is 0.4 to 0.8 nm. This also fits well with our idea that at increased dopant concentrations, the dopant sits in the amorphous region of the film where it can reside closer, on average, to the polarons on the P3HT backbone.

As a check on the validity of our assignments of the peaks observed in the transient spectroscopy, we worked to reconstruct the 0.1 mg/mL UV-Vis spectrum (Figure 2.1), which should result almost entirely from free polarons, by using the fitted peak positions and widths of the fast transient spectral component (Table 2.1), along with the known spectra of neutral P3HT and anionic F4TCNQ. The results, which also make use of a single Gaussian to represent the P1 absorption band, are shown in Fig. 2.12. Clearly, our ability to fit the steady-state UV-Visible absorption spectrum with only amplitudes as adjustable parameters is excellent. This lends credence to the idea that there are indeed 2-D-delocalized P3, P3′ and P2 transitions lying under the sharp F4TCNQ anion peaks in the UV-Vis of doped P3HT.

Finally, we are also able to check our understanding of the various polaronic transitions by working to reproduce the steady-state absorption spectrum of the 5.5 mg/mL-F4TCNQ-doped P3HT sample using the trapped polaron action spectrum extracted from our ultrafast spectroscopic analysis. Here, we started with the 0.1 mg/mL-doped-P3HT steady-state spectrum, and added additional absorption from the action spectrum for trapped polarons that we extracted from the slow transient absorption component. Figure 2.13 shows that again, the results are excellent. Thus, the spectra of trapped polarons that we extracted from our ultrafast spectroscopy experiments are indeed internally-consistent with the measured steady-state spectra at each doping level.

## 2.4 Conclusions

In this paper we have found strong evidence for two populations of quasiparticles present in F4TCNQ-doped P3HT. The transient spectroscopy is consistent with F4TCNQ-doped P3HT consisting primarily of free and trapped polarons, both of which follow the traditional model for 2-D-delocalized polarons in terms of their observed absorption transitions. Neither the band-bending picture of polarons nor the presence of bipolarons accounts for the observed bleaches in our transient absorption measurements. We were able to distinguish free and trapped polarons by monitoring both the position and dynamics of their transient spectra: trapped polarons show blue-shifted features that decay more than an order of magnitude more slowly than free polarons, a direct result of their need to diffuse to return to equilibrium and their generally poor mobility.

By monitoring the relative amounts of free and trapped polarons produced at different excitation wavelengths, we were able to generate an action spectrum to disentangle the steady-state absorption of the two polaronic species. We found that the more highly-doped samples had greater amounts of polarons that were more tightly bound by their counterions. By comparing the action spectra of trapped polarons to theory, we found that the F4TCNQ dopant resides roughly 0.4 nm away from trapped polarons, compared to 0.7 to 0.9 nm for free polarons. For an F4TCNQ anion to be that close to a trapped polaron, it likely must pi-stack with the P3HT backbone, presumably in the amorphous regions of the film.

With an internally-consistent view of the electronic structure of free and trapped polarons in

place, it may now be possible to design new materials to improve carrier mobility by decreasing the fraction of trapped polarons. For example, the use of dopants whose anions are electrostatically shielded from their corresponding holes provides a possible route to preventing the build-up of trapped polarons at high doping levels.[49, 50] Another possibility would be to engineer the crystal structure of a polymer to better accommodate counterions into the lattice in positions far from the backbone, so that more dopants can be accommodated without having to produce significant numbers of trapped polarons. The hope is that with our new understanding, it should be possible to create new materials that do not suffer from increased polaron trapping at high doping concentrations.

## References


(1) Deschler, F.; Riedel, D.; Deák, A.; Ecker, B.; Hauff, E. V.; Da, E. Imaging of morphological changes and phase segregation in doped polymeric semiconductors.*Synthetic Metals* **2015**, *199*, 381–387.

(2) Pingel, P.; Neher, D. Comprehensive picture of P -type doping of P3HT with the molecular acceptor F4TCNQ.*Physical Review B* **2013**, *87*, 115209.

(3) Scholes, D. T.; Hawks, S. A.; Yee, P. Y.; Wu, H.; Lindemuth, J. R.; Tolbert, S. H.; Schwartz, B. J. Overcoming Film Quality Issues for Conjugated Polymers Doped with F 4 TCNQ by Solution Sequential Processing: Hall Effect, Structural, and Optical Measurements.*The Journal of Physical Chemistry Letters* **2015**, *6*, 4786–4793.

(4) Francis, C.; Fazzi, D.; Grimm, S. B.; Paulus, F.; Beck, S.; Hillebrandt, S.; Pucci, A.; Zaumseil, J. Raman spectroscopy and microscopy of electrochemically and chemically doped high-mobility semiconducting polymers.*Journal of Materials Chemistry C* **2017**, *5*, 6176–6184.

(5) Lim, E.; Peterson, K. A.; Su, G. M.; Chabinyc, M. L. Thermoelectric Properties of Poly(3-hexylthiophene) (P3HT) Doped with 2,3,5,6-Tetrafluoro-7,7,8,8-tetracyanoquinodimethane (F 4 TCNQ) by Vapor-Phase Infiltration.*Chemistry of Materials* **2018**, *30*, 998–1010.

(6) Enengl, C.; Enengl, S.; Pluczyk, S.; Havlicek, M.; Lapkowski, M.; Neugebauer, H.; Ehrenfreund, E. Doping Induced Absorption Bands in P3HT: Polarons and Bipolarons.*ChemPhysChem* **2016**, *56*, 607–622.

(7) Yamamoto, J.; Furukawa, Y. Raman characterization and electrical properties of poly(3-hexylthiophene) doped electrochemically in an ionic liquid-gated transistor geometry.*Organic Electronics* **2016**, *28*, 82–87.

(8) Cox, M.; van der Heijden, E. H. M.; Janssen, P.; Koopmans, B. Investigating the influence of traps on organic magnetoresistance by molecular doping.*Physical Review B* **2014**, *89*, 085201.

(9) Yang, S. Y.; Kim, B. N.; Zakhidov, A. A.; Taylor, P. G.; Lee, J. K.; Ober, C. K.; Lindau, M.; Malliaras, G. G. Detection of transmitter release from single living cells using conducting polymer microelectrodes.*Advanced Materials* **2011**, *23*, 184–188.

(10) Lu, G.; Blakesley, J.; Himmelberger, S.; Pingel, P.; Frisch, J.; Lieberwirth, I.; Salzmann, I.; Oehzelt, M.; Di Pietro, R.; Salleo, A.; Koch, N.; Neher, D. Moderate doping leads to high performance of semiconductor/insulator polymer blend transistors.*Nature Communications* **2013**, *4*, 1588.

(11) Bujak, P.; Kulszewicz-Bajer, I.; Zagorska, M.; Maurel, V.; Wielgus, I.; Pron, A. Polymers for electronics and spintronics.*Chemical Society Reviews* **2013**, *42*, 8895.

(12) Sudha Devi, L.; Al-Suti, M. K.; Dosche, C.; Khan, M. S.; Friend, R. H.; Köhler, A. Triplet energy transfer in conjugated polymers. I. Experimental investigation of a weakly disordered compound.*Physical Review B - Condensed Matter and Materials Physics* **2008**, *78*, 1–8.

(13) Khlyabich, P. P.; Burkhart, B.; Thompson, B. C. Efficient Ternary Blend Bulk Heterojunction Solar Cells with Tunable Open-Circuit Voltage.*Journal of the American Chemical Society* **2011**, *133*, 14534–14537.

(14) Scholes, D. T.; Yee, P. Y.; Lindemuth, J. R.; Kang, H.; Onorato, J.; Ghosh, R.; Luscombe, C. K.; Spano, F. C.; Tolbert, S. H.; Schwartz, B. J. The Effects of Crystallinity on Charge Transport and the Structure of Sequentially Processed F 4 TCNQ-Doped Conjugated Polymer Films.*Advanced Functional Materials* **2017**, *27*, 1702654.

(15) Hamidi-Sakr, A.; Biniek, L.; Fall, S.; Brinkmann, M. Precise Control of Lamellar Thickness in Highly Oriented Regioregular Poly(3-Hexylthiophene) Thin Films Prepared by High-Temperature Rubbing: Correlations with Optical Properties and Charge Transport.*Advanced Functional Materials* **2016**, *26*, 408–420.

(16) Bredas, J. L.; Street, G. B. Polarons, bipolarons, and solitons in conducting polymers.*Accounts of Chemical Research* **1985**, *18*, 309–315.

(17) Nowak, M.; Rughooputh, S. D. D. V.; Hotta, S.; Heeger, A. J. Polarons and bipolarons on a conducting polymer in solution.*Macromolecules* **1987**, *20*, 965–968.

(18) Beljonne, D.; Cornil, J.; Sirringhaus, H.; Brown, P. J.; Shkunov, M.; Friend, R. H.; Brédas, J.-L. Optical Signature of Delocalized Polarons in Conjugated Polymers.*Advanced Functional Materials* **2001**, *11*, 229–234.

(19) Heimel, G. The Optical Signature of Charges in Conjugated Polymers.*ACS Central Science* **2016**, *2*, 309–315.

(20) Png, R.-Q.; Ang, M. C.; Teo, M.-H.; Choo, K.-K.; Tang, C. G.; Belaineh, D.; Chua, L.-L.; Ho, P. K. Madelung and Hubbard interactions in polaron band model of doped organic semiconductors.*Nature Communications* **2016**, *7*, 11948.

(21) Kohlstedt, K. Mind the Gap.*ACS Central Science* **2016**, *2*, 278–280.

(22) Kahmann, S.; Fazzi, D.; Matt, G. J.; Thiel, W.; Loi, M. A.; Brabec, C. J. Polarons in Narrow Band Gap Polymers Probed over the Entire Infrared Range: A Joint Experimental and Theoretical Investigation.*The Journal of Physical Chemistry Letters* **2016**, *7*, 4438–4444.

(23) Ghosh, R.; Chew, A. R.; Onorato, J.; Pakhnyuk, V.; Luscombe, C. K.; Salleo, A.; Spano, F. C. Spectral Signatures and Spatial Coherence of Bound and Unbound Polarons in P3HT Films : Theory Versus Experiment.*The Journal of Physical Chemistry C* **2018**, *122*, 18048–18060.

(24) Doan, S. C.; Schwartz, B. J. Ultrafast Studies of Excess Electrons in Liquid Acetonitrile: Revisiting the Solvated Electron/Solvent Dimer Anion Equilibrium.*The Journal of Physical Chemistry B* **2013**, *117*, 4216–4221.

(25) Cornil, J.; Brédas, J.-L. Nature of the optical transitions in charged oligothiophenes.*Advanced Materials* **1995**, *7*, 295–297.

(26) Kim, Y. H.; Hotta, S.; Heeger, A. J. Infrared photoexcitation and doping studies of poly(3-methylthienylene).*Physical Review B* **1987**, *36*, 7486–7490.

(27) Ziemelis, K. E.; Hussain, A. T.; Bradley, D. D. C.; Friend, R. H. Optical Spectroscopy of Field-Induced Charge in Poly(3-hexyl thienylene) Metal-Insulator-Semiconductor Structures: Evidence for Polarons.*Physical Review Letters* **1991**, *66*, 2231–2234.

(28) Arkhipov, V. I.; Emelianova, E. V.; Heremans, P.; Bässler, H. Analytic model of carrier mobility in doped disordered organic semiconductors.*Physical Review B* **2005**, 2–6.

(29) Chew, A. R.; Ghosh, R.; Shang, Z.; Spano, F. C.; Salleo, A. Sequential Doping Reveals the Importance of Amorphous Chain Rigidity in Charge Transport of Semi-Crystalline Polymers.*The Journal of Physical Chemistry Letters* **2017**, *8*, 4974–4980.

(30) Bird, M. J.; Bakalis, J.; Asaoka, S.; Sirringhaus, H.; Miller, J. R. Fast Holes, Slow Electrons, and Medium Control of Polaron Size and Mobility in the DA Polymer F8BT.*The Journal of Physical Chemistry C* **2017**, *121*, 15597–15609.

(31) Kahmann, S.; Loi, M. A.; Brabec, C. J. Delocalisation softens polaron electronic transitions and vibrational modes in conjugated polymers.*Journal of Materials Chemistry C* **2018**, *18*, 10270–10280.

(32) Jacobs, I. E.; Aasen, E. W.; Oliveira, J. L.; Fonseca, T. N.; Roehling, J. D.; Li, J.; Zhang, G.; Augustine, M. P.; Mascal, M.; Moulé, A. J. Comparison of solution-mixed and sequentially processed P3HT:F4TCNQ films: Effect of doping-induced aggregation on film morphology.*Journal of Materials Chemistry C* **2016**, *4*, 3454–3466.

(33) Wang, C.; Duong, D. T.; Vandewal, K.; Rivnay, J.; Salleo, A. Optical measurement of doping efficiency in poly(3-hexylthiophene) solutions and thin films.*Physical Review B* **2015**, *91*, 085205.

(34) Gao, J.; Stein, B. W.; Thomas, A. K.; Garcia, J. A.; Yang, J.; Kirk, M. L.; Grey, J. K. Enhanced Charge Transfer Doping Efficiency in J-Aggregate Poly(3-hexylthiophene) Nanofibers.*The Journal of Physical Chemistry C* **2015**, *119*, 16396–16402.

(35) McFarland, F. M.; Ellis, C. M.; Guo, S. The Aggregation of Poly(3-hexylthiophene) into Nanowires: With and without Chemical Doping.*Journal of Physical Chemistry C* **2017**, *121*, 4740–4746.

(36) Fuzell, J.; Jacobs, I. E.; Ackling, S.; Harrelson, T. F.; Huang, D. M.; Larsen, D.; Moulé, A. J. Optical Dedoping Mechanism for P3HT:F4TCNQ Mixtures.*Journal of Physical Chemistry Letters* **2016**, *7*, 4297–4303.

(37) Reid, O. G.; Pensack, R. D.; Song, Y.; Scholes, G. D.; Rumbles, G. Charge Photogeneration in Neat Conjugated Polymers.*Chemistry of Materials* **2014**, *26*, 561–575.

(38) Lioudakis, E.; Alexandrou, I.; Othonos, A. Ultrafast dynamics of localized and delocalized polaron transitions in P3HT/PCBM blend materials: The effects of PCBM concentration.*Nanoscale Research Letters* **2009**, *4*, 1475–1480.

(39) Saeki, A.; Seki, S.; Koizumi, Y.; Tagawa, S. Dynamics of photogenerated charge carrier and morphology dependence in polythiophene films studied by in situ time-resolved microwave conductivity and transient absorption spectroscopy.*Journal of Photochemistry and Photobiology A: Chemistry* **2007**, *186*, 158–165.

(40) Li, H.; Gauthier-Houle, A.; Grégoire, P.; Vella, E.; Silva-Acuña, C.; Bittner, E. R. Probing polaron excitation spectra in organic semiconductors by photoinduced-absorption-detected two-dimensional coherent spectroscopy.*Chemical Physics* **2016**, *481*, 281–286.

(41) Provencher, F.; Bérubé, N.; Parker, A. W.; Greetham, G. M.; Towrie, M.; Hellmann, C.; Côté, M.; Stingelin, N.; Silva, C.; Hayes, S. C. Direct observation of ultrafast long-range charge separation at polymer-fullerene heterojunctions.*Nature Communications* **2014**, *5*, DOI: 10.1038/ncomms5288.

(42) Menšík, M.; Pfleger, J.; Toman, P. Dynamics of photogenerated polarons and polaron pairs in P3HT thin films.*Chemical Physics Letters* **2017**, *677*, 87–91.

(43) Das, S.; Khlyabich, P. P.; Burkhart, B.; Roberts, S. T.; Couderc, E.; Thompson, B. C.; Bradforth, S. E. Quantifying Charge Recombination in Solar Cells Based on Donor–Acceptor P3HT Analogues.*The Journal of Physical Chemistry C* **2014**, *118*, 6650–6660.

(44) Ohkita, H.; Cook, S.; Astuti, Y.; Duffy, W.; Tierney, S.; Zhang, W.; Heeney, M.; McCulloch, I.; Nelson, J.; Bradley, D. D. C.; Durrant, J. R. Charge Carrier Formation in Polythiophene/Fullerene Blend Films Studied by Transient Absorption Spectroscopy.*Journal of the American Chemical Society* **2008**, *130*, 3030–3042.

(45) Guerrero, A.; Loser, S.; Garcia-Belmonte, G.; Bruns, C. J.; Smith, J.; Miyauchi, H.; Stupp, S. I.; Bisquert, J.; Marks, T. J. Solution-processed small molecule:fullerene bulk-heterojunction solar cells: Impedance spectroscopy deduced bulk and interfacial limits to fill-factors.*Physical Chemistry Chemical Physics* **2013**, *15*, 16456–16462.

(46) Hamidi-sakr, A.; Biniek, L.; Bantignies, J.-l.; Maurin, D.; Herrmann, L.; Leclerc, N.; Lévêque, P.; Vijayakumar, V.; Zimmermann, N. A Versatile Method to Fabricate Highly In-Plane Aligned Conducting Polymer Films with Anisotropic Charge Transport and Thermoelectric Properties : The Key Role of Alkyl Side Chain Layers on the Doping Mechanism.*Advanced Functional Materials* **2017**, *1700173*, 1–13.

(47) Duong, D. T.; Wang, C.; Antono, E.; Toney, M. F.; Salleo, A. The chemical and structural origin of efficient p-type doping in P3HT.*Organic Electronics* **2013**, *14*, 1330–1336.

(48) Hynynen, J.; Kiefer, D.; Yu, L.; Kroon, R.; Munir, R.; Amassian, A.; Kemerink, M.; Müller, C. Enhanced Electrical Conductivity of Molecularly p-Doped Poly(3-hexylthiophene) through Understanding the Correlation with Solid-State Order.*Macromolecules* **2017**, *50*, 8140–8148.

(49) Liang, Z.; Zhang, Y.; Souri, M.; Luo, X.; Boehm, A. M.; Li, R.; Zhang, Y.; Wang, T.; Kim, D.-Y.; Mei, J.; Marder, S. R.; Graham, K. R. Influence of dopant size and electron affinity on the electrical conductivity and thermoelectric properties of a series of conjugated polymers.*Journal of Materials Chemistry A* **2018**, *6*, 16495–16505.

(50) Aubry, T. J.; Axtell, J. C.; Basile, V. M.; Winchell, K. J.; Lindemuth, J. R.; Porter, T. M.; Liu, J.; Alexandrova, A. N.; Kubiak, C. P.; Tolbert, S. H.; Spokoyny, A. M.; Schwartz, B. J. Dodecaborane-based dopants designed to shield anion electrostatics lead to increased carrier mobility in a doped conjugated polymer.*Advanced Materials* **2019**, *31*, 1805647.

# CHAPTER 3

# Driving Force and Optical Signatures of Bipolaron Formation in Chemically-Doped Conjugated Polymers

## 3.1 Introduction

Like any semiconductors, conjugated polymers can be doped to create additional free charge carriers, expanding the potential uses for these materials in a variety of applications, including conductive layers,[1, 2] organic field effect transistors,[1, 3, 4] and thermoelectric devices.[5–8] Most conjugated polymers are *p*-type materials, so the charge carriers created by doping are holes.

For conjugated polymers, most dopants are strong oxidizing agents that remove an electron from the polymer's valence band, creating a polymer radical cation, also called a polaron. The doped polymer's backbone structure reorganizes from benzoid to quinoid to stabilize the positive charge, creating new energy levels in the bandgap and thus new optical transitions,[9–12] which are summarized at the upper left of Figure 3.1. By further oxidation, it is also possible to create a radical dication, or bipolaron, removing the electron in the mid-gap level and causing the level to further rise into the gap, as shown in the lower left of Figure 3.1.[9] It is generally assumed that bipolarons can be created only at very high doping levels,[9] but in this work, we show that for a particular push-pull conjugated polymer, bipolarons can be more stable than single polarons.

Push-pull conjugated polymers, also called donor-acceptor polymers, are copolymers consisting of alternating electron-rich and electron-poor groups along the semiconducting polymer's backbone. This design provides the advantage that the polymer bandgap can be tuned by changing the offset between the donor and acceptor energy levels, which also furnishes the ability to create low-bandgap materials. Many studies have demonstrated successful chemical doping of push-pull polymers,[8,

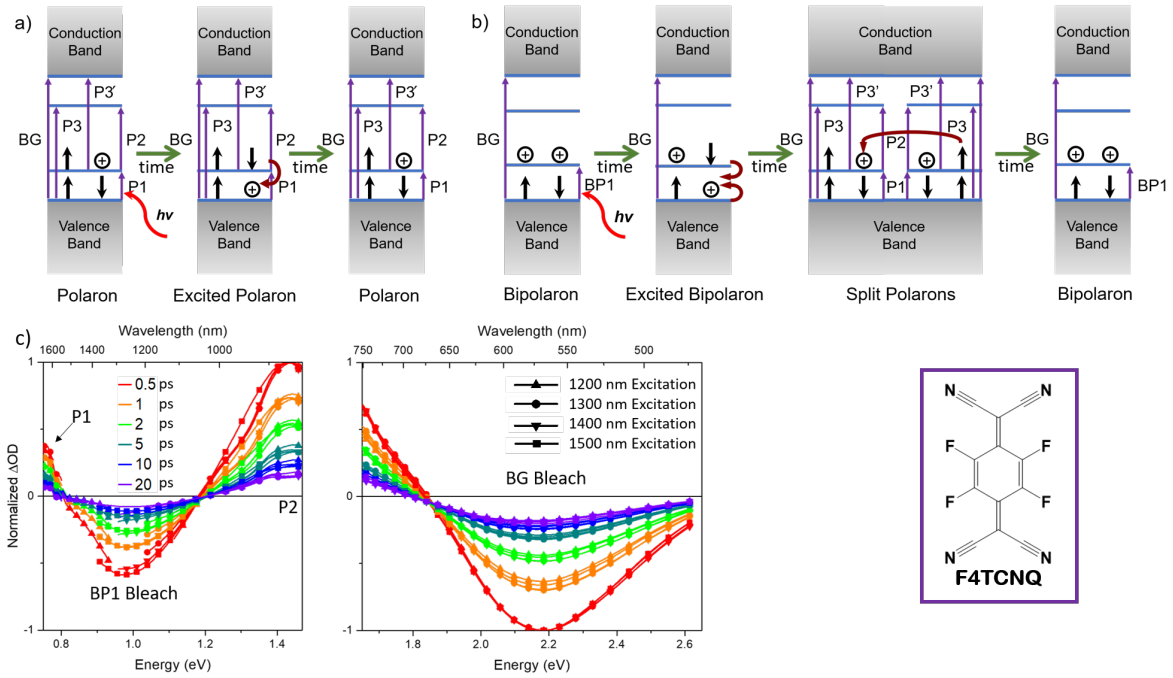


**Figure 3.1: Energy level diagrams of conjugated polymer polarons (a) and bipolarons (b). The left-most diagrams show the basic electronic structure of each kind of carrier, where BG represents the bandgap transition and the optical transitions created by doping are numbered in order of increasing energy; Appendix A contains a discussion of some of the theory underlying these energy level diagrams. The diagrams to the right show the expected dynamics following photoexcitation of the low-energy P1 or BP1 transition. c) Ultrafast transient absorption spectra of 1 mg mL$^{-1}$ $F_4$TCNQ-doped PBTDTP films excited at ∼1.03, ∼0.95, ∼0.89, and ∼0.83 eV (1200 nm (up-pointing triangles), 1300 nm (circles), 1400 nm, (down-pointing triangles) and 1500 nm (squares), respectively), at time delays of 0.5 (red), 1 (orange), 2 (green), 5 (light blue), 10 (dark blue) and 20 (purple) ps between the pump and the probe pulses. All excitation wavelengths (including the additional excitation wavelengths indicated in Figure 3.2 with the data in Appendix A) show similar transient spectral shapes and dynamics with clear isosbestic points, indicating that only a single excited electronic species is present. The gap in the data near 1.55 eV (800 nm) is due to scatter of laser fundamental and the fact that the NIR and visible portions of the data were collected separately. The inset (bottom right) shows the structure of the $F_4$TCNQ (2,3,5,6-tetrafluoro-7,7,8,8-tetracyanoquinodimethane) dopant used to oxidize the polymer backbone.**

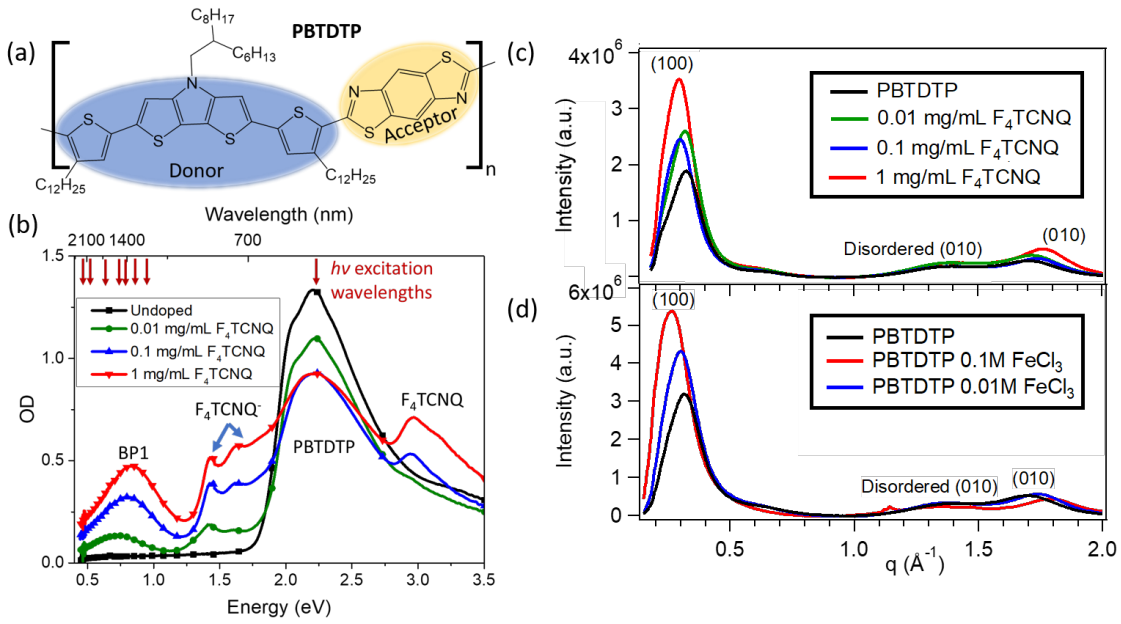


**Figure 3.2: a) Chemical structure of the push-pull conjugated polymer PBTDTP; the donor (push) and acceptor (pull) units are indicated with blue and yellow color, respectively. b) Steady-state optical spectrum of a film of PBTDTP (black curve, squares) and films of PBTDTP doped with $F_4$TCNQ by sequential processing, with the dopant supplied at concentrations of 0.01 (green curve, circles), 0.1 (blue curve, up-pointing triangles) and 1 (red curve, down-pointing triangle) mg mL$^{-1}$ in dichloromethane solution. The red arrows at the top of the panel indicate the excitation wavelengths used for the transient absorption experiments shown in Figure 3.1c and Appendix A. c) and d) GIWAXS measurements of PBTDTP films doped with (c) $F_4$TCNQ or (d) $FeCl_3$ showing the (100) lamellar peak shifting monotonically to smaller $q$ and the (010) crystalline π-stacking peak shifting smoothly to larger $q$ upon doping for both dopants. Further details are given in Appendix A.**

13–18] and there is strong evidence that charge transfer only occurs when the dopant is located near one of the donor units on the copolymer backbone and not near one of the acceptor units.[19]

In this paper, we focus on the nature of the charge carriers and their optical properties in a push-pull conjugated polymer oxidized with the commonly-used molecular dopants $FeCl_3$ and $F_4$TCNQ (2,3,5,6-tetrafluoro-7,7,8,8-tetracyanoquinodimethane),[8, 20–25] whose chemical structure is shown in Figure 3.1a. The push-pull copolymer we have chosen to study, (poly[(4-(2-hexyldecyl)-4H-dithieno[3,2-b:2′,3′-d′]pyrrole)-2,6-diyl-alt-(2,5-bis(3-dodecylthiophen-2-yl)benzo[1,2-d;4,5-[4]d′]bisthiazole)]), PBTDTP, whose molecular structure is also shown in the upper part of Figure 3.2, was synthesized as previously reported,[26] with synthetic details provided in the Supporting Information (SI). The gel permeation chromatography (GPC)-determined molecular weight (against polystyrene standards) in chlorobenzene at 60 °C for the material used in

this study was $M_w$ = 147.6 kDa, $M_w/M_n$ = 2.82.

## 3.2 Results

PBTDTP has a relatively low ionization potential of 4.8 eV,[26] making it easy to dope. It is worth noting that the donor group in PBTDTP extends over 5 conjugated rings, which is larger than other push-pull co-polymers whose chemical doping has been studied.[6, 8, 13–18, 26, 27] We will argue below that the large donor size and thus ability to delocalize the holes is what causes doping of PBTDTP to directly create bipolarons without first creating single polarons.

We prepared samples of both $F_4$TCNQ-doped and $FeCl_3$-doped PBTDTP via solution sequential processing,[28] starting with polymer films cast from a hot 100 $^{o}$C 1.5 mg mL$^{-1}$ ortho-dichlorobenzene solution at 2000 rpm for 60 s after which the films dried for an hour. Doping was accomplished by casting a solution of $F_4$TCNQ in dichloromethane at 0.01, 0.1 or 1 mg mL$^{-1}$ concentration on top of the pre-cast polymer film at 4000 rpm for 10 s (see Appendix A for more details on $FeCl_3$ doping and sample preparation).

We characterized the structure of the doped PBTDTP films using two-dimensional grazing-incidence wide-angle x-ray scattering (GIWAXS, Figures 3.2c,d for $F_4$TCNQ- and $FeCl_3$-doped films, respectively). We find that doping increases the lamellar spacing and decreases the π-stack spacing of the polymer, indicating that the dopant resides in the polymer side chain regions (see the Supporting Information (SI) for peak positions).[25, 29] Further discussion of texturing using in- and out-of-plane diffraction is also presented in Appendix A. The polymer structure changes smoothly with increasing dopant concentration, suggesting that only a single doped species is formed. The contraction of the π-stacking distance upon doping further indicates that any charge carriers created are likely delocalized across multiple chains.[6]

Despite this evidence for delocalized charge carriers, when we investigated the electrical properties using standard 4-point probe methods,[29] we found that 1 mg mL$^{-1}$ $F_4$TCNQ-doped PBTDTP films had barely-measurable conductivities between $5 \times 10^{-4}$ S cm$^{-1}$ and $1 \times 10^{-3}$ S cm$^{-1}$, and films doped with lower amounts of $F_4$TCNQ had conductivities lower than our detection limit. This indicates that the chemical doping process did not create mobile charge carriers, even

though field-effect transistors fabricated with PBTDTP showed a hole mobility of $5.3 \times 10^{-4}$ cm$^2$ V$^{-1}$ s$^{-1}$, comparable to other conjugated polymers.[26]

Figure 3.2b shows the steady-state optical spectroscopy of $F_4$TCNQ-doped PBTDTP films. As expected with the addition of increasing amounts of dopant, the neutral polymer bandgap absorption at ∼2.2 eV (565 nm) decreases, and new peaks appear corresponding to absorption by the $F_4$TCNQ anion at ∼3.54, ∼1.80 and ∼1.76 eV (350, 690 and 705 nm, respectively).[30] More importantly, we also see a single new peak characteristic of the absorption of charged species on the polymer at ∼0.83 eV (1500 nm). Figure 3.2b shows that the position and shape of this polymer charge carrier absorption is independent of dopant concentration, and we show in Appendix A that the properties of this peak also do not depend on whether $F_4$TCNQ or $FeCl_3$ is used as the dopant.

In most chemically-doped conjugated polymers, the new low-energy optical absorption that results from polarons, labelled P1 in Figure 3.1a, appears near 0.5 eV (∼2480 nm).[29] We[31, 32] and others[33, 34] have argued that when the dopant counterion resides close to the polaron on the polymer backbone the polaron can be trapped by the attractive Coulomb interaction, lowering its mobility and blue-shifting the absorption of the P1 transition. As shown in Figure 3.1b, bipolarons are also expected to have an optical transition (BP1) that is higher in energy than that of a single polaron.[9] Given the blue-shifted carrier absorption and the poor electrical conductivity of chemically-doped PBTDTP, this leads to the question of whether the immobile carriers are Coulombically-trapped polarons or bipolarons.

In previous work, we showed that we could distinguish free and Coulombically-trapped polarons using ultrafast transient absorption spectroscopy.[31] The idea behind the experiment is shown in Figure 3.1a. By exciting the polaron P1 transition, an electron from the valence band is moved to the half-filled state in the bandgap (left energy level diagram); in essence, the excitation is a photoinduced charge transfer taking an electron from a neutral region of the polymer and filling the hole, thus moving the hole to a new location on the polymer backbone (center diagram). Once the backbone relaxes to accommodate the charge, the stable polaron now resides in a new physical location (right diagram). The optical signatures of this process are a bleach (loss) of the bandgap transition, a bleach of the P1 transition, and an increase in absorption of the P2 transition, all of which uniformly and smoothly recover on a time scale of a few ps.[31] If the photoexcited carriers

are Coulombically-trapped polarons, then the photoinduced P2 transition is blue-shifted, and the recovery time lengthens to tens of ps because the relocalized carrier needs time to diffuse back to the place where it was Coulombically trapped. Thus, time-resolved spectroscopy is capable of separating the presence of free and trapped polaron species.[31]

Figure 3.1c shows the results of ultrafast transient absorption experiments on $F_4$TCNQ-doped PBTDTP films. The data show the same transient absorption spectral shape and dynamics following excitation at any wavelength under the carrier absorption band (the data for additional excitation wavelengths are shown in Appendix A). The spectral pattern, however, does not match the behavior expected for the transient absorption from either free or trapped polarons. In particular, the transient spectra show a new induced absorption band appearing at energies lower than the steady-state NIR absorption band, a peak that could not appear for either excited free or excited trapped polarons. Moreover, the recovery of the transiently induced signals occurs on a time scale longer than that seen for the excitation of polarons.

Remarkably, however, the transient absorption spectra seen in Figure 3.1c make perfect sense if the steady-state NIR absorption is due entirely to the BP1 optical transition of bipolarons. Figure 3.1b shows that exciting the low-energy BP1 transition would move a charge from a neutral region of the polymer to fill one of the pair of holes, leading to two separate polarons in separate places on the polymer backbone. After rapid stabilization of the relocalized holes, the bipolaron can only recover if the two newly-created polarons diffuse to find each other and recombine, a process that should be slower than reorganization of the backbone to stabilize a single polaron. Figure 3.1b also shows that the expected optical signatures following bipolaron excitation are a bleach of the BP1 transition, a loss of the bandgap transition, and the appearance of new polaronic absorptions, specifically the P1 and P2 polaron transitions, which correspond perfectly with the data in Figure 3.1c.

The clear isosbestic points seen in Figure 3.1c indicate that only a single excited species was created, which based on the above arguments must be bipolarons. We verified that only bipolarons are present in our doped PBTDTP samples by performing two additional sets of ultrafast transient absorption measurements, both of which are shown in Appendix A (Figures A.6 and A.7). First we excited the NIR absorption as far red as $\sim$0.56 eV (2200 nm), a wavelength where any single

polarons would be expected to absorb more intensely than bipolarons. The results are identical to the data in Figure 3.1c, indicating that there is no secondary electronic species (such as single polarons) hiding under the broad steady-state NIR absorption band. Second, we also excited the bandgap transition at ∼2.25 eV (550 nm). As shown in Appendix A, the optical signatures we observe for this experiment are exactly what is expected for bipolarons and not for single polarons. Thus, transient absorption spectroscopy can unambiguously identify the presence of bipolarons in doped conjugated polymer films. We note that the appearance of new P1 and P2 peaks match other experiments where polarons were photogenerated in semiconducting polymers[13, 14, 35]; here, we generate these peaks by photo-splitting of bipolarons.

## 3.3 Computational Results

Although the low electrical conductivity, steady-state and ultrafast spectroscopy experiments all point clearly to the fact that chemically-doped PBTDTP forms solely bipolarons and not single polarons, the question is why? We are aware of no other conjugated polymer systems where only bipolarons are observed with no stable polarons, and in fact, there are very few reports of bipolarons on conjugated polymers achieved by chemical doping.[36, 37] The relatively high valence band of PBTDTP means that strong oxidants such as $FeCl_3$ and $F_4TCNQ$ likely have the electrochemical potential to oxidize polarons to bipolarons, but this does not explain why bipolarons form even at low doping concentrations. Thus, to understand the reason PBTDTP favors bipolarons instead of polarons, we modeled the system using Density Functional Theory (DFT). Briefly, our calculations were performed using the PBE0 hybrid functional with the 6-31g** basis set on geometry-optimized PBTDTP oligomers consisting of 4 polymer repeat units (32 rings along the backbone) and the side chains truncated to single methyl groups;[38] the trend of the results we obtained did not vary with either the choice of functional or basis set, and full details are given in Appendix A. We note that we do not expect DFT to give an accurate description of the electronic structure of the polymers studied in this work; rather, we use DFT as the only affordable quantum chemistry theory available to gain a qualitative understanding of the relative stabilities of polarons and bipolarons in these systems.

To understand the energetic cost for polaron and bipolaron formation, we started by calculating

the total energy of neutral PBTDTP and subtracting that energy from the same calculation on singly-ionized PBTDTP. We found the energy difference to be 4.94 eV, in excellent agreement with the experimentally-measured 4.8-eV ionization energy of the material.[26] When we then remove a second electron from PBTDTP to create a singlet bipolaron, the calculated energetic cost was slightly higher at 5.49 eV; in other words, in the calculation, the singlet bipolaron is expected to be only 0.55 eV more unstable than making two separated polarons. We also calculated the properties of triplet bipolarons,[39] but found that for this system they dissociated into two single polarons, as discussed in Appendix A.

Our calculations do not predict PBTDTP bipolarons to be more stable than single polarons, in contrast to experiment; however, we can get a rough sense of what the 0.55-eV energetic cost means by comparing to calculations of bipolaron stability on other conjugated polymers. Thus, we repeated the same type of calculations for poly(3-hexylthiophene-2,5-diyl) (P3HT) hexadecamers, also with methyl-truncated side groups (see Appendix A for details). For P3HT, metastable bipolarons have been observed experimentally following chemical doping with $FeCl_3$, but only at very high doping concentrations.[36] Our calculations indicate that the P3HT polaron is 0.64 eV more stable than the bipolaron, as shown in Appendix A. Thus, our calculations predict that bipolarons are $\sim$100 meV more stable on PBTDTP than P3HT, consistent with our experimental observations.

To see why bipolarons are more stable on PBTDTP, we compared the relative energies of the PBTDTP neutral, polaron, and bipolaron species as we changed the physical size of the donor moiety, as shown in Figure 3.3b and Table A.4 in Appendix A. The trend in energies is quite clear: removing thiophenes from the donor moiety destabilizes the singlet bipolaron relative to the polaron. When the two thiophenes on the donor unit are removed, the calculated singlet bipolaron energy is 0.70 eV less stable than the single polaron. This shows that the presence of the two thiophenes, i.e., the large donor unit size, is primarily what stabilizes the singlet bipolaron.

To understand why donor size is related to bipolaron stability, Figure 3.3 shows the calculated bond length changes of the bipolaron species relative to the neutral polymer. The benzoid-to-quinoid transition that helps to stabilize the positive charges produces a bond-order alternation that is a clear signature of where the charges reside. Panel c) shows that the singlet bipolaron on PBTDTP spreads over all four donor and three of the acceptor units, but that the amount of charge that resides on

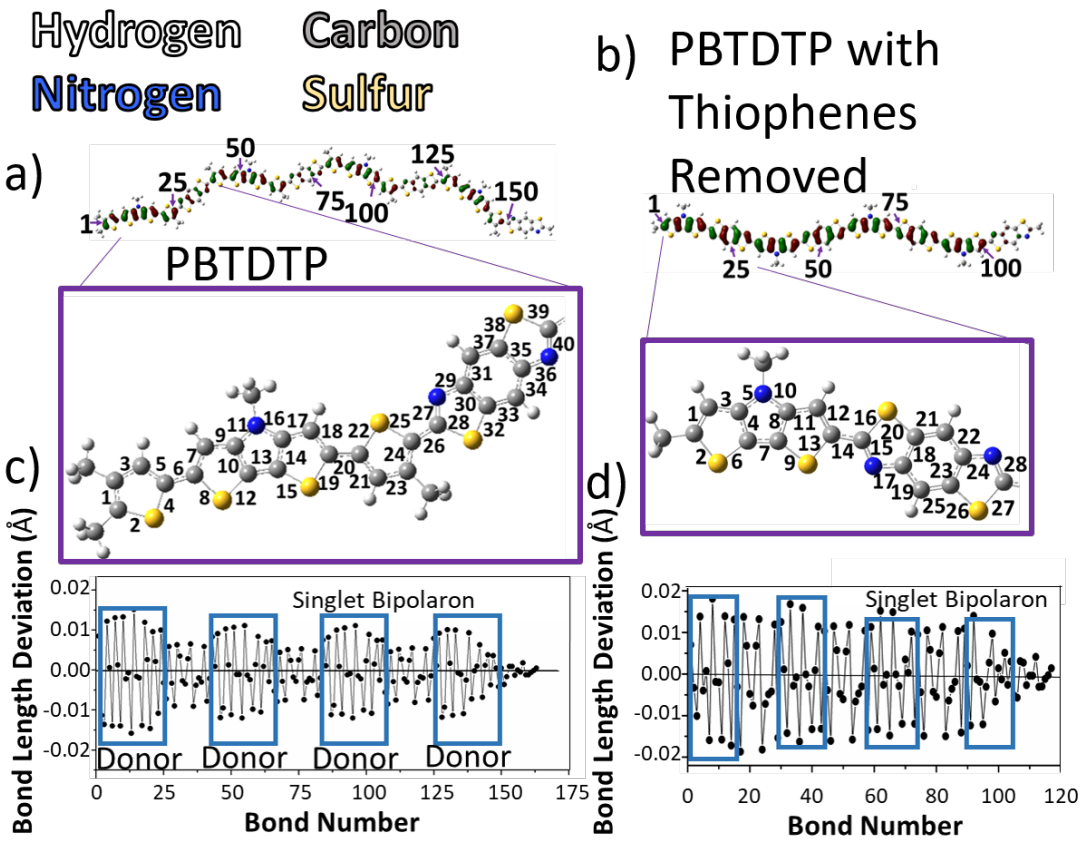


**Figure 3.3: a) Singlet bipolaron LUMO orbital of the side-chain truncated PBTDTP oligomer used for the DFT calculations, showing the definitions of the bond numbers and atom types for four repeat units of the polymer. b) Singlet bipolaron LUMO orbital of bond-number definitions for four repeat units of the PBTDTP polymer with the two 'extra' thiophene rings that were present in the donor unit removed throughout the oligomer. c) Bond length deviation (difference in bond length between the neutral and charged oligomers) of the singlet bipolaron for PBTDTP using the PBE0 DFT functional; see Appendix A for calculation details. The bonds corresponding to the donor units are boxed in blue. The singlet bipolaron is delocalized across all four of the donor and three of the acceptor units, but there is significantly more bond alternation on the donor units, indicating that the bipolaron prefers to avoid the higher-energy acceptor units. d) Bond length deviation for the singlet bipolaron for PBTDTP oligomers with the 'extra' donor thiophenes removed. Without the thiophenes, the bipolaron resides nearly equally on the donor and acceptor units, explaining why larger donor units provide for more stable bipolarons.**

the acceptor units is small. From the DFT calculations, we can determine the NBO charges on each atomic site, and find that there is a $\sim$4.1:1 donor charge:acceptor charge ratio, as discussed in Appendix A. When the two thiophene rings are removed from the donor unit, panel d) shows that the lack of room to hold the positive charges on the donor units forces the positive charges to spend essentially the same amount of time on the high-energy acceptor units as the donor units, making the bipolaron less energetically stable. Indeed, the NBO charges show a $\sim$1.6:1 donor charge:acceptor charge ratio when the two thiophenes are absent. In fact, nearly every (but not all,[40]) other push-pull copolymer that has been chemically doped in the literature has four or fewer rings in the donor unit, and all of these polymers form solely polarons, consistent with the idea that the bipolaron is destabilized with smaller donor units; this is discussed in more detail in Appendix A.

## 3.4 Conclusion

In summary, we have found that in a push-pull conjugated polymer with a large donor unit, bipolarons form stably even at low doping concentrations. Both steady-state UV-Vis and structural measurements confirm that a single charge carrier species smoothly appears upon doping, with no secondary species or single polarons present at low doping levels. We were able to verify the identity of the bipolaronic charge carriers using ultrafast transient absorption spectroscopy, which shows clear optical signatures for bipolarons that are distinct from free and Coulombically-bound single polarons. The bipolarons have poor mobility, explaining the lack of electrical conductivity in chemically-doped PBTDTP. The reason PBTDTP favors bipolaron formation at all doping levels is due to its chemical structure: our DFT calculations indicate that making the donor unit smaller destabilizes the bipolaron by forcing it to delocalize more over the higher-energy acceptor units. All of these findings can be used to inform the rational design of new push-pull polymers for better charge mobility upon chemical doping.

## References


(1) Bujak, P.; Kulszewicz-Bajer, I.; Zagorska, M.; Maurel, V.; Wielgus, I.; Pron, A. Polymers for electronics and spintronics.*Chemical Society Reviews* **2013**, *42*, 8895.

(2) Zhang, Y.; Elawad, M.; Yu, Z.; Jiang, X.; Lai, J.; Sun, L. Enhanced performance of perovskite solar cells with P3HT hole-transporting materials via molecular p-type doping.*RSC Advances* **2016**, *6*, 108888–108895.

(3) Lu, G.; Blakesley, J.; Himmelberger, S.; Pingel, P.; Frisch, J.; Lieberwirth, I.; Salzmann, I.; Oehzelt, M.; Di Pietro, R.; Salleo, A.; Koch, N.; Neher, D. Moderate doping leads to high performance of semiconductor/insulator polymer blend transistors.*Nature Communications* **2013**, *4*, 1588.

(4) Tan, B.; Pan, H.; Li, H.; Minus, M. L.; Budhlall, B. M.; Sobkowicz, M. J. Improving charge carrier mobility of polymer blend field effect transistors with majority insulating polymer phase.*The Journal of Physical Chemistry C* **2018**, *122*, 2918–2930.

(5) Hynynen, J.; Kiefer, D. Influence of crystallinity on the thermoelectric power factor of P3HT vapour-doped with F4TCNQ.*RSC Adv.* **2018**, 1593–1599.

(6) Liang, Z.; Zhang, Y.; Souri, M.; Luo, X.; Boehm, A. M.; Li, R.; Zhang, Y.; Wang, T.; Kim, D.-Y.; Mei, J.; Marder, S. R.; Graham, K. R. Influence of dopant size and electron affinity on the electrical conductivity and thermoelectric properties of a series of conjugated polymers.*Journal of Materials Chemistry A* **2018**, *6*, 16495–16505.

(7) Lim, E.; Peterson, K. A.; Su, G. M.; Chabinyc, M. L. Thermoelectric Properties of Poly(3-hexylthiophene) (P3HT) Doped with 2,3,5,6-Tetrafluoro-7,7,8,8-tetracyanoquinodimethane (F 4 TCNQ) by Vapor-Phase Infiltration.*Chemistry of Materials* **2018**, *30*, 998–1010.

(8) Suh, E. H.; Jeong, Y. J.; Oh, J. G.; Lee, K.; Jung, J.; Kang, Y. S.; Jang, J. Doping of donor-acceptor polymers with long side chains via solution mixing for advancing thermoelectric properties.*Nano Energy* **2019**, *58*, 585–595.

(9) Bredas, J. L.; Street, G. B. Polarons, bipolarons, and solitons in conducting polymers.*Accounts of Chemical Research* **1985**, *18*, 309–315.

(10) Beljonne, D.; Cornil, J.; Sirringhaus, H.; Brown, P. J.; Shkunov, M.; Friend, R. H.; Brédas, J.-L. Optical Signature of Delocalized Polarons in Conjugated Polymers.*Advanced Functional Materials* **2001**, *11*, 229–234.

(11) Heimel, G. The Optical Signature of Charges in Conjugated Polymers.*ACS Central Science* **2016**, *2*, 309–315.

(12) Png, R.-Q.; Ang, M. C.; Teo, M.-H.; Choo, K.-K.; Tang, C. G.; Belaineh, D.; Chua, L.-L.; Ho, P. K. Madelung and Hubbard interactions in polaron band model of doped organic semiconductors.*Nature Communications* **2016**, *7*, 11948.

(13) Cobet, C.; Gasiorowski, J.; Menon, R.; Hingerl, K.; Schlager, S.; White, M. S.; Neugebauer, H.; Sariciftci, N. S.; Stadler, P. Influence of molecular designs on polaronic and vibrational transitions in a conjugated push-pull copolymer.*Scientific Reports* **2016**, *6*, 35096.

(14) Kahmann, S.; Fazzi, D.; Matt, G. J.; Thiel, W.; Loi, M. A.; Brabec, C. J. Polarons in Narrow Band Gap Polymers Probed over the Entire Infrared Range: A Joint Experimental and Theoretical Investigation.*The Journal of Physical Chemistry Letters* **2016**, *7*, 4438–4444.

(15) Bird, M. J.; Bakalis, J.; Asaoka, S.; Sirringhaus, H.; Miller, J. R. Fast Holes, Slow Electrons, and Medium Control of Polaron Size and Mobility in the DA Polymer F8BT.*The Journal of Physical Chemistry C* **2017**, *121*, 15597–15609.

(16) Vardeny, S. R.; Baniya, S.; Lafalce, E.; Peyghambarian, N.; Vardeny, Z. V. Electronic and vibrational spectroscopy studies of PffBT4T π-conjugated donor–acceptor copolymer.*Journal of Photonics for Energy* **2018**, *8*, 1.

(17) Anderson, M.; Ramanan, C.; Fontanesi, C.; Frick, A.; Surana, S.; Cheyns, D.; Furno, M.; Keller, T.; Allard, S.; Scherf, U.; Beljonne, D.; D'Avino, G.; von Hauff, E.; Da Como, E. Displacement of polarons by vibrational modes in doped conjugated polymers.*Physical Review Materials* **2017**, *1*, 055604.

(18) Baniya, S.; Vardeny, S. R.; Lafalce, E.; Peygambarian, N.; Vardeny, Z. V. Amplitude-Mode Spectroscopy of Charge Excitations in PTB7 π -Conjugated Donor-Acceptor Copolymer for Photovoltaic Applications.*Physical Review Applied* **2017**, *7*, 064031.

(19) Di Nuzzo, D.; Fontanesi, C.; Jones, R.; Allard, S.; Dumsch, I.; Scherf, U.; von Hauff, E.; Schumacher, S.; Da Como, E. How intermolecular geometrical disorder affects the molecular doping of donor–acceptor copolymers.*Nature Communications* **2015**, *6*, 6460.

(20) Saska, J.; Gonel, G.; Bedolla-valdez, Z. I.; Aronow, S. D.; Shevchenko, N. E.; Dudnik, A. S.; Moule, A. J.; Mascal, M. A freely soluble, high electron affinity molecular dopant for solution processing of organic semiconductors.**2019**, 4–10.

(21) Yu, S.; Frisch, J.; Opitz, A.; Cohen, E.; Bendikov, M.; Koch, N.; Salzmann, I. Effect of molecular electrical doping on polyfuran based photovoltaic cells.*Applied Physics Letters* **2015**, *106*, DOI: 10.1063/1.4921484.

(22) Scholes, D. T.; Yee, P. Y.; McKeown, G. R.; Li, S.; Kang, H.; Lindemuth, J. R.; Xia, X.; King, S. C.; Seferos, D. S.; Tolbert, S. H.; Schwartz, B. J. Designing conjugated polymers for molecular doping: The roles of crystallinity, swelling, and conductivity in sequentially-doped selenophene-Based copolymers.*Chemistry of Materials* **2019**, *31*, 73–82.

(23) Yim, K.-H.; Whiting, G. L.; Murphy, C. E.; Halls, J. J. M.; Burroughes, J. H.; Friend, R. H.; Kim, J.-S. Controlling electrical properties of conjugated polymers via a solution-based p-Type Doping.*Advanced Materials* **2008**, *20*, 3319–3324.

(24) Cox, M.; van der Heijden, E. H. M.; Janssen, P.; Koopmans, B. Investigating the influence of traps on organic magnetoresistance by molecular doping.*Physical Review B* **2014**, *89*, 085201.

(25) Hamidi-sakr, A.; Biniek, L.; Bantignies, J.-l.; Maurin, D.; Herrmann, L.; Leclerc, N.; Lévêque, P.; Vijayakumar, V.; Zimmermann, N. A Versatile Method to Fabricate Highly In-Plane Aligned Conducting Polymer Films with Anisotropic Charge Transport and Thermoelectric Properties : The Key Role of Alkyl Side Chain Layers on the Doping Mechanism.*Advanced Functional Materials* **2017**, *1700173*, 1–13.

(26) Ahmed, E.; Subramaniyan, S.; Kim, F. S.; Xin, H.; Jenekhe, S. A. Benzobisthiazole-based donor-acceptor copolymer semiconductors for photovoltaic cells and highly stable field-effect transistors.*Macromolecules* **2011**, *44*, 7207–7219.

(27) Francis, C.; Fazzi, D.; Grimm, S. B.; Paulus, F.; Beck, S.; Hillebrandt, S.; Pucci, A.; Zaumseil, J. Raman spectroscopy and microscopy of electrochemically and chemically doped high-mobility semiconducting polymers.*Journal of Materials Chemistry C* **2017**, *5*, 6176–6184.

(28) Scholes, D. T.; Hawks, S. A.; Yee, P. Y.; Wu, H.; Lindemuth, J. R.; Tolbert, S. H.; Schwartz, B. J. Overcoming Film Quality Issues for Conjugated Polymers Doped with F 4 TCNQ by Solution Sequential Processing: Hall Effect, Structural, and Optical Measurements.*The Journal of Physical Chemistry Letters* **2015**, *6*, 4786–4793.

(29) Scholes, D. T.; Yee, P. Y.; Lindemuth, J. R.; Kang, H.; Onorato, J.; Ghosh, R.; Luscombe, C. K.; Spano, F. C.; Tolbert, S. H.; Schwartz, B. J. The Effects of Crystallinity on Charge Transport and the Structure of Sequentially Processed F 4 TCNQ-Doped Conjugated Polymer Films.*Advanced Functional Materials* **2017**, *27*, 1702654.

(30) Pingel, P.; Neher, D. Comprehensive picture of P -type doping of P3HT with the molecular acceptor F4TCNQ.*Physical Review B* **2013**, *87*, 115209.

(31) Voss, M. G.; Scholes, D. T.; Challa, J. R.; Schwartz, B. J. Ultrafast transient absorption spectroscopy of doped P3HT films: distinguishing free and trapped polarons.*Faraday Discussions* **2018**, DOI: 10.1039/C8FD00210J.

(32) Aubry, T. J.; Axtell, J. C.; Basile, V. M.; Winchell, K. J.; Lindemuth, J. R.; Porter, T. M.; Liu, J.; Alexandrova, A. N.; Kubiak, C. P.; Tolbert, S. H.; Spokoyny, A. M.; Schwartz, B. J. Dodecaborane-based dopants designed to shield anion electrostatics lead to increased carrier mobility in a doped conjugated polymer.*Advanced Materials* **2019**, *31*, 1805647.

(33) Ghosh, R.; Chew, A. R.; Onorato, J.; Pakhnyuk, V.; Luscombe, C. K.; Salleo, A.; Spano, F. C. Spectral Signatures and Spatial Coherence of Bound and Unbound Polarons in P3HT Films : Theory Versus Experiment.*The Journal of Physical Chemistry C* **2018**, *122*, 18048–18060.

(34) Ghosh, R.; Luscombe, C. K.; Hambsch, M.; Mannsfeld, S. C. B.; Salleo, A.; Spano, F. C. Anisotropic polaron delocalization in conjugated homopolymers and donor–acceptor copolymers.*Chemistry of Materials* **2019**, acs.chemmater.9b01704.

(35) Li, H.; Gauthier-Houle, A.; Grégoire, P.; Vella, E.; Silva-Acuña, C.; Bittner, E. R. Probing polaron excitation spectra in organic semiconductors by photoinduced-absorption-detected two-dimensional coherent spectroscopy.*Chemical Physics* **2016**, *481*, 281–286.

(36) Yamamoto, J.; Furukawa, Y. Electronic and Vibrational Spectra of Positive Polarons and Bipolarons in Regioregular Poly(3-hexylthiophene) Doped with Ferric Chloride.*Journal of Physical Chemistry B* **2015**, *119*, 4788–4794.

(37) Wang, C.; Duong, D. T.; Vandewal, K.; Rivnay, J.; Salleo, A. Optical measurement of doping efficiency in poly(3-hexylthiophene) solutions and thin films.*Physical Review B* **2015**, *91*, 085205.

(38) Frisch, M. J. et al. Gaussian 09 Revision D.01, Gaussian Inc. Wallingford CT, 2009.

(39) Zozoulenko, I.; Singh, A.; Singh, S. K.; Gueskine, V.; Crispin, X.; Berggren, M. Polarons, bipolarons, and absorption spectroscopy of PEDOT.*ACS Applied Polymer Materials* **2019**, *1*, 83–94.

(40) Provencher, F.; Bérubé, N.; Parker, A. W.; Greetham, G. M.; Towrie, M.; Hellmann, C.; Côté, M.; Stingelin, N.; Silva, C.; Hayes, S. C. Direct observation of ultrafast long-range charge separation at polymer-fullerene heterojunctions.*Nature Communications* **2014**, *5*, DOI: 10.1038/ncomms5288.

# APPENDIX A

# Supporting Information for Chapter 3

## A.1 Experimental and Computational Details

### A.1.1 Sample Preparation of Doped PBTDTP films

A mixture of 1[1] (210 mg, 0.246 mmol), 4-(2-hexyldecyl)-2,6-bis(trimethyltin)-4H-dithieno[3,2-b:2′,3′-d′]pyrrole 2[2] (180 mg, 0.246 mmol), tris(dibenzylideneacetone)dipalladium (0) (4.5 mg, 0.00491 mmol), tris-o-tolyphosphine (6.0 mg, 0.0197 mmol) in 5.4 mL of chlorobenzene was refluxed for 72 h. The reaction solution was poured into 200 mL of 5% hydrochloric acid:methanol solution and stirred for 5 h. The filtered solid was subjected to Soxhlet extraction with methanol and hexane for 24 h each. PBTDTP-1 was extracted with chloroform to give a shiny green solid (68.8 mg) whereas the chloroform-insoluble fraction PBTDTP-2 (172 mg) remained in the filter paper (241 mg, 90%). $^1$H NMR ($C_6D_4Cl_2$, 60 °C): δ 8.43-8.17 (m, 4H), 7.30-7.00 (m, 2H), 4.10 (s, br, 2H), 3.18 (s, br, 4H), 1.91-0.98 (m, 77H). Gel permeation chromatography (GPC) against polystyrene standards in chlorobenzene at 60 °C: PBTDTP-1: $M_w$ = 32.1 kDa, $M_n$ = 10.3 kDa, PDI = 3.12. PBTDTP-2: $M_w$ = 147.6 kDa, $M_n$ = 52.4 kDa, PDI = 2.82. The higher molecular weight fraction, that is PBTDTP-2, was used in our current study and simply named PBTDTP.

PBTDTP (specifically PBTDTP-2, the higher molecular weight batch, as synthesized in Ref. [1]) was also doped with iron (III) chloride. This was accomplished by casting a 0.1 M solution of $FeCl_3$ in tetrahydrofuran (THF) on top of the pre-cast polymer film at 4000 rpm for 10 s. The solution of 0.1 M iron (III) chloride in tetrahydrofuran doped PBTDTP quite well: other than the fact that the iron (II) chloride anion absorbs in a different spectral region than the $F_4$TCNQ anion, the $FeCl_3$-doped PBTDTP films have a similar absorption spectra to that shown in the main text (Figure A.2). This indicates the carrier absorption in doped PBTDTP is not specific to a single

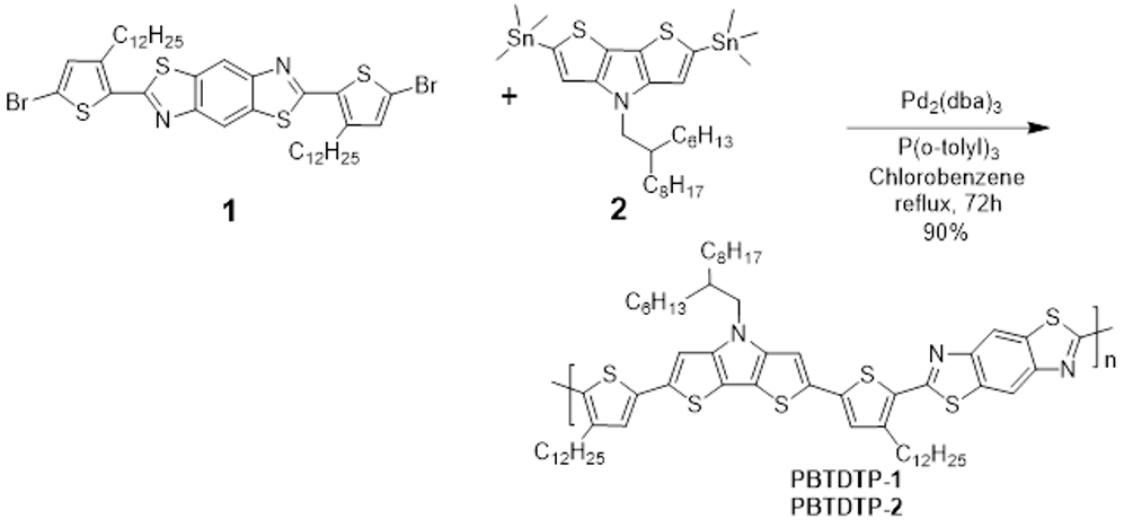


**Figure A.1: Synthetic route to PBTDTP copolymer[1].**

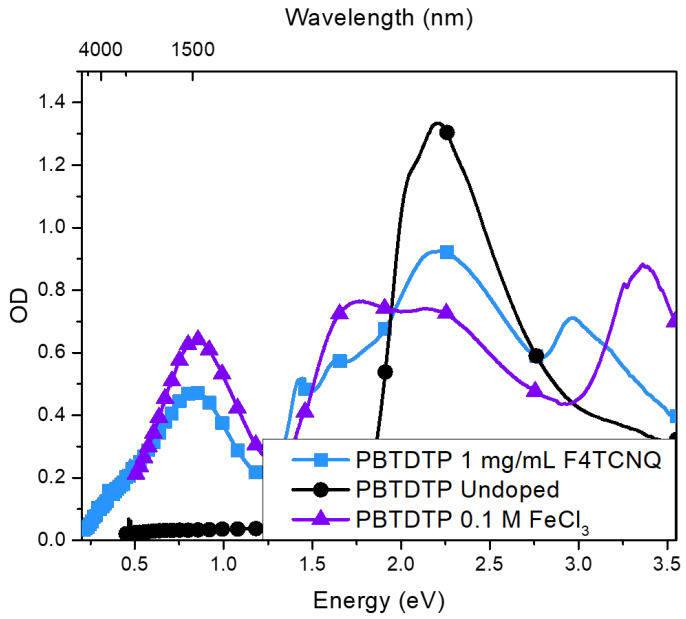


**Figure A.2: UV-Vis of 0.1 M iron (III) chloride:THF-Doped and 1 mg $F_4$TCNQ:1 mL DCM-Doped PBTDTP showing similar bipolaron peaks in the near infrared around 0.84 eV; the differences in the visible region are due to the different absorbances of the two dopant anions. The IR data below ~0.44 eV (2800 nm) is scaled to align with the UV-Vis absorption for the $F_4$TCNQ-doped film.**

dopant system, and the unique behavior of PBTDTP is a more general phenomenon.

| Table A1.1 - Physical properties of PBTDTP | | | | | | | | | |
|---|---|---|---|---|---|---|---|---|---|
| Polymer | $T_m$:$T_c$ (°C) | Abs $\lambda^b_{max}$ (nm) | Abs $\lambda^c_{max}$ (nm) | $E_g^{opt}$ (eV) | PL $\lambda^b_{max}$ (nm) | PL $\lambda^c_{max}$ (nm) | $E_{HOMO}$ (eV)[e] | $E_{LUMO}$ (eV)[e] | $E_g$ (eV)[e] |
| PBTDTP | [a] | 574 | 562 | 1.83 | 650 | [d] | -4.79 | -3.30 | 1.49 |

**Table A.1: Physical properties of PBTDTP. [a] Thermal transition was not observed up to 390 °C [b] In ($1 \times 10^{-6}$ M solution [c] Thin film [d]PL emission was not observed [e]Thin film cyclic voltammetry**

PTB7 (CAL Organic Semiconductors, PDI 1.8-2.2, $M_n > 25{,}000$) solutions were made by dissolving 10 mg of PTB7 in 1 mL of chlorobenzene. 25 $\mu$L of polymer solution was added to a 1.5 by 1.5 cm glass substrate and spun at 1000 RPM for 60 seconds and then 3000 RPM for 5 seconds. A 100 $\mu$L of 25 mM $FeCl_3$:acetonitrile was pipetted on top of the polymer films to dope the polymer. The doping solution was allowed to soak into the film for 10 s then spun at 4000 RPM for 10 s.

The UV-Vis-NIR spectra of doped PTB7 shows that upon doping with $FeCl_3$ the bandgap (BG) transition decreases, and the P2 and P1 peak appear, along with the IR active vibrations (IRAV), as is typical of polaron formation. The energies of the P1 and P2 peaks satisfy the relation, 2P1 + P2=BG as expected for polarons, showing that PTB7 forms polarons unlike PBTDTP.

### A.1.2 Conductivity Measurements

Four-point probe conductivity measurements were performed in the Van der Pauw geometry using a custom-built apparatus with a Keithley 2400 Sourcemeter. The max current sourced was fixed at 1 mW total power. The current was swept from negative to positive and then rotated 90° and repeated. The I-V curves were then fit to the Van der Pauw equation to extract the sheet resistance of the films. Samples were made using a glass substrate with the leads attached at the corners of the 1.5 by 1.5 cm substrate. The thickness of each film was determined from a Dektak Profilometer measuring the depth of multiple lines etched into each film.

For PBTDTP films doped with both $FeC_3$ and $F_4TCNQ$, only the 1 mg $mL^{-1}$ $F_4TCNQ$ doped PBTDTP film had a measurable conductivity. All other films had a sheet resistance indistinguishable

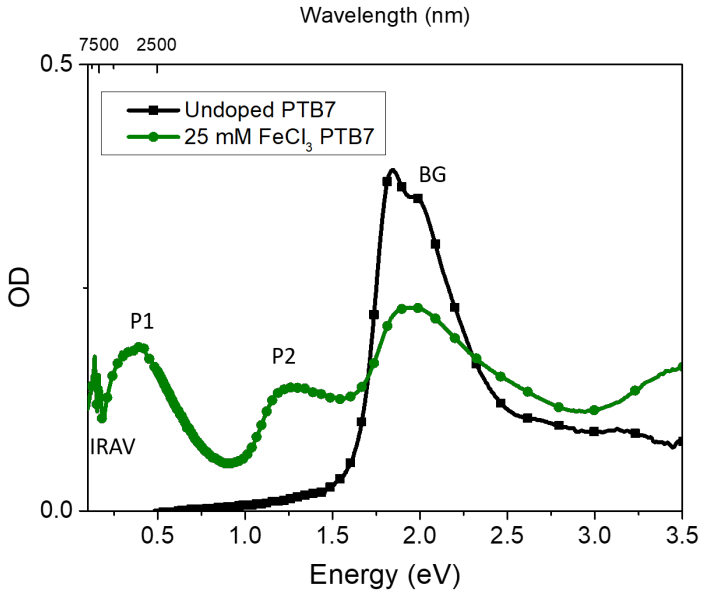


**Figure A.3: UV-Vis-NIR of 25mM iron (III) chloride:acetonitrile-Doped PTB7 showing polaron peaks, P1 and P2 and loss of the bandgap transition upon doping. The IR data below ∼0.44 eV (2800 nm) is scaled to align with the UV-Vis absorption for the $F_4$TCNQ-doped film.**

from the open circuit resistance of the four-point probe set-up. The 1 mg mL$^{-1}$ $F_4$TCNQ doped PBTDTP film had a sheet resistance $3 \times 10^7 \Omega \times \square^{-1}$ and a calculated conductivity ranging from $5 \times 10^{-4}$ to $1 \times 10^{-3}$ S cm$^{-1}$.

In comparison, PTB7 doped with a 25 mM solution of $FeCl_3$ in acetonitrile had its conductivity determined by four-point probe as well, using the same set-up as PBTDTP. Three films were tested three times each. Sheet resistance for PTB7 doped films ranged from 47,000 to 65,000 $\Omega \times \square^{-1}$ with a film thickness ranging from 81 to 84 nm, yielding an average conductivity of 2.2 S cm$^{-1}$

### A.1.3 Structural Studies of Doped PBTDTP

We examined the molecular structure of our pristine and doped PBTDTP films using 2-D grazing-incidence wide-angle X-ray scattering (GIWAXS). In both the raw and radially-integrated diffraction patterns obtained from the pure polymer (Figure A.4a), we see a lamellar (100) peak, which represents the distance between polymer backbones along the side chain direction, at $q = 0.32$ Å$^{-1}$. We also see two peaks in the region that is usually assigned to the π-stacking or (010) peaks at

$q = 1.37$ Å$^{-1}$ and 1.71 Å$^{-1}$. While these two peaks could be two different π-related peaks, each with a different indexing, the low crystallinity of this polymer and the texture of the peaks in question makes this unlikely. Instead, the lower-$q$ (010) peak is usually attributed to disordered π-stacking, while the higher-$q$ (010) peak is associated with more ordered and tightly packed π-stacking. For complex polymers like these, it is often observed that that those domains that lie face-on to a flat surface are more ordered (i.e., higher crystallinity) with smaller π-stacking distances; those face-on domains can be seen in the enhanced 1.71 Å$^{-1}$ out-of-plane scattering peak in Figure A.4a.[3] The in-plane scattering and the diffraction collected at 45° are similar, so this scattering represents the isotropic, more disordered components of the polymer film.

**Table A.2: GIWAXS Peak Positions of $F_4$TCNQ-Doped PBTDTP [Å$^{-1}$]**

| Doping Level | (100) | Disordered (010) | (010) |
|---|---|---|---|
| Pure PBTDTP | 0.32 | 1.37 | 1.71 |
| 0.01 mg mL$^{-1}$ | 0.31 | 1.38 | 1.72 |
| 0.1 mg mL$^{-1}$ | 0.30 | 1.39 | 1.74 |
| 1 mg mL$^{-1}$ | 0.29 | 1.40 | 1.77 |

**Table A.3: GIWAXS Peak Positions of $FeCl_3$-Doped PBTDTP [Å$^{-1}$]**

| Doping Level | (100) | Disordered (010) | (010) |
|---|---|---|---|
| Pure PBTDTP | 0.31 | 1.37 | 1.70 |
| 0.01 M | 0.30 | 1.38 | 1.74 |
| 0.1 M | 0.27 | 1.37 | 1.79 |

Upon doping with either $F_4$TCNQ (Figure A.4b) or $FeCl_3$, (Figure A.4c), we see a shift of the (100) lamellar peak to higher $d$-spacing ($q = 0.29$ Å$^{-1}$), indicating that the $F_4$TCNQ anions are infiltrating into the lamellar gallery. We also see an increase in the (100) diffraction intensity, indicative of an increase in overall polymer crystallinity. Such increases have been observed previously for semi-disordered polymers upon doping.[4] At the same time, doping causes the more ordered π-stacking peak to shift to lower $d$-spacing. These shifts are monotonic with increasing concentration of either dopant indicating that only a single doped structure is formed, a fact that is

consistent with the optical absorption upon doping with either $F_4TCNQ$ or $FeCl_3$. The smooth shifts are thus consistent with the direct formation of bipolarons upon chemical doping. The decrease in the π-stacking peak *d*-spacing further indicates delocalization of charges across multiple polymer polymer chains.[4] This delocalization is likely responsible for the increase in ordering indicated by the increased diffraction intensity. In- and out-of-plane diffraction for the $F_4TCNQ$ doped polymer further shows that the polymer maintains its dominantly face-on orientation upon doping, indicating that the dopant infiltrates into existing crystalline and semi-crystalline domains and does not significantly restructure the film.

### A.1.4 Discussion of the Optical Transitions in Doped Conjugated Polymers

A semiconducting polymer natively adopts a benzoid arrangement of single and double bonds along its backbone. When the polymer becomes *p*-doped, the double bonds shift position forming a quinoid arrangement, creating a cation radical, or polaron, on the polymer backbone. The reordering of the double and single bonds distorts the lattice locally, as seen in Figure 3.1, bringing the local energy levels into the band gap. Further *p*-doping converts the cation radical into a dication, or bipolaron, without necessarily causing any further significant rearrangement of the positions of the double and single bonds.[5]

Figure A.5a shows the positions of the half-filled state that rises up from the valence band and the empty state that falls from the conduction band upon polaron formation (also cf. Figure 3.1).[5] Haare et al. have pointed out that the absolute energy levels of the polaron and bipolaron may shift relative to vacuum, so that it would be harder to oxidize the polaron than the neutral polymer.[6] The band tightening gives rise to several new optical transitions: the P1 transition going from the valence band to the half-filled state, the P2 transition going between the two new intergap states, and the P3 and P3′ transitions going from the valence band to the empty intergap state or from the half-filled intergap state to the conduction band.[5] The transitions, by convention, are labelled in order of increasing energy. The P3 and P3′ are formally optically forbidden and degenerate, but in the case of 2-D-delocalization of the polaron across the doped chain and a neighboring undoped chain, the degeneracy can be broken and the P3 and P3′ transitions can become allowed.[7, 8] Cobet

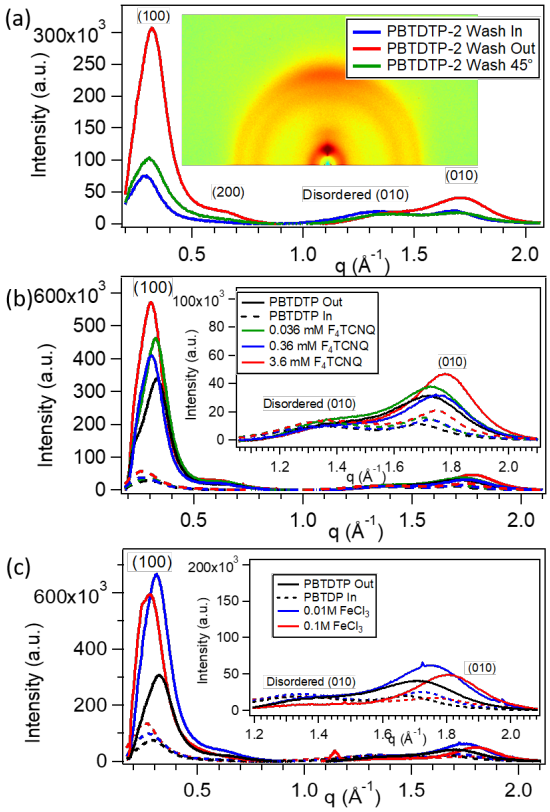


**Figure A.4: a) Raw and radially-integrated GIWAXS data collected on undoped PBTDTP films. For better comparison, all samples were washed with the same solvent used for SqP doping. Here, data labeled 'out' corresponds to out-of-plane diffraction, 'in' corresponds to in-plane diffraction, and '45°' corresponds to a slice centered at 45° off the out-of-plane. This 45° slice represents the isotropic portion of the sample. Panels (b) and (c) show the separate in- and out-of-plane scattering portions of the $F_4TCNQ$-doped and $FeCl_3$-doped PBTDTP films, respectively. Both dopants cause the (100) crystalline lamellar peak to shift monotonically to smaller $q$ and the (010) crystalline π-stacking peak to shift to larger $q$. The monotonic changes and similar structure shows that only a single doped species is created independent of the choice of dopant. All orientation effects observed in the undoped diffraction are retained in the doped samples, despite the peak shifts.**

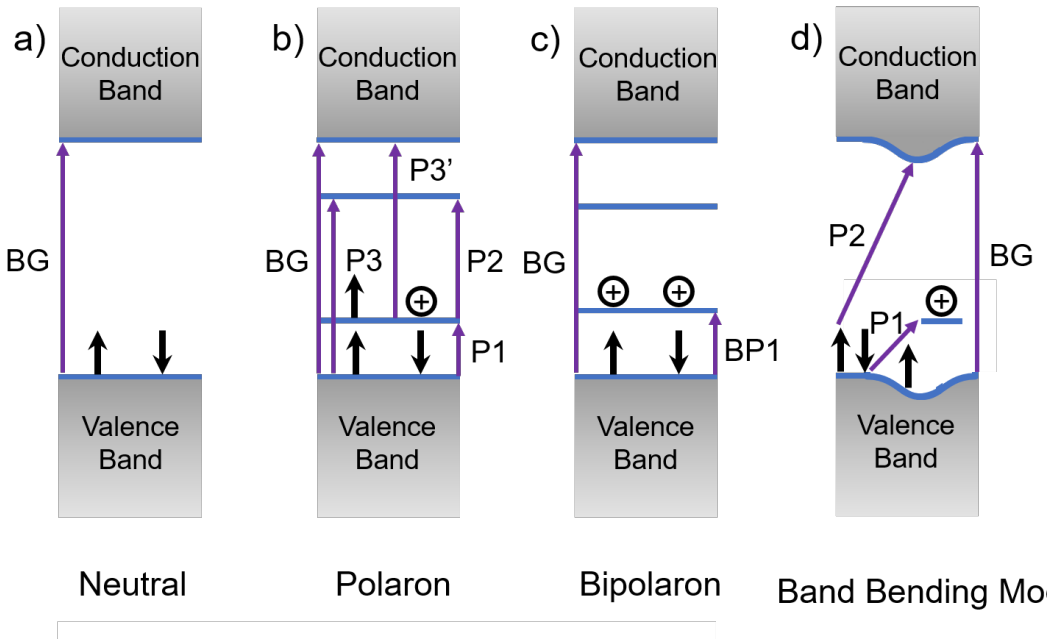


**Figure A.5: Energy level diagram showing the undoped polymer (a), the traditional model for polarons (b), the traditional model for bipolarons (c), and the new band-bending model of polarons (d), and the corresponding transitions between the different energy levels.**

*et al*. have shown that push-pull copolymers have less 2-D-delocalization than their homopolymer counterparts.[9]

More recently, a band-bending model, developed by Heimel and Png, predicts a different arrangement of doped conjugated polymer energy levels from the more traditional picture.[10–13] According to the band-bending model, when a semiconducting polymer is doped, the valence band state splits into two half-states, with one half-occupancy state rising into the bandgap and the other half occupancy state bending below the edge of the valence band due to the distortion of the localized charge. The conduction band also bends down due to the localized charge. This gives rise to an equivalent P1 transition going from the undistorted region of the valence band to the half-occupancy intergap state and the P2 transition going from the undistorted region of the valence band to the lowered region of the conduction band.[10, 13] The band-bending model does not predict a P3 or P3′ transition.[10]

The band-bending model also has not been successfully applied to bipolarons,[10] in contrast to the traditional picture in which a bipolaron is formed by removing an electron from the half-filled state, causing the two intergap states to further narrow in energy. This creates a BP1 transition going

from the valence band to the lower of the two intergap states. The transition from the valence band to the upper intergap state would be termed BP2, but this transition is not seen, as it is symmetry forbidden, similar to the case of the P3 transition with single polarons.[5, 14] Bipolarons form to reduce the energetic penalty for the benzoid-to-quinoid lattice distortion at the expense of increased Coulomb repulsion. Bipolarons are expected to show less 2-D-delocalization and thus less symmetry breaking, maintaining the forbidden nature of the BP2 transition.

Our previous work found that the band bending model did not correspond to the observed transitions seen in the ultrafast spectroscopy of doped P3HT.[15] Although the band-bending model predicts no P3 nor P3$'$ transition exists, the transient absorption measurements showed the bleach and increase of P3 and P3$'$ respectively. Moreover, the band bending model suggests that photoexcitation of P1 should lead to a bleach at P2, but instead, an increase in absorption was observed.[15]

For the PBTDTP bipolarons discussed in the main text, we cannot distinguish between the two models, as in both cases we expect to see bipolarons split into two polarons each with a P2 and P1 absorption appearing in the transient absorption measurements. In addition, the spectroscopic measurements cannot distinguish between triplet bipolarons or singlet bipolarons as they would have the same ground-state transitions, and when excited to split into two polarons, two spin-up polarons would look the same as two polarons of opposite spin in the transient absorption measurements. Based on the results of previous work and the fact that the band-bending model was unable to predict stable bipolarons despite us finding bipolarons, we discount the band-bending model and favor the long-standing model.[15]

### A.1.5 Ultrafast Transient Absorption Spectroscopy of Doped-PBTDTP Films

The ultrafast transient absorption measurements used a commercial Ti:sapphire regenerative amplifier (Coherent, Inc.) and a Helios transient absorption spectrometer. Together they provide $\sim$75-fs time resolution. The amplified laser system produces 1.55-eV (800 nm) light pulses at a 1 kHz repetition rate with $\sim$3 mJ of energy. The 1.55-eV beam is split, with part of the beam sent to pump an optical parametric amplifier (Topas), which created the $\sim$1 $\mu$J at $\sim$2.25, $\sim$1.03, $\sim$0.95,

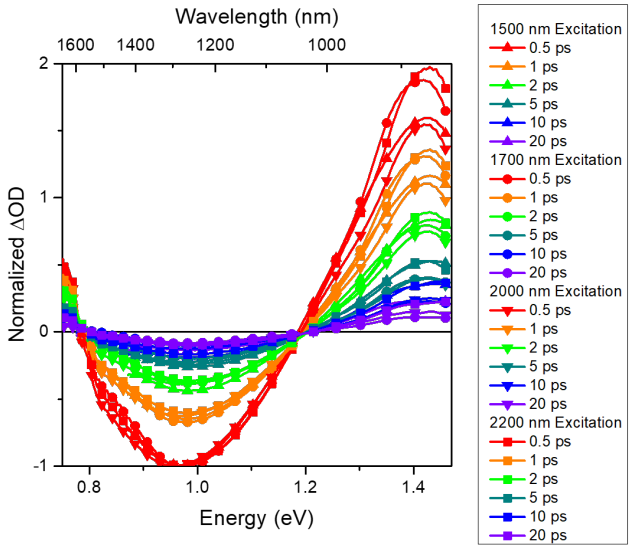


**Figure A.6: Ultrafast transient absorption spectra of 1 mg mL$^{-1}$ $F_4$TCNQ:DCM doped PBTDTP excited at ∼0.83, ∼0.73, 0.62, and ∼0.56 eV (1500 nm, 1700 nm, 2000 nm, and 2200 nm, respectively), at time delays of 0.5, 1, 2, 5, an 10 and 20 ps between the pump and the probe pulses. All excitation wavelengths show similar spectral shapes and decay patterns, indicating that a single electronic species was excited. The gaps in the data in the NIR are due to scatter from the pump excitation wavelength.**

∼0.89, ∼0.83, ∼0.73, 0.62, and ∼0.56 eV (550, 1200, 1300, 1400, 1500, 1700, 2000, and 2200 nm respectively) to serve as the pump beam. The other fraction of the 1.55-eV light was sent through a sapphire plate to generate white light continuum in either the visible (3.1 to 1.6 eV) or NIR (1.42 to 0.75 eV) to probe the sample. The scatter from the 1.55-eV fundamental beam obscures data collected near 1.55 eV. A double-pass delay stage controls the timing between the pump and probe pulses. Scans were averaged over 5 seconds per time point, with the 10 adjacent points in time and wavelength averaged together. At least 3 scans were averaged together in any of the data shown in the main text or this SI. In addition, scans for 1.03 eV to 0.83 eV and 0.56 eV had data collected with the pump and probe polarizations both parallel and perpendicular that were combined in the appropriate ratio to produce the equivalent magic angle spectra. No polarization anisotropy was found for any of the five excitation wavelengths. 0.73 eV and 0.62 eV were collected with the pump and probe polarized parallel and 2.25 eV was collected with the pump and probe perpendicularly polarized.

As mentioned in the main text, we scanned the pump pulse further into the near infrared to see if there was a second electronic species hiding under the broad NIR UV-Vis peak. The P1 band

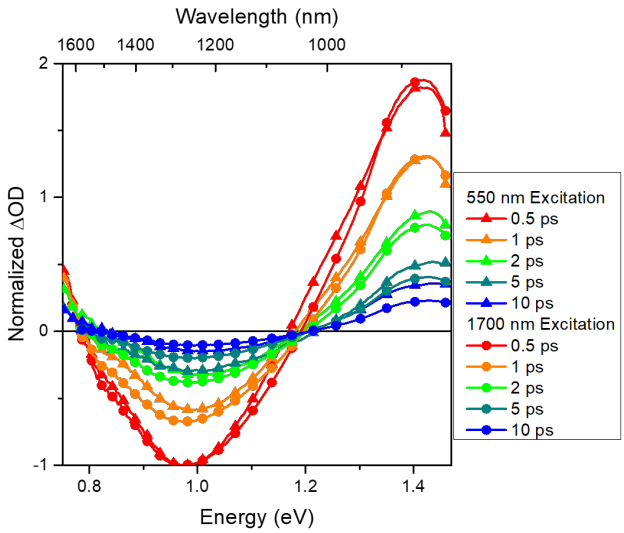


**Figure A.7: Ultrafast transient absorption spectra of 1 mg mL$^{-1}$ $F_4$TCNQ:DCM doped PBTDTP excited at ∼2.25 eV and ∼0.73 eV (550 nm and 1700 nm), at time delays of 0.5, 1, 2, 5, and 10 ps between the pump and the probe pulses. All excitation wavelengths show similar spectral shapes and decay patterns, indicating that exciting either the bandgap transition or the BP1 transition can generate polaronic states, confirming the assignment of the near-IR absorption as arising from bipolarons.**

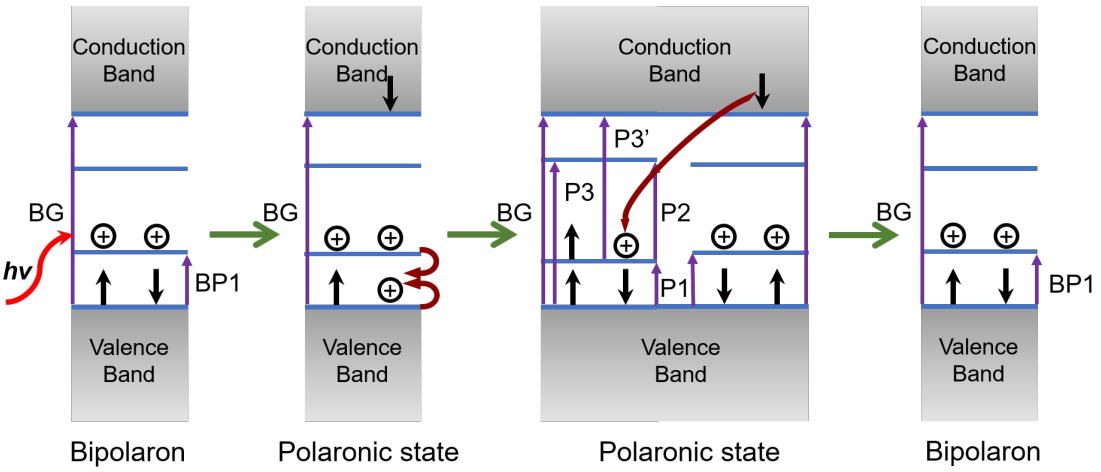


**Figure A.8: Energy level diagrams of conjugated polymer bipolarons undergoing photoexcitation. The left-most diagrams show the basic electronic structure of the bipolaron, where BG represents the bandgap transition, and the optical transitions created by doping are numbered in order of increasing energy; The diagrams to the right show the expected dynamics following photoexcitation of the bandgap transition.**

of single polarons in conjugated polymers nearly always absorbs near 0.5 eV.[16] This means that exciting near 0.5 eV should reveal any small population of polarons present underneath the broad BP1 absorption band. However, as seen in Figure A.6, shifting the excitation wavelength into the NIR does not alter the observed transient absorption spectra or affect the presence of the clean isosbestic points. This implies that there is no single polaron absorption peak obscured by the red tail of the bipolaron BP1 absorption. In addition, the lack of wavelength dependence on the spectra and the clean isosbestic points also indicates that there is only one population of bipolarons present in the film. There is no secondary population of bipolarons in distinctly amorphous regions that acts spectroscopically distinct from the bipolarons in the semicrystalline region of the film.

A second experiment confirming the assignment of the charge carriers in doped PBTDTP to bipolarons is transient absorption spectroscopy following excitation of the bandgap transition of the $F_4$TCNQ-doped PBTDTP films. As seen in Figure A.8, exciting an electron across the bandgap leaves one unpaired electron and promotes one electron to the conduction band. The promoted electron is not seen in the NIR; however, the unpaired electron acts like a polaron formed from a split bipolaron. Indeed, the spectral shape and kinetics match with the transient absorption following excitation of the BP1 transition, confirming the assignment of the BP1 transition. Note that exciting the P1 transition of free or trapped polarons in the traditional or band-bending models would not give rise to P1 and P2 transtions increasing, and thus would not match the spectra seen by exciting the bandgap transition. Thus, the results of this transient absorption experiment further confirms the assignment of bipolarons being the species present in $F_4$TCNQ-doped PBTDTP films.

### A.1.6 Computational predictions of PBTDTP Polarons and Bipolarons

Calculations on PBTDTP, PBTDTP with the two donor unit thiophenes removed (PBTDTP-2Th), and P3HT were optimized using the PBE0 hybrid functional with Grimme's D3 dispersion correction and with the 6-31g** basis set; a polarizable continuum PCM of a dielectric constant of 3 also was used to simulate a conjugated polymer matrix environment. All sidechains were approximated with methyl groups for ease of calculation. Our calculations used 4 repeat units for PBTDTP and PBTDTP-2Th, while our P3HT calculations used 16 repeat units. In addition, these calculations

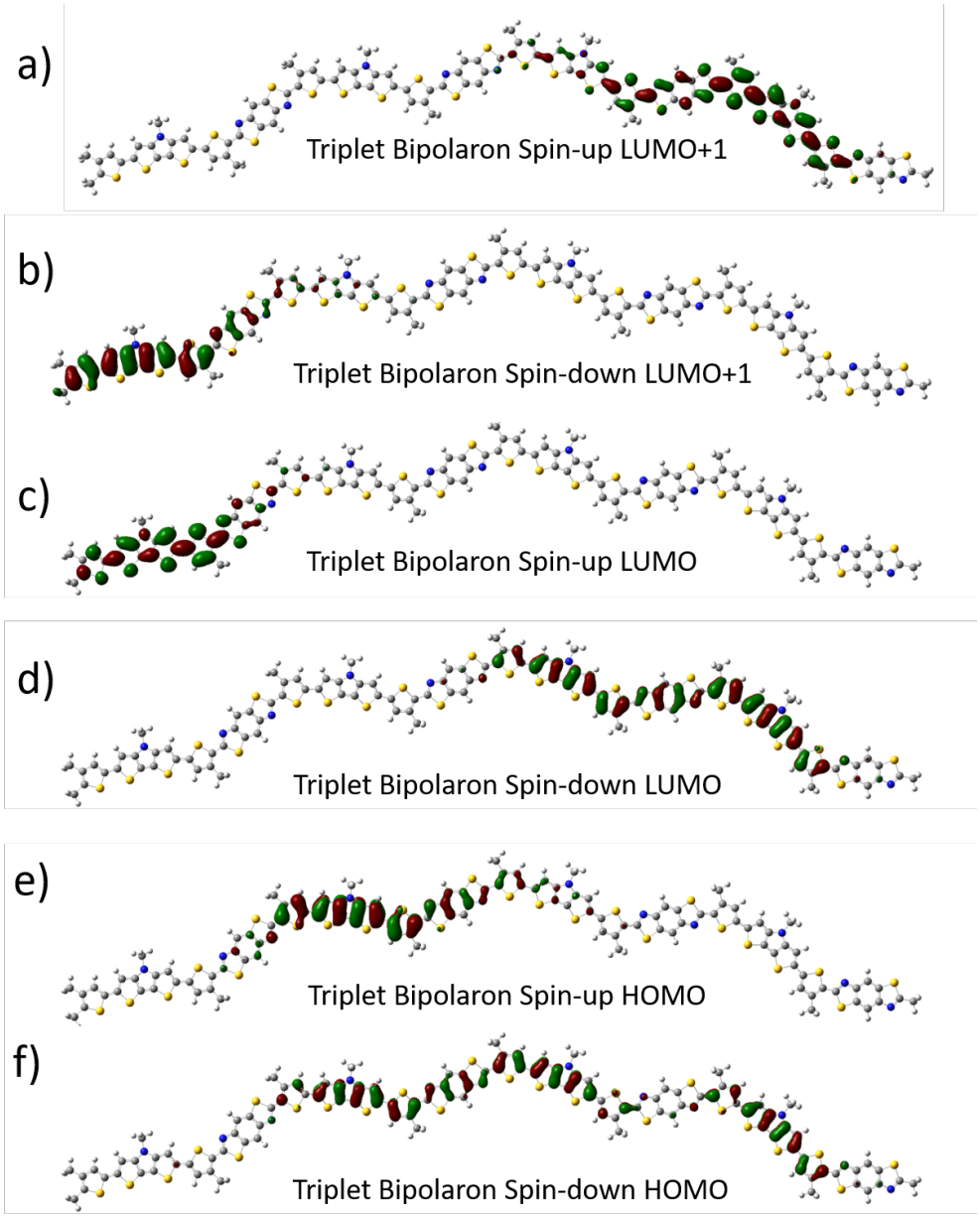


**Figure A.9: Orbital pictures of the a) triplet bipolaron PBTDTP spin-up LUMO+1, b) triplet bipolaron PBTDTP spin-down LUMO+1, c) triplet bipolaron PBTDTP spin-up LUMO, d) triplet bipolaron PBTDTP spin-down LUMO, e) triplet bipolaron PBTDTP spin-up HOMO, f) and triplet bipolaron PBTDTP spin-down HOMO, all calculated with the PBE0 functional.**

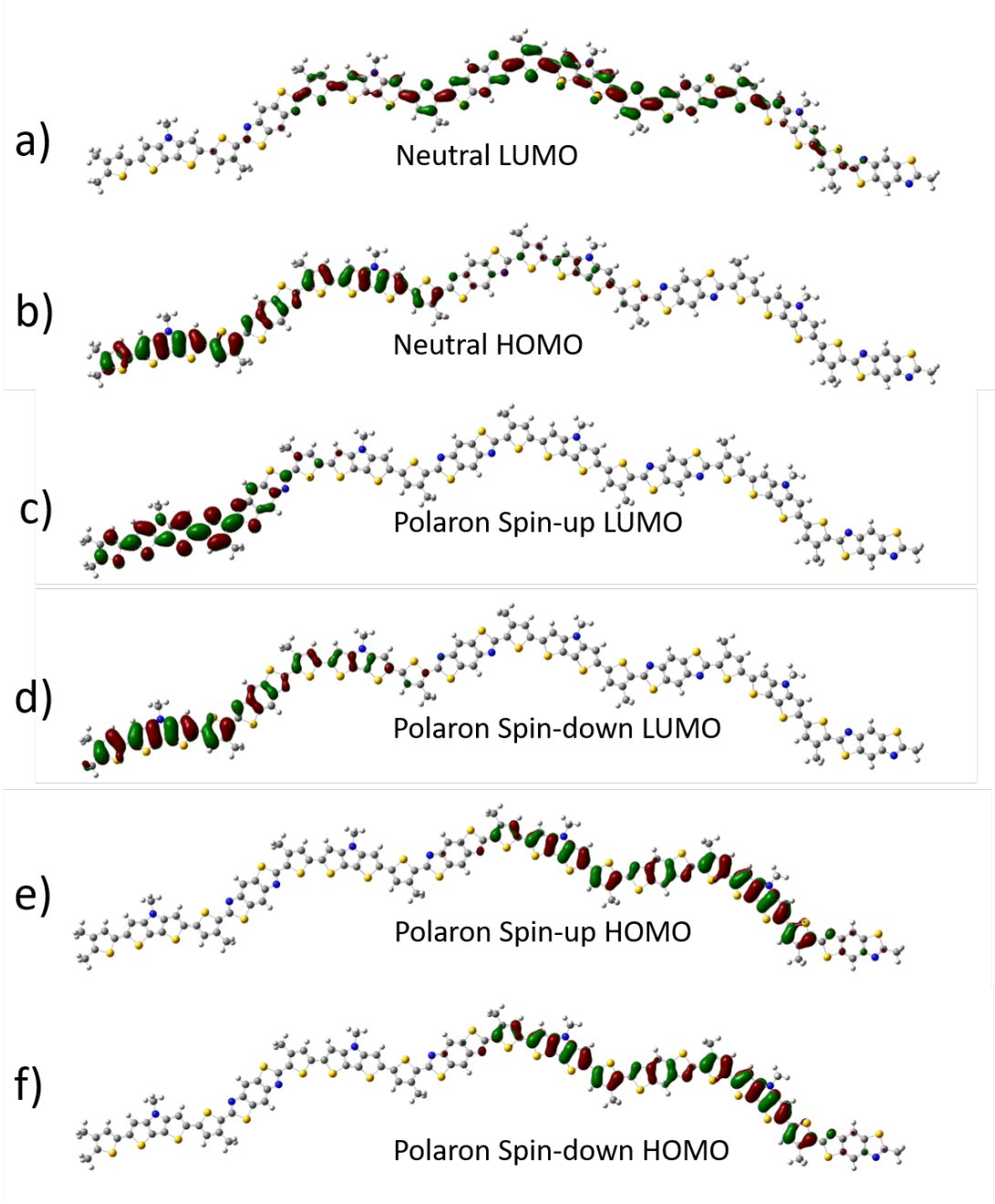


**Figure A.10: Orbital pictures of the a) neutral PBTDTP LUMO, b) neutral PBTDTP HOMO, c) spin-up PBTDTP polaron LUMO, d) spin-down PBTDTP polaron LUMO, e) spin-up PBTDTP polaron HOMO, and f) spin-down PBTDTP polaron HOMO all calculated with the PBE0 functional.**

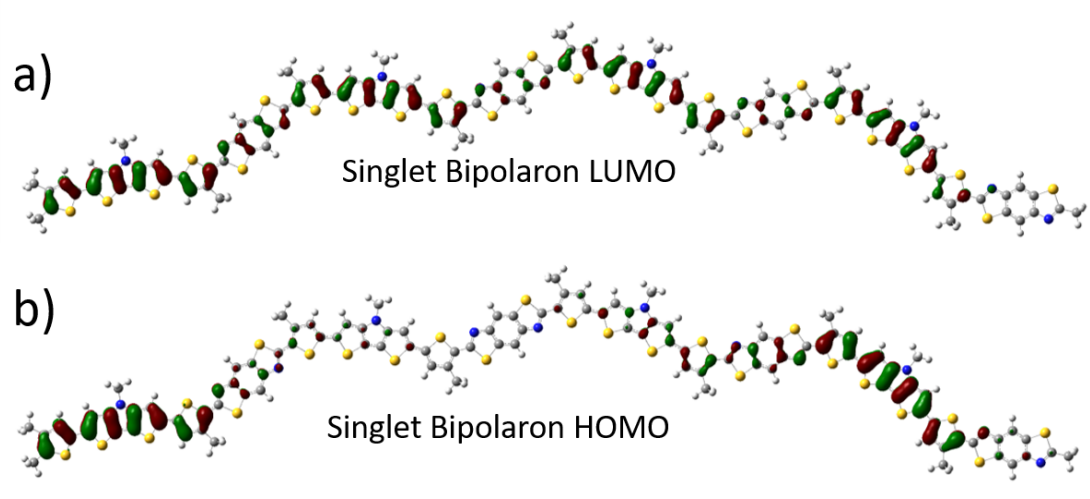


**Figure A.11: Orbital pictures of the a) PBTDTP singlet bipolaron LUMO and b) PBTDTP singlet bipolaron HOMO, all calculated with the PBE0 functional.**

were repeated using the B3LYP functional, which gave qualitatively similar results for both PBTDTP and P3HT as far as bipolaron stability is concerned. The orbitals of the HOMO and LUMO from each calculation are shown in Figures A.9-A.14 and A.18. Figures A.15-A.17 show the charge density and bond length deviation compared to the neutral polymer, and confirm that the LUMO (or LUMO and LUMO+1) correspond to the location of the most dramatic bond length changes and thus the location of the polaronic or bipolaronic charges.

**Table A.4: Total Energies Above Neutral Polymer (eV)**

| | | | |
|---|---|---|---|
| Polymer | Polaron | Singlet Dication | Triplet Dication |
| PBTDTP | 4.94 | 10.43 | 10.07 |
| PBTDTP-2Th | 5.22 | 11.14 | 10.82 |
| P3HT | 4.67 | 9.98 | 9.73 |
| PTB7 | 5.19 | 10.97 | 10.77 |

Based on the calculations, we note that for PBTDTP singlet bipolarons are energetically disfavored relative to two polarons (Table S3); however, the relative trend between PBTDTP singlet bipolaron energy and PBTDTP-2Th singlet bipolaron energy goes as expected. We do not expect DFT to be accurate within ∼0.1 eV on the absolute scale, but the accuracy for energy differences should be on that order. Surveying the literature, DFT techniques are used to characterize polarons

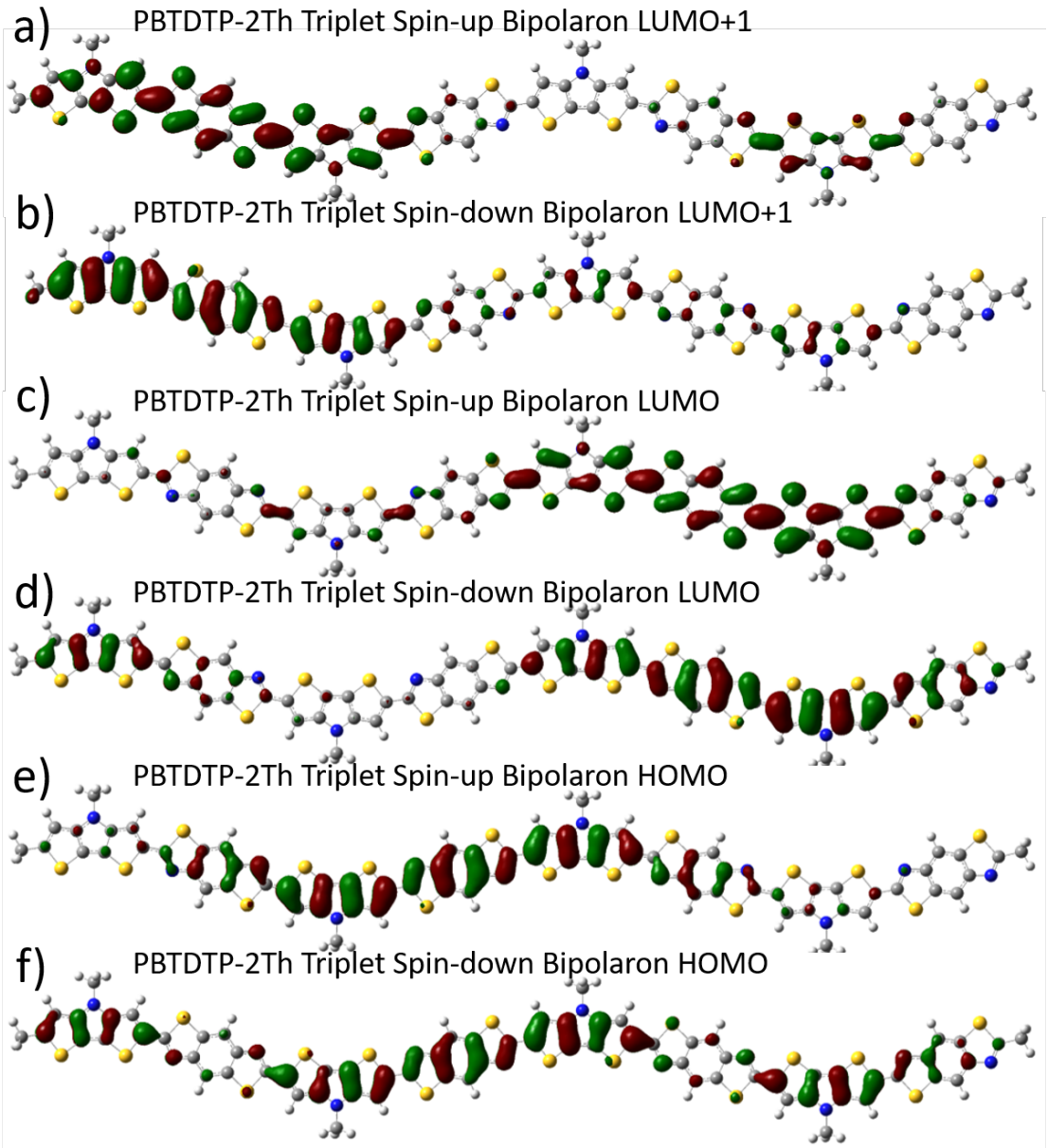


**Figure A.12: PBTDTP-2Th PBE0 orbitals for the triplet bipolaron spin-up LUMO+1 (a), triplet bipolaron spin-down LUMO+1 (b), triplet bipolaron spin-up LUMO (c), triplet bipolaron spin-down LUMO (d), triplet bipolaron spin-up HOMO (e), and triplet bipolaron spin-down HOMO (f).**

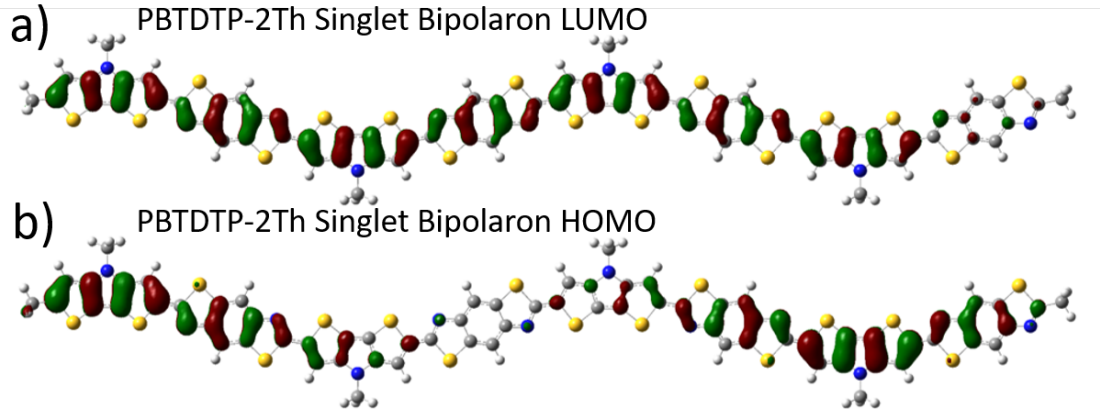


**Figure A.13: PBTDTP-2Th PBE0 orbitals for the singlet bipolaron LUMO (a) and singlet bipolaron HOMO (b).**

and bipolarons on semiconducting polymers and have qualitative and descriptive accuracy.[10, 12, 17–23] For PBTDTP-2Th, making a bipolaron is 0.64 eV disfavored compared to making two polarons, 0.09 eV more than that of PBTDTP. Comparing PBTDTP to PTB7 shows that bipolarons are 0.04 eV less favored energetically for PBTDTP than PTB7, but this is near the limits of the accuracy of these methods. Comparing PBTDTP to P3HT, we note that the trend continues, with bipolarons in P3HT being more disfavored energetically than PBTDTP by 0.15 eV. This trend holds true regardless of the choice of basis set or functional. One of the reasons our calculations predict unstable bipolarons in contrast to experiment is that the calculations do not include factors such as stabilization/trapping by a nearby counteranion or delocalization between π-stacks of neighboring polymers, either of which might lead to bipolarons being favored more than polarons. But even without these effects, our current level of theory shows qualitatively that the chemical structure of PBTDTP encourages bipolaron formation more than other polymers with smaller donor units. Finally, as mentioned in the main text, the triplet bipolaron appears lower in energy than the singlet bipolaron. However, analysis of the orbital, bond order alternation and charge plots above shows that the triplet bipolaron effectively is two separate polarons that are attempting to distance themselves from each other by localizing to opposite sides of the polymer backbone. We note that one paper[17] recently found triplet bipolarons to be lower in energy than singlet bipolarons in PEDOT, but it appears that the triplet dication is better described as two separate polarons in this system.

To identify what states correspond to the charge location, we compare the Mulliken and NBO

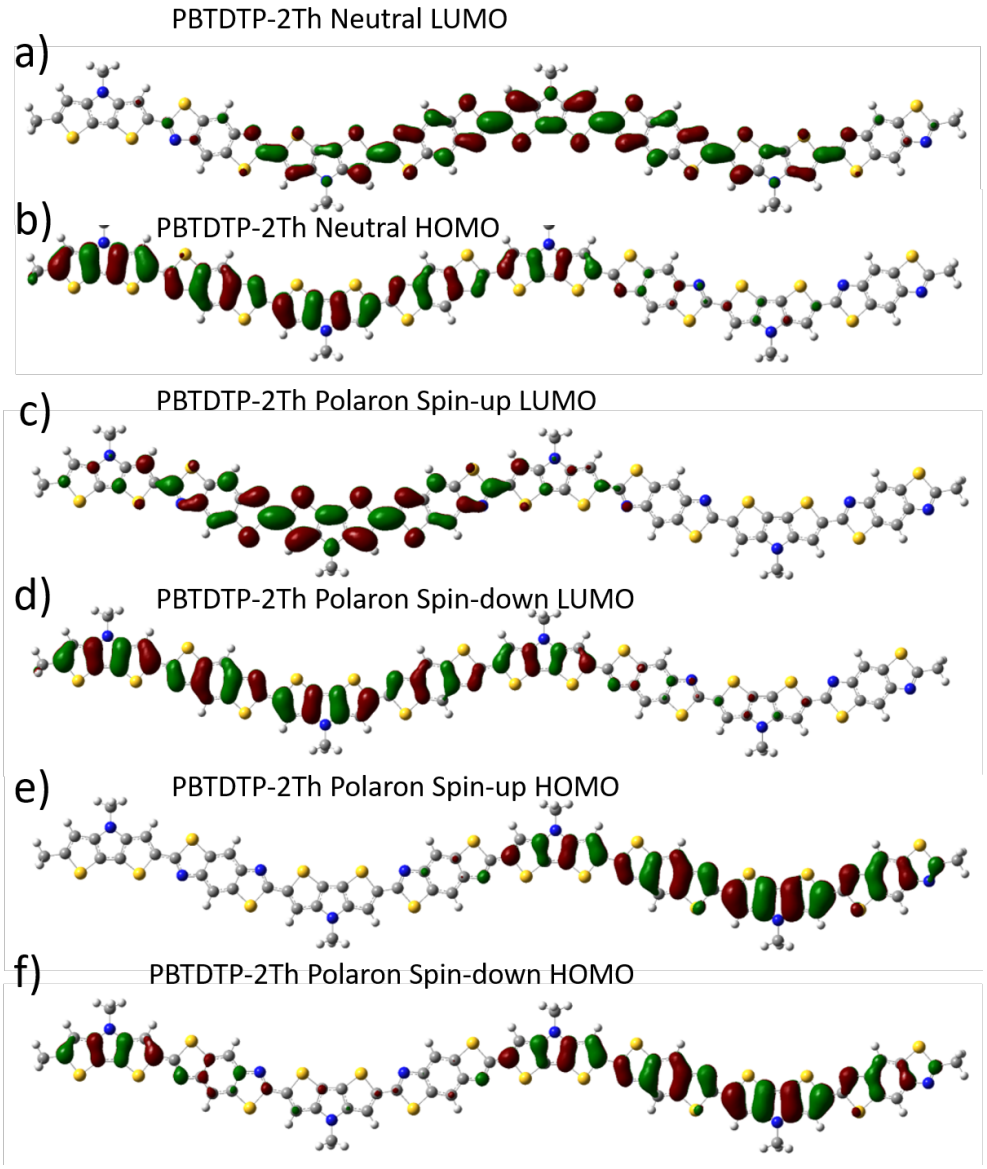


**Figure A.14: PBTDTP-2Th PBE0 orbitals for the neutral LUMO (a), neutral HOMO (b), polaron spin-up LUMO (c), polaron spin-down LUMO (d), polaron spin-up HOMO (e), and polaron spin-down HOMO (f).**

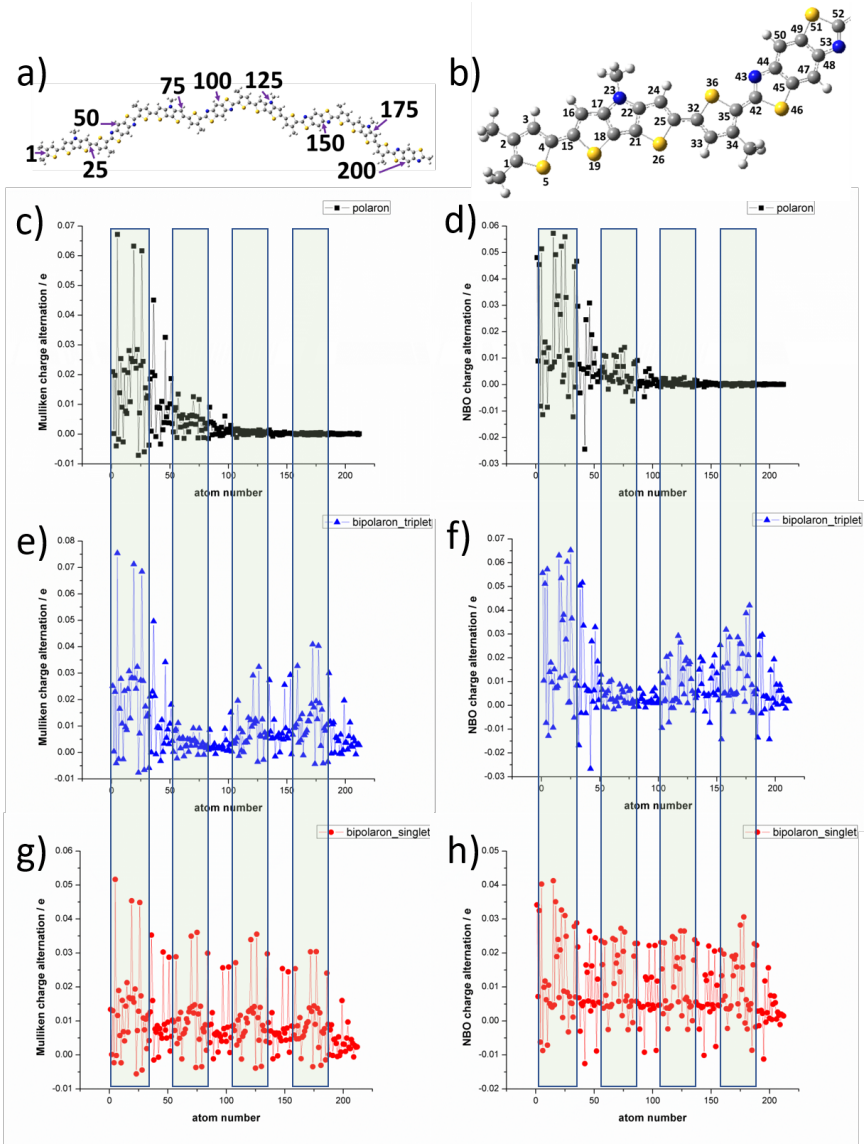


**Figure A.15: Charge density deviation plots of PBTDTP show the difference between the Mulliken and NBO charges of the neutral oligomer and the charged oligomer. The atom numbering scheme is shown in (a) and (b), and the charge density differences per atom are shown for the polaron (c, d), triplet bipolaron (e,f) and singlet bipolaron (g,h). The Mulliken charge density plots are on the left and the NBO charge density plots are on the right. The location of the donor regions are highlighted in green.**

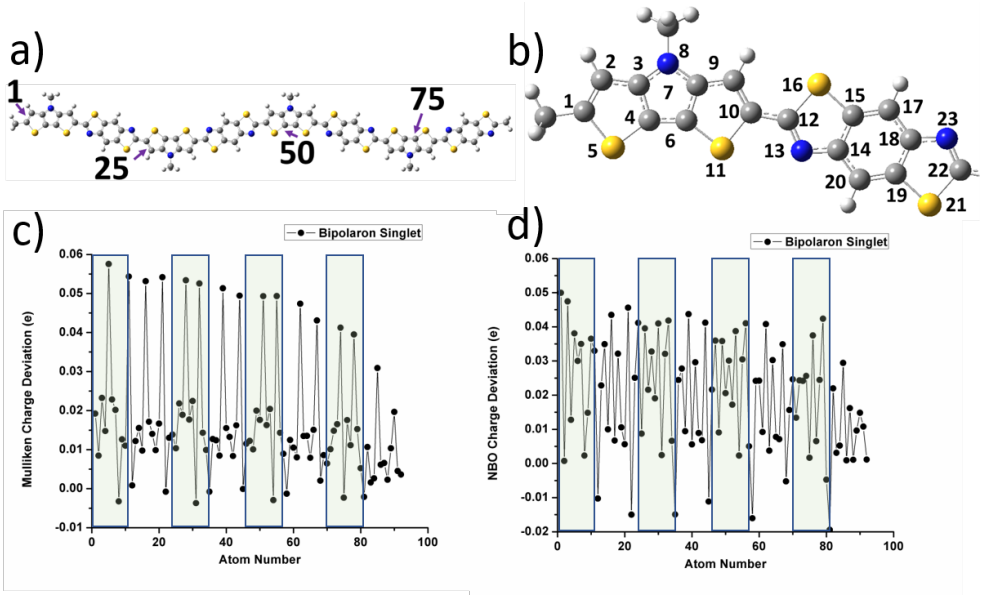


**Figure A.16: Charge density deviation plots of PBTDTP-2Th show the difference between the neutral oligomer and the charged oligomer. The atom numbering scheme is shown in (a) and (b), and the charge density differences per atom are shown for the singlet bipolaron (c, d). The Mulliken charge density plots are on the left and the NBO charge density plots are on the right. The location of the donor regions are highlighted in green.**

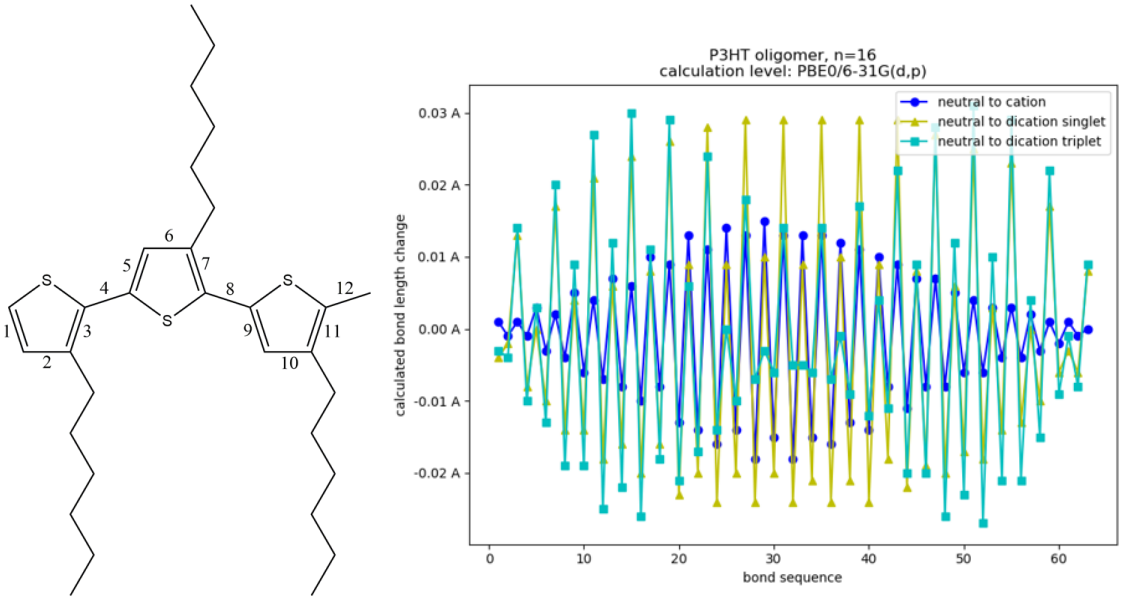


**Figure A.17: Bond order labelling schema for P3HT hexadecamers (left) and bond order alternation deviation plot (right) of the difference between the neutral geometry of P3HT and cation, triplet dication, and singlet dication geometries.**

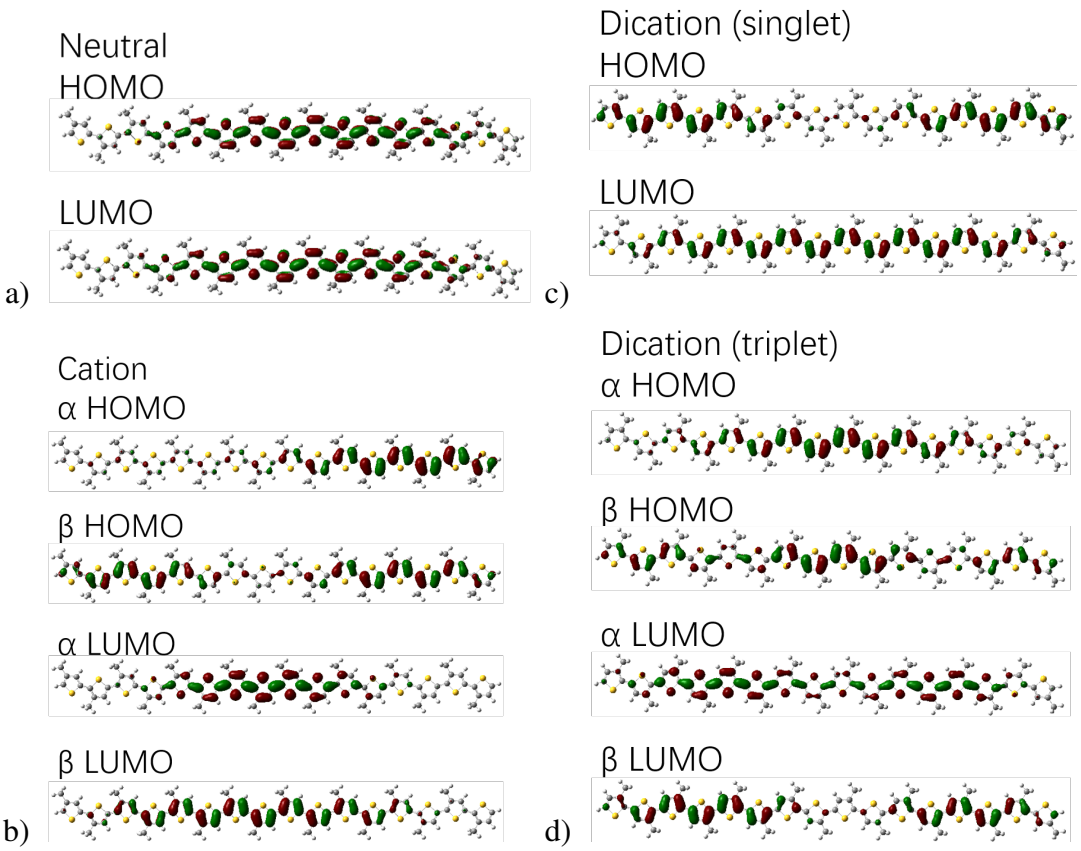


**Figure A.18: Orbital pictures of the a) neutral P3HT hexadecamer orbitals, b) cation P3HT hexadecamer orbitals, c) dication singlet P3HT hexadecamer orbitals, and d) dication triplet P3HT hexadecamer orbitals, all calculated with the PBE0 functional**

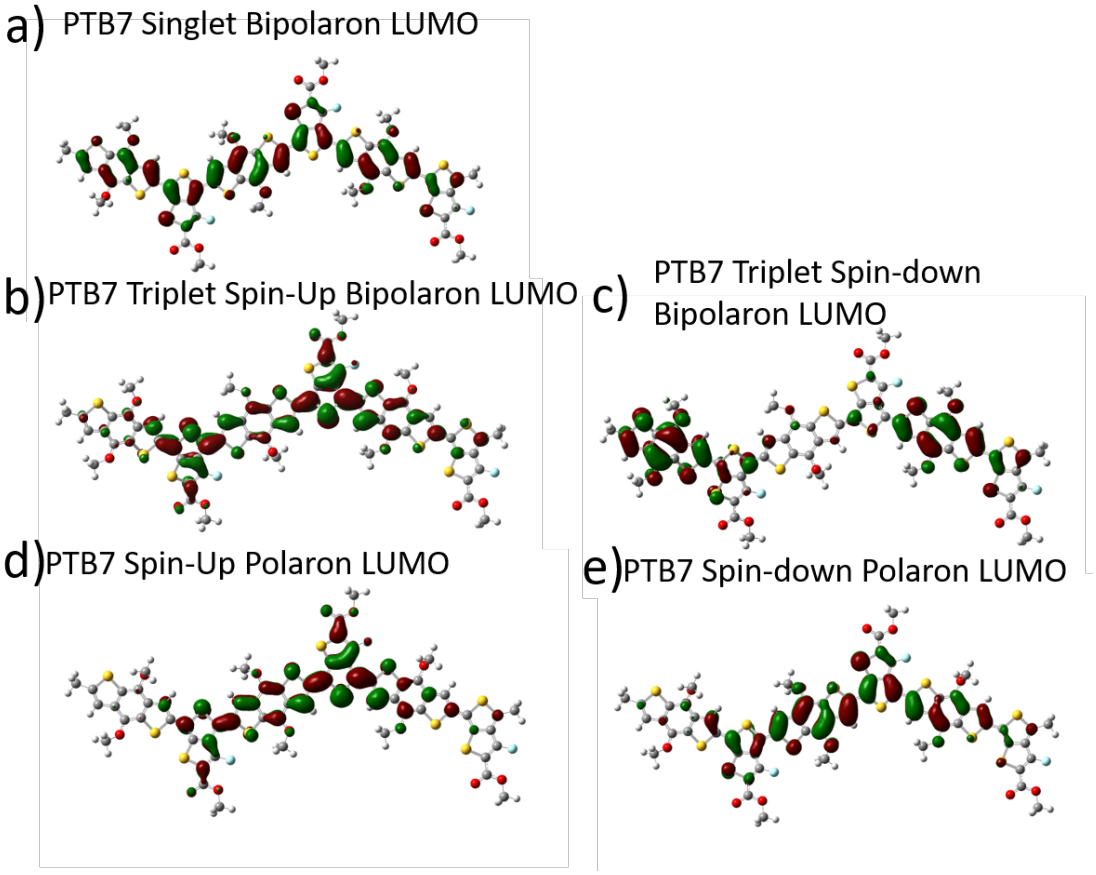


**Figure A.19: Orbital pictures of the a) singlet bipolaron LUMO, b) triplet spin-up bipolaron LUMO, c) triplet spin-down bipolaron LUMO, d) spin-up polaron LUMO, and e) spin-down polaron LUMO.**

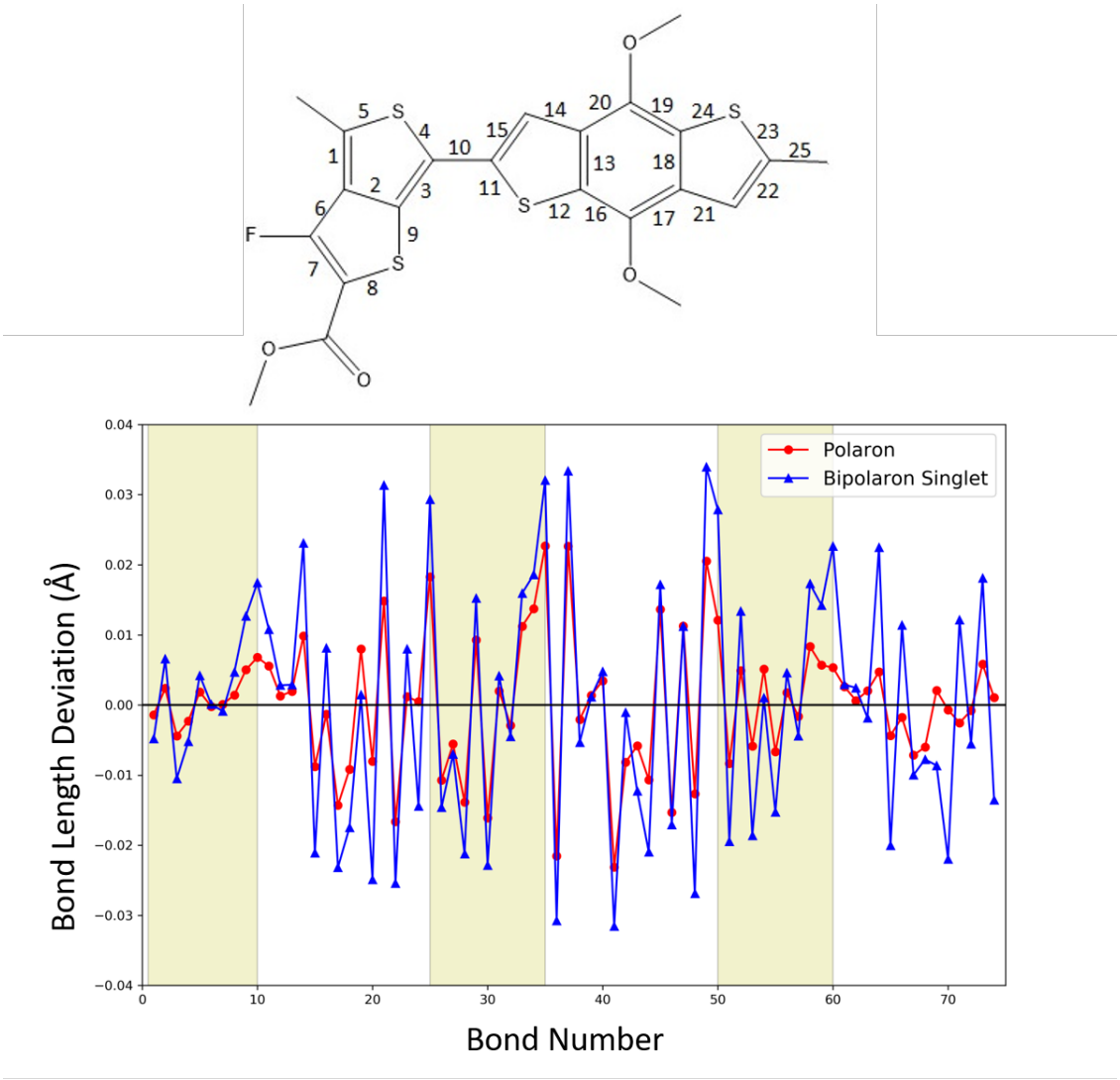


**Figure A.20: Top) The bond labeling scheme of PTB7 oligomer. Bottom) The bond length deviation relative to the neutral PTB7 structure of the PTB7 polaron (red) and singlet bipolaron (blue). The acceptor region is highlighted in yellow.**

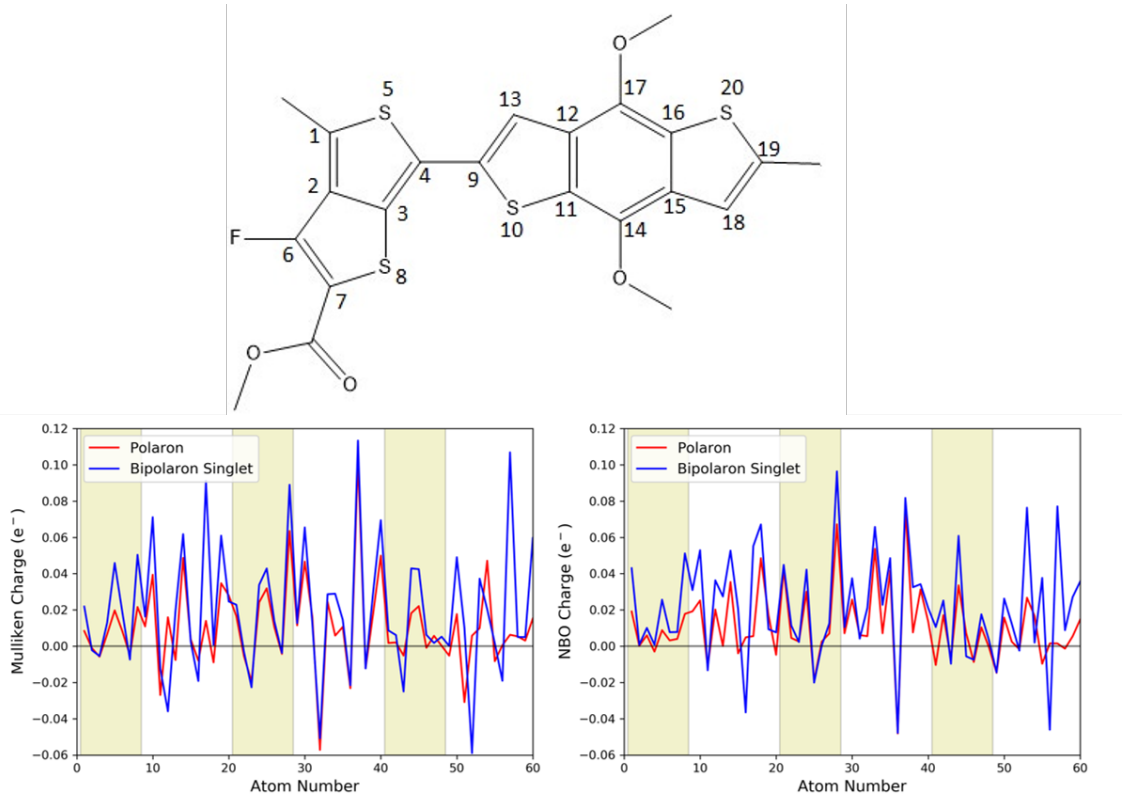


**Figure A.21: Top) The atom labeling scheme of the PTB7 oligomer. Bottom) The Mulliken (left) and NBO (right) charge density plots as a difference from the neutral PTB7 oligomer. The polaron is shown in red and the singlet bipolaron is shown in blue. The acceptor region is highlighted in yellow.**

charge density plots in Figures A.15 and A.17 with the HOMO and LUMO orbitals. (Figures A.9-A.12) The location of the polaron is based on the unoccupied SOMO level, specifically the spin-down LUMO. In the case of the singlet bipolaron, the location of the charges and bond distortion matches well with the LUMO state as expected. In the case of the triplet bipolaron, since the spin-down LUMO and LUMO+1 states are quasi-degenerate and the bipolaron is doubly-charged, the location of the charges and bond distortion reflects a mixture of those two states. There is good agreement between the bond deviation position and both Mulliken and NBO charge density plots, indicating that the bond deviations are representative of the location of the bipolaron charges. For PBTDTP, the singlet bipolaron predominantly resides primarily on the donor regions, while for PBTDTP-2th and PTB7, the singlet bipolaron occupies both the donor and acceptor regions.

**Table A.5: Polymer Donor Size and Doping Results Literature Comparison**

| Polymer | Number of Donor Rings | Doped Species |
|---|---|---|
| PBTDTP[1] (this work) | 5 | Bipolarons |
| PCDTBT[24] | 5 | Polarons |
| DPPT-TT[18] | 4 | Polarons |
| PDPP-4T[25] | 4 | Polarons |
| PDPP-T-TT-T[25] | 4 | Polarons |
| PffBT4T[26] | 4 | Polarons |
| F8BT[21] | 3 | Polarons |
| PTB7[27] (and this work) | 3 | Polarons |
| PBDTTT-c[9] | 3 | Polarons |
| PCDTPT[28] | 3 and 3 | Polarons |
| PCDTFBT[28] | 3 and 3 | Polarons |
| PCPDTBT[29] | 3 | Polarons |
| TAF copolymers[13] | 3 | Polarons |
| PCPDTPT[22] | 3 | Polarons |

### A.1.7 Other work on push-pull polymer doping

Table S4 shows the size of the donor moieties in a variety of chemically-doped push-pull conjugated polymers in the literature. For all of these studies, with the exception of PCDTBT studied by Provencher and co-workers,[24] the donor unit size was smaller than that of PBTDTP, the polymer studied in this paper. All of the other studies found only polarons upon chemical doping. We note that in the case of PCDTBT, the acceptor unit, benzothiadiazole, is much smaller than that of PBTDTP, and has its most electron-poor region (the thiadiazole part) located off of the main polymer backbone. As such, we posit that the acceptor unit in PCDTBT does not act as a significant barrier to polaron delocalization, and thus allows polarons to spread more easily along the polymer backbone, which favors polarons more relative to bipolarons. Thus, as discussed in the main text, the choice of donor and acceptor units in push-pull conjugated polymers deeply affect charge delocalization and spatial confinement of the chemically doped carriers.

## References


(1) Ahmed, E.; Subramaniyan, S.; Kim, F. S.; Xin, H.; Jenekhe, S. A. Benzobisthiazole-based donor-acceptor copolymer semiconductors for photovoltaic cells and highly stable field-effect transistors.*Macromolecules* **2011**, *44*, 7207–7219.

(2) Noone, K. M.; Strein, E.; Anderson, N. C.; Wu, P. T.; Jenekhe, S. A.; Ginger, D. S. Broadband absorbing bulk heterojunction photovoltaics using low-bandgap solution-processed quantum dots.*Nano Letters* **2010**, *10*, 2635–2639.

(3) Hwang, Y.-J.; Courtright, B. A. E.; Ferreira, A. S.; Tolbert, S. H.; Jenekhe, S. A. 7.7% efficient all-polymer solar cells.*Advanced Materials* **2015**, *27*, 4578–4584.

(4) Yee, P. Y.; Scholes, D. T.; Schwartz, B. J.; Tolbert, S. H. Dopant-induced ordering of amorphous regions in regiorandom P3HT.*The Journal of Physical Chemistry Letters* **2019**, *10*, 4929–4934.

(5) Bredas, J. L.; Street, G. B. Polarons, bipolarons, and solitons in conducting polymers.*Accounts of Chemical Research* **1985**, *18*, 309–315.

(6) Van Haare, J. A.; Havinga, E. E.; Van Dongen, J. L.; Janssen, R. A.; Cornil, J.; Brédas, J. L. Redox states of long oligothiophenes: Two polarons on a single chain.*Chemistry - A European Journal* **1998**, *4*, 1509–1522.

(7) Beljonne, D.; Cornil, J.; Sirringhaus, H.; Brown, P. J.; Shkunov, M.; Friend, R. H.; Brédas, J.-L. Optical Signature of Delocalized Polarons in Conjugated Polymers.*Advanced Functional Materials* **2001**, *11*, 229–234.

(8) Chew, A. R.; Salleo, A.; Science, M. Spectroscopic studies of dopant-induced conformational changes in poly ( 3-hexylthiophene ) thin fi lms.*MRS Communications* **2017**, 728–734.

(9) Cobet, C.; Gasiorowski, J.; Menon, R.; Hingerl, K.; Schlager, S.; White, M. S.; Neugebauer, H.; Sariciftci, N. S.; Stadler, P. Influence of molecular designs on polaronic and vibrational transitions in a conjugated push-pull copolymer.*Scientific Reports* **2016**, *6*, 35096.

(10) Heimel, G. The Optical Signature of Charges in Conjugated Polymers.*ACS Central Science* **2016**, *2*, 309–315.

(11) Kohlstedt, K. Mind the Gap.*ACS Central Science* **2016**, *2*, 278–280.

(12) Kahmann, S.; Fazzi, D.; Matt, G. J.; Thiel, W.; Loi, M. A.; Brabec, C. J. Polarons in Narrow Band Gap Polymers Probed over the Entire Infrared Range: A Joint Experimental and Theoretical Investigation.*The Journal of Physical Chemistry Letters* **2016**, *7*, 4438–4444.

(13) Png, R.-Q.; Ang, M. C.; Teo, M.-H.; Choo, K.-K.; Tang, C. G.; Belaineh, D.; Chua, L.-L.; Ho, P. K. Madelung and Hubbard interactions in polaron band model of doped organic semiconductors.*Nature Communications* **2016**, *7*, 11948.

(14) Cornil, J.; Brédas, J.-L. Nature of the optical transitions in charged oligothiophenes.*Advanced Materials* **1995**, *7*, 295–297.

(15) Voss, M. G.; Scholes, D. T.; Challa, J. R.; Schwartz, B. J. Ultrafast transient absorption spectroscopy of doped P3HT films: distinguishing free and trapped polarons.*Faraday Discussions* **2018**, DOI: 10.1039/C8FD00210J.

(16) Pingel, P.; Neher, D. Comprehensive picture of P -type doping of P3HT with the molecular acceptor F4TCNQ.*Physical Review B* **2013**, *87*, 115209.

(17) Zozoulenko, I.; Singh, A.; Singh, S. K.; Gueskine, V.; Crispin, X.; Berggren, M. Polarons, bipolarons, and absorption spectroscopy of PEDOT.*ACS Applied Polymer Materials* **2019**, *1*, 83–94.

(18) Francis, C.; Fazzi, D.; Grimm, S. B.; Paulus, F.; Beck, S.; Hillebrandt, S.; Pucci, A.; Zaumseil, J. Raman spectroscopy and microscopy of electrochemically and chemically doped high-mobility semiconducting polymers.*Journal of Materials Chemistry C* **2017**, *5*, 6176–6184.

(19) Di Nuzzo, D.; Fontanesi, C.; Jones, R.; Allard, S.; Dumsch, I.; Scherf, U.; von Hauff, E.; Schumacher, S.; Da Como, E. How intermolecular geometrical disorder affects the molecular doping of donor–acceptor copolymers.*Nature Communications* **2015**, *6*, 6460.

(20) Fuzell, J.; Jacobs, I. E.; Ackling, S.; Harrelson, T. F.; Huang, D. M.; Larsen, D.; Moulé, A. J. Optical Dedoping Mechanism for P3HT:F4TCNQ Mixtures.*Journal of Physical Chemistry Letters* **2016**, *7*, 4297–4303.

(21) Bird, M. J.; Bakalis, J.; Asaoka, S.; Sirringhaus, H.; Miller, J. R. Fast Holes, Slow Electrons, and Medium Control of Polaron Size and Mobility in the DA Polymer F8BT.*The Journal of Physical Chemistry C* **2017**, *121*, 15597–15609.

(22) Yurash, B.; Cao, D. X.; Brus, V. V.; Leifert, D.; Wang, M.; Dixon, A.; Seifrid, M.; Mansour, A. E.; Lungwitz, D.; Liu, T.; Santiago, P. J.; Graham, K. R.; Koch, N.; Bazan, G. C.; Nguyen, T.-Q. Towards understanding the doping mechanism of organic semiconductors by Lewis acids.*Nature Materials* **2019**, *18*, 1327–1334.

(23) Gao, J.; Roehling, J. D.; Li, Y.; Guo, H.; Moulé, A. J.; Grey, J. K. The Effect of 2,3,5,6-Tetrafluoro-7,7,8,8-Tetracyanoquinodimethane Charge Transfer Dopants on the Conformation and Aggregation of Poly(3-Hexylthiophene).*Materials Chemistry C* **2013**, *1*, 5638.

(24) Provencher, F.; Bérubé, N.; Parker, A. W.; Greetham, G. M.; Towrie, M.; Hellmann, C.; Côté, M.; Stingelin, N.; Silva, C.; Hayes, S. C. Direct observation of ultrafast long-range charge separation at polymer-fullerene heterojunctions.*Nature Communications* **2014**, *5*, DOI: 10.1038/ncomms5288.

(25) Liang, Z.; Zhang, Y.; Souri, M.; Luo, X.; Boehm, A. M.; Li, R.; Zhang, Y.; Wang, T.; Kim, D.-Y.; Mei, J.; Marder, S. R.; Graham, K. R. Influence of dopant size and electron affinity on the electrical conductivity and thermoelectric properties of a series of conjugated polymers.*Journal of Materials Chemistry A* **2018**, *6*, 16495–16505.

(26) Vardeny, S. R.; Baniya, S.; Lafalce, E.; Peyghambarian, N.; Vardeny, Z. V. Electronic and vibrational spectroscopy studies of PffBT4T π-conjugated donor–acceptor copolymer.*Journal of Photonics for Energy* **2018**, *8*, 1.

(27) Baniya, S.; Vardeny, S. R.; Lafalce, E.; Peygambarian, N.; Vardeny, Z. V. Amplitude-Mode Spectroscopy of Charge Excitations in PTB7 π -Conjugated Donor-Acceptor Copolymer for Photovoltaic Applications.*Physical Review Applied* **2017**, *7*, 064031.

(28) Suh, E. H.; Jeong, Y. J.; Oh, J. G.; Lee, K.; Jung, J.; Kang, Y. S.; Jang, J. Doping of donor-acceptor polymers with long side chains via solution mixing for advancing thermoelectric properties.*Nano Energy* **2019**, *58*, 585–595.

(29) Anderson, M.; Ramanan, C.; Fontanesi, C.; Frick, A.; Surana, S.; Cheyns, D.; Furno, M.; Keller, T.; Allard, S.; Scherf, U.; Beljonne, D.; D'Avino, G.; von Hauff, E.; Da Como, E. Displacement of polarons by vibrational modes in doped conjugated polymers.*Physical Review Materials* **2017**, *1*, 055604.